DOI: 10.1002/anie.200602750

Analytical Methods

Scanning Electrochemical Microscopy for Direct Imaging of Reaction Rates

Gunther Wittstock, Malte Burchardt, Sascha E. Pust, Yan Shen, and Chuan Zhao*

Keywords:
electrochemistry · interfaces · scanning electrochemical microscopy · scanning probe microscopy · ultramicroelectrodes

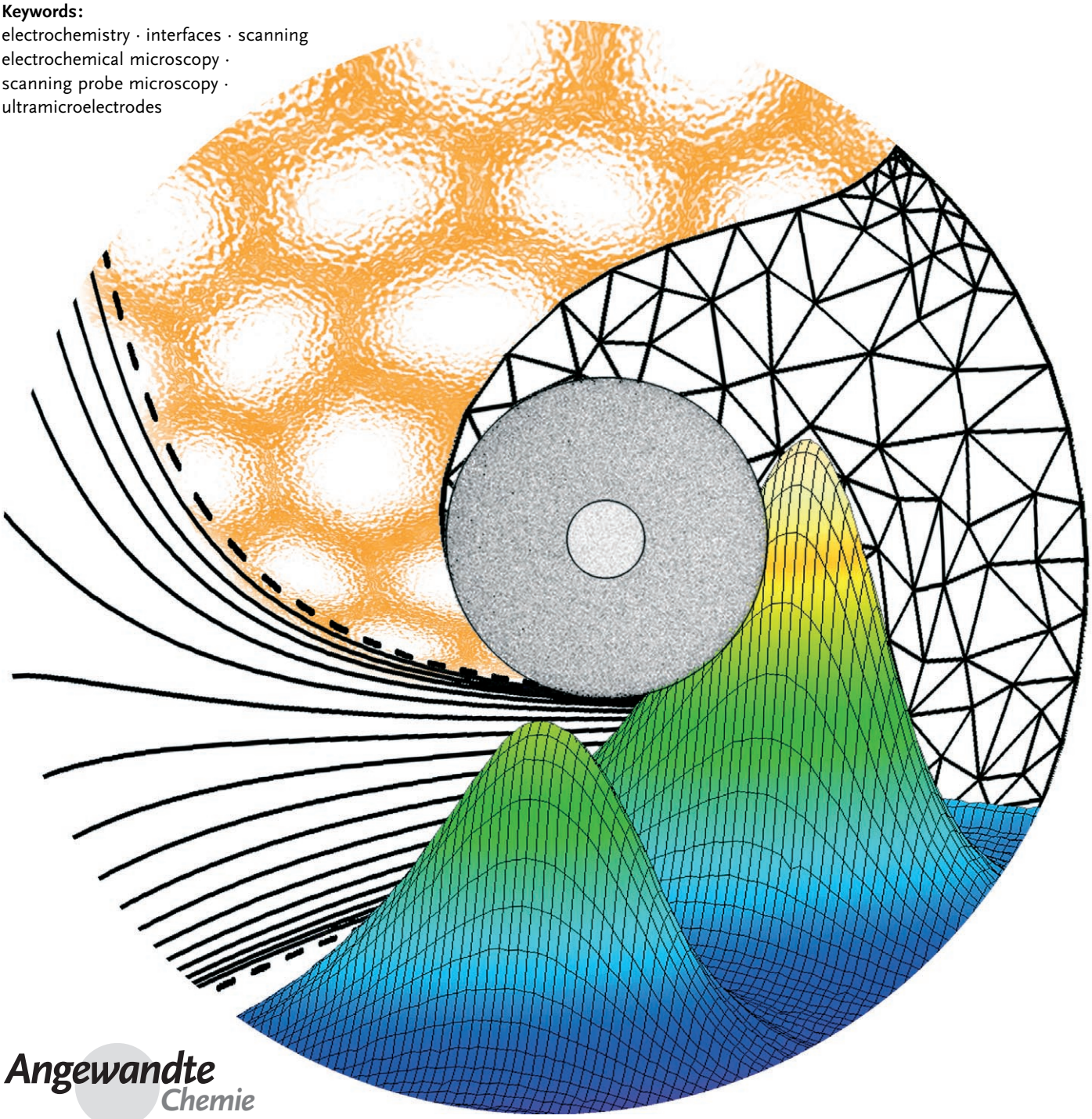

Not only in electrochemistry but also in biology and in membrane transport, localized processes at solid–liquid or liquid–liquid interfaces play an important role at defect sites, pores, or individual cells, but are difficult to characterize by integral investigation. Scanning electrochemical microscopy is suitable for such investigations. After two decades of development, this method is based on a solid theoretical foundation and a large number of demonstrated applications. It offers the possibility of directly imaging heterogeneous reaction rates and locally modifying substrates by electrochemically generated reagents. The applications range from classical electrochemical problems, such as the investigation of localized corrosion and electrocatalytic reactions in fuel cells, sensor surfaces, biochips, and microstructured analysis systems, to mass transport through synthetic membranes, skin and tissue, as well as intercellular communication processes. Moreover, processes can be studied that occur at liquid surfaces and liquid–liquid interfaces.

From the Contents

1. Introduction

What do the screening of a combinatorial library of oxygen reduction catalysts for fuel cells[1] and the evaluation of in vitro fertilized bovine embryos[2] have in common? Both studies made use of scanning electrochemical microscopy (SECM). Bard and co-workers supplied reduction catalysts with oxygen originating from water electrolysis at a movable microelectrode.[1] By plotting the reduction currents at the catalyst array against the position of the microelectrode, the most effective catalyst composition could be identified. Shiku et al. used a positionable microelectrode for the measurement of oxygen consumption of bovine embryos, which allowed conclusions about their metabolic activity.[2] These and further very diverse applications of SECM are rooted in two fundamentally new developments of the last two decades: the broad application of microscopic electrodes and the diverse usage of the scanning probe principle.

The properties of small electrodes have been investigated intensively since the 1980s.[3,4] One of their advantages is the formation of a hemispherical diffusion field that allows more efficient mass transfer than that at macroscopic electrodes. The special diffusion properties lead to a rapid establishment of a steady-state diffusion-limited current $i_{T,\infty}$, which is given for a disk-shaped electrode surrounded by an insulating sheath by Equation (1),[5] in which n is the number of

$$i_{T,\infty} = g\, n\, F\, D\, c^*\, r_T \qquad (1)$$

transferred electrons per molecule, F the Faraday constant, D the diffusion coefficient, c^* the bulk concentration of the reagent, and r_T the radius of the disk-shaped active electrode area. The geometry-dependent factor g assumes the value of 4 for a disk-shaped electrodes embedded in an infinitely large insulator.[5]

The properties of such electrodes become apparent in typical experiments when the electrode diameter is smaller than 30 μm. Electrodes with such properties are termed ultramicroelectrodes (UMEs).[3,4] Furthermore, it shall be implied in the following contribution that electrodes that possess a disk-shaped active electrode area surrounded by an insulating sheath are meant when the abbreviation UME is used without other specifications. The steady-state diffusion-limited current yields a current density that is larger than the current density at macroscopic electrodes under conditions of forced convection (for example, at a rotating disk electrode). Consequently, relative movement between UME and solution causes only negligible enhancement of the faradaic current. Engstrom et al. used UMEs as sensors for recording concentration profiles above macroscopic electrodes in 1986.[6] In retrospect, this experiment represents the first scanning electrochemical microscopy experiment. A parallel development resulted from the application of scanning tunneling microscopy in electrochemical environments (ECSTM, electrochemical scanning tunneling microscopy), which shares some similarities with SECM in the general setup of the instrument. Bard and co-workers observed unusually large currents in ECSTM experiments in which the tip was located outside the tunneling distance.[7] In 1989, Kwak and Bard formulated a quantitative description of the diffusion-limited current at a UME as a function of the distance d above a macroscopic planar sample.[8] It was

[*] Prof. Dr. G. Wittstock, M. Burchardt, S. E. Pust, Dr. Y. Shen, Dr. C. Zhao
Carl von Ossietzky Universität Oldenburg
Institut für Reine und Angewandte Chemie und Institut für Chemie und Biologie des Meeres
26111 Oldenburg (Germany)
Fax: (+49) 441-798-3979
E-mail: gunther.wittstock@uni-oldenburg.de

evident that despite the instrumental similarities to ECSTM, the experiments involved a different interaction principle, which resulted in entirely new applications. The term "scanning electrochemical microscopy" was coined. According to the international use, acronyms such as SECM and ECSTM are used to designate the method as well as the corresponding microscope. SECM studies are described in more that 1000 original communications[9] and have been summarized in partially focused reviews, from which only a selection can be cited herein.[10–19]

An SECM consists of a positioning system that moves a UME as a local probe with respect to the sample (Figure 1). Depending on the size of the UME, different positioning technologies can be used; the technical requirements increase with the decreasing size of the UME. The UME is connected to a potentiostat as an amperometric mircoelectrode, and the electrochemical cell is completed by a reference electrode and an auxiliary electrode. The sample to be investigated can be connected to a bipotentiostat as second working electrode. In this respect, the SECM setup of UME and sample (Figure 2a) is similar to an electrochemical thin-layer cell (Figure 2b).[20] The important point is that redox-active

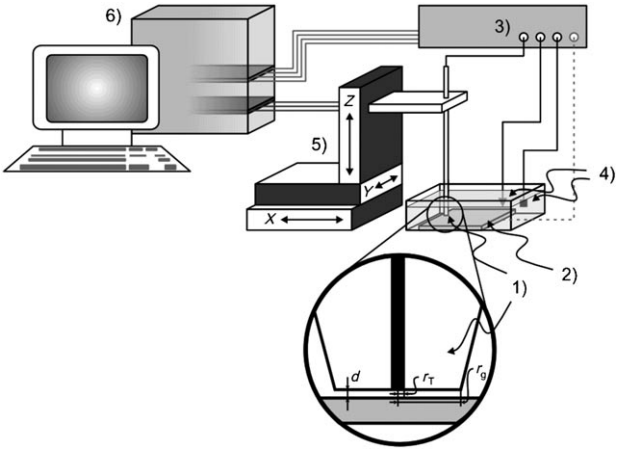

Figure 1. Important components of an SECM. 1) Disk-shaped amperometric ultramicroelectrode, 2) sample, 3) mono- or bipotentiostat, 4) reference and auxiliary electrodes, 5) positioning system, 6) control PC.

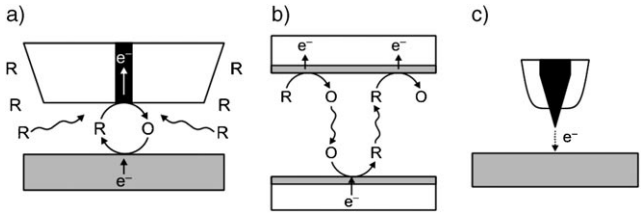

Figure 2. Comparison of the principles of a) SECM; b) electrochemical thin-layer cell; c) ECSTM. R stands for the reduced form and O for the oxidized form of a redox couple.

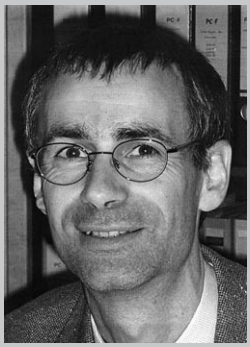

Gunther Wittstock was born in Schwerin in 1965. He studied chemistry at the University of Leipzig and then obtained a PhD in analytical chemistry under H. Emons and G. Werner in 1994. After his habilitation with R. Szargan in Leipzig, he accepted a call to a full professorship for physical chemistry at the University of Oldenburg in 2001. His research interests include the investigation of local reactions at solid–liquid interfaces, the combination of biochemical and biomimetic functional units with solid-state surfaces, and local electrochemical surface modification.

Malte Burchardt was born in Delmenhorst in 1979. He finished his studies in chemistry at the University of Oldenburg in 2004. Since then he has been a PhD student in the group of Prof. Wittstock. His research interests are the fabrication and characterization of patterned functional polyelectrolyte multilayer films.

Sascha E. Pust was born in Lingen (Ems) in 1980. He finished his chemistry studies at the University of Oldenburg in 2006, and is currently a PhD student under the guidance of Prof. Wittstock. He investigates grain-resolved electrochemical properties of passive layers on biphasic titanium alloys.

Yan Shen was born in Inner Mongolia, P.R. China, in 1973. She received a BSc degree in 1997, an MSc degree in physical chemistry from the Jilin University under Prof. Hengbin Zhang in 2000, and a PhD from the Changchun Institute of Applied Chemistry, Chinese Academy of Sciences under the supervision of Prof. Shaojun Dong in 2003. She was an Alexander von Humboldt Fellow and studied the kinetics of dye-sensitized oxide films and of the electrochemical oxygen reduction in the group of Prof. Wittstock at the University of Oldenburg.

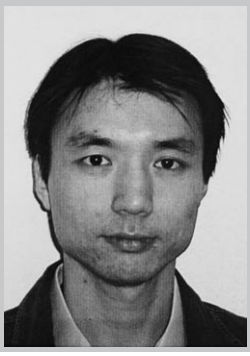

Chuan Zhao was born in 1974 in Shannxi, P.R. China. He studied chemistry and received his PhD in 2002 under the supervision of Prof. Junfeng Song at Northwest University, China. His dissertation focused on organic electrochemistry and flow electroanalysis. From 2002 to 2006, he was a postdoctoral researcher in the group of Prof. Wittstock at the University of Oldenburg. His research activities involve scanning electrochemical microscopy and surface chemistry, as well as their applications to biosensors and fundamental cell biology.

substances can undergo multiple oxidation-reduction cycles at both electrodes of the thin-layer cell. The ECSTM (Figure 2c) shares with SECM the possibility to position the local probe.

Corresponding to this analogy, the local probe in SECM is often called a "tip", although in most cases disk-shaped UMEs are used. The probe dimensions such as radius (r_T),[*] current (i_T), and electrode potential (E_T) are therefore indexed with "T", and the corresponding quantities for the sample with "S" (sample, specimen, substrate). The current originates from the quantum-mechanical tunneling effect in ECSTM,[21] that is, without electrochemical conversion, whereas the current between the sample and the UME in SECM is mediated only by dissolved substances that enter into (electro)chemical reactions at the UME and the sample. The UME can thus move at a separation distance that is much larger than the tunneling distance. Owing to the different interaction principles of ECSTM and SECM, the corresponding images provide complementary information. The lateral resolution of ECSTM is always superior to SECM because of the shorter range of the tunneling effect. Although this distinction appears to be clear, the interpretation of some experiments triggers intensive and interesting debates,[22–27] because the instrumental details of SECM become similar to those used in ECSTM with increasing lateral resolution. Categorization of the experiments exclusively on the basis of the equipment used appears to be ever less convincing.

2. Two-Dimensional Mapping of Reaction Rates

SECM imaging experiments can be carried out in generation-collection (GC) or in feedback (FB) mode. Extensive theoretical treatments are available that have been obtained by numerical solution of the diffusion equations. The detailed quantitative treatment of many SECM experiments is a major advantage of this technique. In this Review, the basic principles of both working modes are discussed, and the results of theoretical work are summarized. For more detailed discussion, the reader should consult the original papers or specialized reviews.[10,11,13,15]

2.1. Feedback Mode

2.1.1. Principle

For measurements in FB mode, one redox form of a quasi-reversible redox couple is added to the supporting electrolyte as a mediator. In the following discussion it is assumed that the reduced form R is added, although the same explanations hold for the addition of the oxidized form O of the mediator if the reaction directions are reversed. At the UME, a potential E_T is applied at which diffusion-controlled conversion of the mediator occurs according to Equation (2) and thus a steady-state faradaic current $i_{T,\infty}$ results according to Equation (1). The index "∞" indicates the quasi-infinite separation distance d of the UME and the sample surface (Figure 3a). If the UME approaches an insulating, inert surface, the surface hinders the diffusion of R towards the UME (Figure 3b) and the faradaic current i_T decreases. The term "negative feedback" has commonly been adopted to describe this phenomenon.[17]

$$R \rightarrow O + n\,e^- \qquad (2)$$

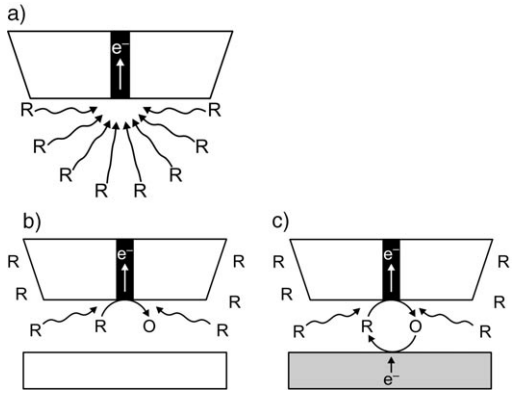

Figure 3. Principle of the feedback mode. a) Steady-state diffusion-limited current in the bulk solution; b) hindered diffusion when the UME approaches the sample (negative feedback); c) mediator regeneration by a heterogeneous reaction at the sample (positive feedback).

If, however, the UME moves towards a surface at which R can be regenerated by (electro)chemical conversion, a new reagent source becomes available for Equation (2) and $i_T(d)$ increases with respect to $i_T(d)$ at an inert sample (Figure 3c). The term "positive feedback" is predominantly used for this principle.[17] The mediator can be regenerated through three types of reaction: electrochemical conversion of the mediator at the sample as the reverse of Equation (2), an (enzyme-) catalyzed reaction with consumption of O and regeneration of R, or local oxidation of the sample material by O.

2.1.2. Importance of the UME Radius

Figure 4 shows the change of i_T with d. Such curves can be recorded with high accuracy by a slow approach of the UME towards the sample surface ("approach curve"). They show the normalized current $I_T = i_T/i_{T,\infty}$ as a function of the normalized distance $L = d/r_T$. The normalized curves [Eqs. (3) and (4); Section 2.1.4] are independent of the mediator concentration, the diffusion coefficients, and r_T. However, the achievable lateral resolution and the required absolute distance d for a given normalized current (corresponding to the contrast) are directly proportional to r_T. An improvement in the lateral resolution in FB mode depends directly on the application of smaller UMEs, which leads to considerable experimental problems in the vertical positioning of the UME if $r_T \leq 1$ μm. This problem will be discussed together with implementation of constant–distance experiments in Section 6.

[*] Following the usage in the field of microelectrodes, the UME radius is often abbreviated as a rather than r_T.

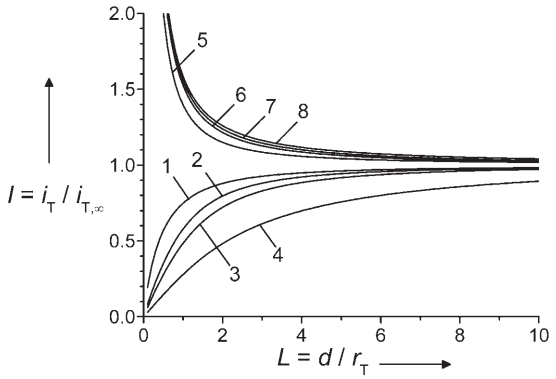

Figure 4. Calculated current–distance curves for hindered diffusion (curves 1–4) and diffusion-controlled regeneration of the mediator at the sample (curves 5–8) for *RG* values of 1.5 (curves 1 and 5), 5.1 (2 and 6), 10.2 (3 and 7) and 1002 (4 and 8). The curves were calculated according to approximations[34] obtained from digital simulations.

2.1.3. *Importance of the Insulating Sheath*

The current in Figure 3b can be considered as a background signal that originates from the conversion of R species that diffuse from the solution bulk to the UME. For a reaction occurring at the surface of the sample to be detected, it must cause a measurable additional flux of R towards the UME (Figure 3c). The smaller the normalized current $I_T = i_T/i_{T,\infty}$ is in the absence of any reaction at the sample, the easier it is to detect the additional contribution from the sample reaction. Because both i_T and $i_{T,\infty}$ are proportional to the bulk concentration of R, I_T depends only on L and the thickness of the insulating sheath that forms an open thin-layer cell with the sample surface. The geometry of microdisk electrodes can be characterized by the *RG* value, which describes the ratio between the radius r_{glass} of the insulating sheath and the radius r_T of the active electrode surface. To calculate $i_{T,\infty}$ according to Equation (1), the geometry-dependent factor g has to be modified (e.g. $g = 4.07$ for $RG = 10$, $g = 4.44$ for $RG = 2$, $g = 4.95$ for $RG = 1.2$).[28]

As illustrated in curves 1–4 of Figure 4, not only $i_{T,\infty}$ but the whole current–distance curve for hindered diffusion changes: The larger the *RG* value, the smaller I_T is at a given L. The normalized currents for the positive FB show only a minor dependence on *RG*.

Under the assumption of idealized geometries, on which many SECM simulations are based, an enhancement in sensitivity can be expected with increasing *RG* because the signal difference between positive FB and hindered diffusion is enlarged for any given d. In fact, the preparation of UMEs with defined size and shape of the active area and the insulating sheath is demanding. The active electrode area is often recessed after polishing or eccentrically located within the insulating sheath, or the electrode plane is tilted with respect to the sample surface. In the latter case, the insulating sheath may make mechanical contact with the sample even though the active electrode area is still a considerable distance from the sample surface. This phenomenon is more difficult to control with UMEs with large *RG* values or dimensions in the nanometer range.

Several approaches can be found in the literature, each of which have their merits for specific applications: 1) Perfectly shaped UMEs can be produced and applied to ideally smooth samples if the corresponding effort is made and the electrode size is relatively large. In those cases the simulations are directly applicable. UMEs with an *RG* value of 5–20 seem to represent a sensible compromise between manageability, sensitivity, and positionability. 2) For small deviations from the ideal shape and for samples with a small roughness, idealized simulations still provide a good approximation because the error is small relative to other experimental uncertainties. 3) With very small UMEs, one forgoes a quantitative description of the signals in favor of higher lateral resolution and a clearer qualitative result. Alternatively, attempts can be made to carry out simulations for individual electrodes of complex shapes.[29–31]

2.1.4. *Influence of Sample Topography and Size*

The UME current i_T has been obtained for a given r_T, probe geometry (defined by *RG* for a disk-shaped UME), and d for the limiting case of a quasi-infinitely large sample that is either insulating and inert, or causes a diffusion-controlled positive feedback by solving the diffusion equations with different numerical methods.[8,32–39] The simulation results for various values of d can be described by analytical approximations for both limiting cases. From the various, almost equivalent formulae,[40] only one shall be given herein. The approach of a UME with $RG = 10$ towards an inert, insulating sample is described well by Equation (3).[34]

$$I_T^{ins}(L) = \frac{i_T}{i_{T,\infty}} = \frac{1}{0.40472 + \frac{1.60185}{L} + 0.58819\exp(\frac{-2.37294}{L})} \quad (3)$$

The curves 1–4 in Figure 4 for other *RG* values are obtained by substitution of the numeric constants with suitable values.[34] Equation (4) gives the UME current at

$$I_T^{cond}(L) = \frac{i_T}{i_{T,\infty}} = 0.72627 + \frac{0.76651}{L} + 0.26015\exp\left(\frac{-1.41332}{L}\right) \quad (4)$$

the sample for the diffusion-controlled regeneration of the mediator, and hence the maximum possible signal at any given value of d, at a UME with $RG = 10$.[34]

Again, further sets of numerical constants are available to obtain curves for different *RG* values.[34] Figure 4 shows simulated current–distance curves for the two limiting cases and for UMEs with different *RG* values. If the *RG* value and the reactivity of the sample are known, such curves enable a vertical positioning of the UME. The strong dependence of the current–distance curves on the local reactivity of the sample (see Section 2.1.5.) prohibits the use of i_T as an input signal for an electronic feedback loop to keep d constant. Such an approach is routinely taken in STM and scanning force microscopy (SFM). Up to now, most SECM experiments have been performed by moving the UME in one plane (constant height mode). The interpretation of results from rough samples is almost impossible without additional information.[41] A detailed description of current-independent

distance-control mechanisms and the development of smaller probes is given in Section 6.

The curves in Figure 4 were derived for planar, quasi infinitely large samples of uniform reactivity. Indeed, a good agreement is found with experimental results if the radius of the investigated sample region is large enough ($r_S \geq r_T + 1.5\,d$).[42,43] If regions of uniform reactivity are smaller, i_T lies between the limiting cases shown in Figure 4.

2.1.5. *Influence of Heterogeneous Kinetics at the Sample Surface*

At constant d, the UME current i_T is a direct measure of the kinetics of mediator regeneration at the sample. The curves in Figure 4 represent only the limiting cases in which mediator regeneration either does not occur at all (curves 1–4) or proceeds at a diffusion-controlled rate (curves 5–8). Each finite reaction rate yields a unique approach curve that lies between the limiting cases. For reactions at the sample that follow a first-order rate law with respect to O, the normalized approach curves are independent on the total concentration of the mediator. These curves have been calculated[42] and verified experimentally.[44] An analytical approximation [Eq. (5)–(6)] is often used which is valid for $RG = 10$ and normalized distances $0.1 \leq L \leq 1.5$.[45]

$$I_T(L) = \frac{i_T}{i_{T,\infty}} = I_T^{ins}(L) + I_S^{kin}(L)\left(1 - \frac{I_T^{ins}(L)}{I_T^{cond}(L)}\right) \quad (5)$$

$$I_S^{kin}(L,k_{eff}) = \frac{0.78377}{L(1+\frac{1}{\kappa L})} + \frac{0.68 + 0.3315\exp(\frac{-1.0672}{L})}{1 + \frac{(11/\kappa L)+7.3}{110-40L}} \quad (6)$$

The expressions of Equations (3) and (4) can be used for I_T^{ins} and I_T^{cond}. The parameter $\kappa = k_{eff} r_T/D$ is a dimensionless rate constant. A first-order heterogeneous rate constant k_{eff} [$cm\,s^{-1}$] can be determined if the UME radius r_T and the diffusion coefficient D are known. Figure 5 shows a selection of curves for different reaction rates at the sample. This plot is of significant importance for many SECM applications. A two-dimensional image provides direct mapping of the local reaction rate at the sample if the working distance d is kept constant. Alternatively, one may position the UME above selected regions of the sample, record an approach curve, and extract a local reaction rate constant by fitting the experimental data to the models discussed above. Such data are often not accessible through other techniques. Examples are discussed in Section 3.

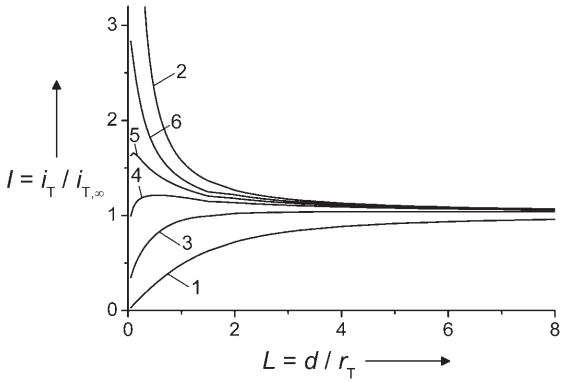

Figure 5. Calculated current–distance curves of a UME ($RG = 10$) for hindered diffusion (Eq. (3), curve 1), diffusion-controlled recycling of the mediator (Eq. (4), curve 2), and kinetically limited mediator recycling (Eqs. (5) and (6)) with $\kappa = k_{eff} r_T/D = 0.3$ (3), 1.0 (4), 1.8 (5), 3.6 (6).

The situation becomes more complicated if the conversion at the sample is an enzymatic reaction, which can often be described by the Michaelis–Menten formalism.[46] In such cases the reaction rate approaches a zero-order rate law with respect to the reagents at high mediator and substrate concentrations. The background signal (curves 1–4 in Figure 4) is, however, proportional to the bulk mediator concentration (Section 5.1.1).

2.2. Generation-Collection Mode

2.2.1. *Principle*

The generation-collection (GC) mode works in a solution that does not initially contain any substance that can be converted at the UME at a potential E_T. If an oxidizable or reducible substance is formed at the sample, this compound can be detected at the UME if it is located close to the active region (Figure 6a). Specifically, this mode is called sample-generation/tip-collection (SG/TC) mode. GC experiments can be performed with potentiometric microelectrodes (Figure 6b).[14,47–58] These electrodes have the advantage that they disturb the sample diffusion layers much less because they are passive sensors.[59–64] However, the positioning of such electrodes is difficult because the hindered diffusion according to Equation (3) cannot be used. Therefore, bifunctional electrodes as well as combined scanning probe techniques have been employed (Section 6).[58,65]

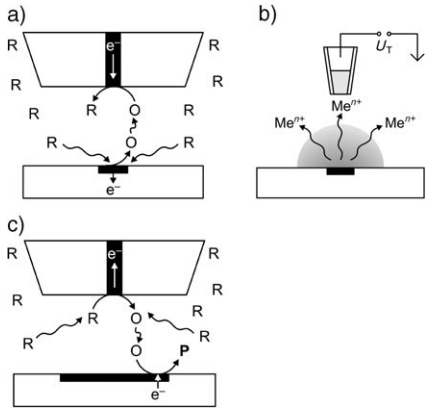

Figure 6. Principle of the generation-collection mode. a) SG/TC mode with an amperometric UME, b) SG/TC mode with a potentiometric microelectrode (e.g. ion-selective electrodes), c) TG/SC mode.

The possibility of using the UME as a local generator and the sample as a collector (TG/SC, tip-generation/sample-collection, Figure 6c) was demonstrated very early.[66] In the initial experiments, reagents were injected locally over a microstructured macroscopic electrode from a positionable capillary[67] or by means of an enzymatic reaction occurring in movable capillary filled with an enzyme-containing gel.[68]

More recently, important applications emerged from electrochemical "time-of-flight" experiments (Section 3), UME-induced microstructuring (Section 4), or the screening of oxygen-reduction catalysts (Section 5.4).

2.2.2. Quantification in the GC Mode

The conceptual simplicity of the GC mode with amperometric UMEs is contrasted by some difficulties in the quantitative interpretation of the results:[13]

- If the active regions of the sample are large, no steady-state situation is established, and the local concentrations depend not only on the position of the UME but also on the time that has passed since the onset of the reaction at the sample.
- The moving probe disturbs the macroscopic diffusion layer of the sample through convection, by hindering the diffusion of reagents to the sample region underneath the UME, and by overlap of the diffusion layers from the sample and the UME.
- An enhancement of the current according to the principle of positive feedback (Section 1.2) can reach significant values if $d < 3r_T$.

These circumstances have delayed a precise theoretical treatment that expands earlier approximate descriptions.[69] To minimize the quantitative problems, it is sensible to work with as small as possible UMEs (small r_T and small RG). In such cases, the disturbance of the sample diffusion layer is minimized and FB effects can also be neglected at small values of d. An illustrative example is the three-dimensional measurement of the diffusion layer of a UME with diameter of 40 μm as sample with another UME that had a diameter as small as 80 nm as the probe.[70] In this way, the quantification problems mentioned were avoided or minimized. The lateral resolution is always poorer in GC mode than in the corresponding FB experiments. Furthermore, it is difficult to detect small active regions in the vicinity of large active areas.[71]

The GC mode offers a much higher sensitivity than FB mode because the flux of reagents coming from the sample is measured essentially without a background signal.[72] This makes the GC mode particularly appropriate for the investigation of immobilized enzymes and cells. Moreover, it is also suitable in situations in which FB experiments are principally impossible.[73,74] Examples can be found in Sections 5.3–5.6.

3. Kinetic Investigations without Lateral Movement of the UME

A considerable part of the SECM literature describes exclusively the use of approach curves and avoids two-dimensional imaging experiments. Strictly speaking, such experiments do not represent microscopy. Nevertheless, these experiments have fundamental importance for methodical developments and many fields of applications, because the understanding of any scanning probe experiment requires knowledge of the underlying signal–distance relationship. Quantitative data can be extracted much more easily from approach curves than from 2D images. Ultimately, the problem of vertical positioning for an imaging experiment can be circumvented because i_T is recorded at all relevant distances. From the perspective of applications, such measurements are important because they enable new experiments concerning interfacial processes that are otherwise not accessible. For these reasons, some important principles are introduced herein mostly without further details.

3.1. Steady-State Measurements in Feedback Mode

The rates of heterogeneous reactions were studied mostly in FB mode by using Equations (3)–(6). The reaction at the sample, which is first order with respect to the mediator, can also be replaced by more complicated models. In those cases, approach curves are recorded at different mediator concentrations. For studying electrochemical reactions at the sample, different sample potentials E_S are often applied as well.

3.1.1. General Advantages

Relative to conventional electrochemical methods, kinetic studies in FB mode possess numerous advantages. Very high diffusive mass fluxes can be realized at small values of d under steady-state conditions, which moves the limits of diffusion control towards faster electrochemical kinetics. In contrast to experiments at rotating electrodes, it is not necessary to produce mechanically highly precise electrodes that can be electrically contacted during rotation. Technically demanding, extremely fast potential changes like in chronoamperometry or in fast-scan cyclic voltammetry are not required. Hence, correction for double-layer charging currents is not necessary. Because the currents at the UME are in the nanoampere range, the ohmic drop resulting from an uncompensated resistance $U_{drop} = i_T R_{sol}$ (R_{sol}: uncompensated solution resistance) is normally smaller than 1 mV. The favorable mass transport conditions and the absence of experimental artifacts enabled the determination of a lower limit of the heterogeneous standard rate constants of very fast redox couples.[75]

In contrast to cyclic voltammetry, large potential excursions can be avoided. This is important, for example, for kinetic investigations of electrodes covered by a self-assembled monolayer (SAM) or a potential-dependent passive layer. Depending on the SAM system, a potential change may induce phase transitions or even desorption at the substrate, which may influence the redox kinetics.

3.1.2. Experiments without Externally Applied Sample Potential

The most important advantage of the method lies in the possibility to investigate mass and charge transfer processes at interfaces that cannot be connected easily to an external potential source (Figure 7).

The simplest examples are prototypes of chip structures with microelectrodes and uncovered connecting pads. A cyclic voltammogram would essentially reflect the reaction at

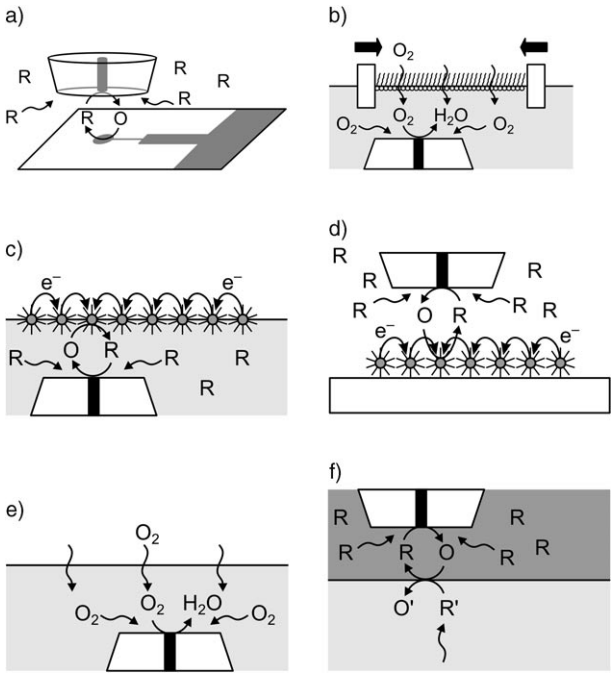

Figure 7. Investigation of interfaces that are difficult to connect to an external potential source. a) Microstructure on a chip with noncovered connecting pad; b) polymer film or lipid film at the gas–liquid interface; c) monolayer-protected metal nanoparticles at the gas–liquid interface; d) monolayer-protected metal nanoparticles on an insulating support; e) gas–liquid interface with mass transport from the gas phase; f) arrangement for the investigation of liquid–liquid interfaces, possibly with a thin film at the phase boundary.

the surface of the large connecting pads (Figure 7a). Further examples include thin films that have been prepared at gas–liquid interfaces (Figure 7b-c,e) or liquid–liquid interfaces (Figure 7f). In these cases, the application of an external potential with a potentiostat is impossible or very complicated.

However, the potential can be controlled by the mediator solution: The bulk solution contains essentially only one redox form (in this case R). Therefore, an electronically conductive immersed body assumes an electrochemical potential that is negative with respect to the formal potential $E^{\circ\prime}$ of the mediator according to the Nernst equation. In the space between the UME and the sample, the concentration ratio [O]/[R] is shifted by electrolysis at the UME in favor of O. A concentration cell is thus formed (Figure 8), which provides the driving force for lateral charge transport and the interfacial reactions at the sample. O will be reduced to R at the sample beneath the UME. To the same extent, R will be converted to O far away from the UME. As the total conversion during the experiment is negligible with respect to the total mediator concentration in the electrochemical cell, this mechanism can be sustained over a sufficiently long period. The sole prerequisite is that the investigated sample region is significantly larger than the UME ($r_S \geq r_T + 1.5\,d$).[42] If this condition is not met and the sample is not connected externally, even conducting materials behave in an FB experiment like an inert and insulating sample following Equation (3).

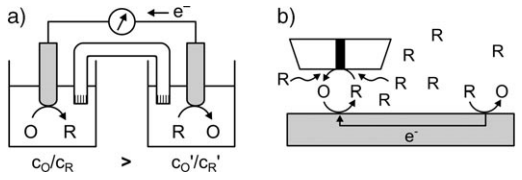

Figure 8. a) Conventional electrochemical concentration cell; b) formation of a concentration cell in SECM FB experiments.

3.1.3. Gas–Liquid Interfaces

Processes at gas–liquid interfaces can be investigated if the UME is mounted face-up in an electrolyte solution and approaches the gas–liquid interface from below (submarine electrode).[15,76] The interface blocks the diffusion of the mediator in exactly the same way as a solid–liquid interface in the conventional setup. If, however, the substance converted at the UME (e.g. O_2) is subject to a distribution equilibrium between gas and liquid phases, the gas phase will partially replenish the substance in the exhausted solution volume between the UME and the interface. Consequently, i_T will be larger than expected from Equation (3). Thus, the kinetics of the phase transfer for O_2 could be determined. If the experiment is carried out in a Langmuir trough, the influence of an organized monolayer at the interface on the phase-transfer kinetics can be studied.[77–79] Furthermore, such systems open up the unique possibility to investigate lateral transport processes, such as those of protons along monolayers of amphiphilic molecules.[80,81]

A Langmuir trough was also used to prepare extremely thin conducting polymer layers[82–85] and monolayer-protected metal clusters at the gas–liquid interface[86–90] or on an insulating substrate.[91] The extent of mediator regeneration at the thin film is determined essentially by the kinetics of the charge transfer between the mediator and the polymer/cluster and the charge-transfer processes within the thin film and can be estimated by comparison of experimental data with digital simulations.

3.1.4. Interfaces between Immiscible Electrolyte Solutions

Interfaces between two immiscible electrolyte solutions (ITIES) have received attention in basic electrochemistry for a number of years. Their fundamental importance rests in the possibility to observe charge-transfer reactions between molecules of very different polarity. The practical significance lies in the pharmacokinetic characterization of charged substances and basic research on hydrometallurgical extraction methods.[92] The interfaces allow very diverse charge-transfer processes.[93–95] Besides the transfer of ions,[96–98] electrons can be exchanged between molecules dissolved in the polar and nonpolar phases. The driving force for this reaction is determined by the difference in the formal potentials as well as by external polarization of the interface.[99–103]

Because several charge-transfer processes occur simultaneously in most cases (e.g. e^- and X^- in Figure 9a), the

interpretation of macroscopic experiments concerning ITIES is often complicated. SECM opened up important new possibilities (Figure 9).[15,33,76,104–110] Because only a small part of the interface is disturbed by the UME or by the pipette, other charge-compensating processes can occur at the macroscopic interface without limiting the overall rate. Further variations result from the change of concentrations and formal potentials of the involved redox systems and the introduction of thin films at the liquid–liquid interface.[100,111–114] The possibilities are even more diverse if the ITIES is prepared and stabilized at the orifice of a pipette.[93,99,115]

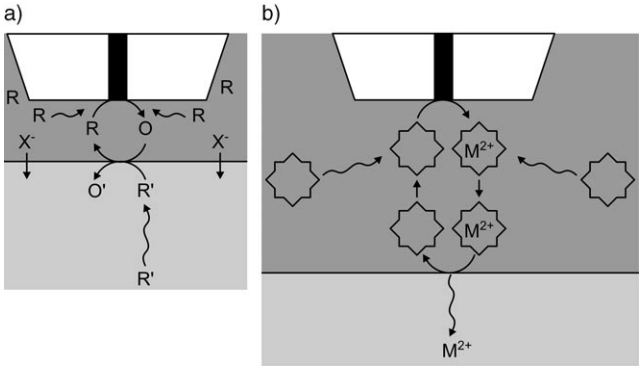

Figure 9. Arrangement for the investigation of liquid–liquid interfaces. a) Electron transfer between two different redox systems; b) a ligand in the organic phase assumes the function of the mediator for the transfer of a cation.

3.2. Electrochemical Time-of-Flight Experiments

The TG/SC mode is applicable for realizing electrochemical "time-of-flight" experiments. (Figure 10).[116] A reactive species (O) is generated at the UME and diffuses towards the sample, where it is converted back into R. If the sample is much larger than the UME, O will reach the sample quantitatively in uncomplicated cases and the sample current i_S equals i_T (collection efficiency $\theta = i_S/i_T \approx 1$).

If, however, O takes part in a subsequent homogeneous reaction during the diffusion to the sample, the amount of O that reaches the sample decreases and θ falls below one. The timescale for the homogeneous reaction in an experiment can be adjusted by varying d. Rate constants for the homogeneous reaction can be determined from the measured $\theta = f(L)$ by using digital simulations for mechanistically different follow-up reactions.[117–119] The measurements are reminiscent of rotating ring–disk electrode experiments, but they are more reliable because of the higher collection efficiency in the absence of a homogeneous reaction.[118]

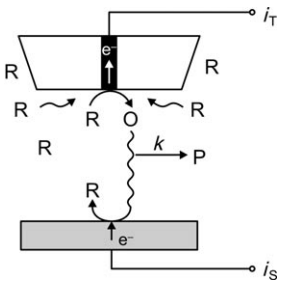

Figure 10. Arrangement of electrochemical time-of-flight experiments for the investigation of electron-transfer reactions and homogeneous follow-up reactions.

Among the investigated compounds and reactions are the reduction of metal–organic compounds with subsequent homogeneous decomposition,[120] intermediates of the electrochemical BH_4^- oxidation,[121] and the reductive dimerization of dimethyl fumarate and fumaronitrile.[118] Furthermore, the fate of electrochemically generated radicals has been investigated (acrylonitrile radical anion,[122] NAD•,[6] $O_2^{\bullet-}$,[123] $RNO_2^{\bullet-}$[124]).

3.3. Transient Feedback Measurements

Although the steady-state character of FB experiments described so far is considered as one of the main advantages of the technique, it has recently become obvious that chronoamperometric measurements [$i_T = f(d,t)$] provide additional information. This is particularly evident when the sample changes during the experiment, for example, when only a limited number of redox equivalents is available for conversion at an insulating sample surface. One possible approach is a double potential pulse experiment (Figure 11).[76] In a potential jump at the UME, a small and defined amount of reagents (e.g. metal ions) is generated (Figure 11 a) and spread by diffusion. Subsequently, this reagent is collected at the UME in a reverse potential jump (Figure 11 c).

The collected amount of reagents depends on the geometry (calibration is necessary by a control experiment over an inert surface; Figure 11 e, curve 1), but can be decreased by consumption in a heterogeneous reaction or through a phase-transfer reaction at the sample (Figure 11 b). The decrease in the collection efficiency is controlled by the kinetics of the interfacial reaction and the capacity of the interface (e.g. the number of binding sites, Figure 11 d). The reaction at the sample can be phase transfer at liquid–liquid interfaces[96] or gas–liquid interfaces with a Langmuir layer[78,112] or an adsorption reaction at a Langmuir layer[125] or a mineral surface.[126]

3.4. Local Disturbance of Heterogeneous Equilibria

The local disturbance of a heterogeneous equilibrium has been applied mainly to induce desorption or dissolution reactions, as well as for kinetic studies of these processes. The UME is positioned, for example, above an ionic crystal that is equilibrated with a saturated solution of crystal constituents. An electrochemical conversion of the dissolved equilibrium species causes a local undersaturation of the solution. In response, local dissolution of the sample takes place, the

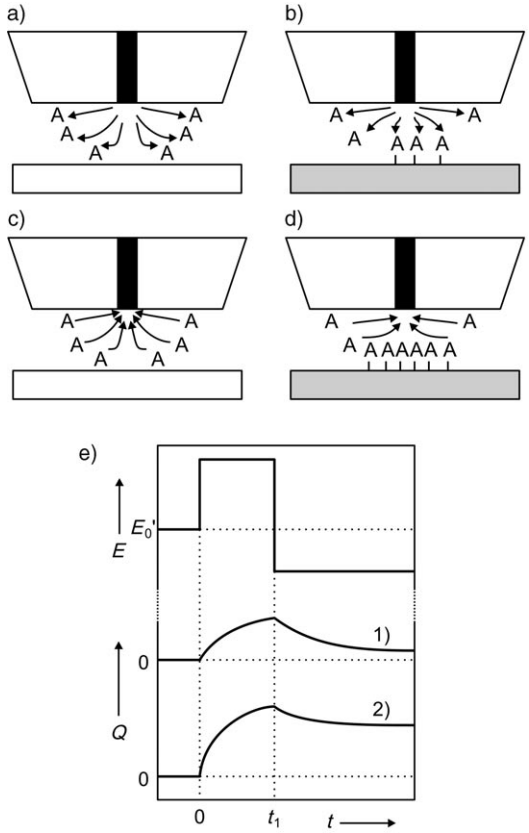

Figure 11. Principle of double potential step experiments in an SECM arrangement. a) Reagent generation in the forward step above an inert sample (spreading by diffusion); b) reagent generation above a reactive sample (diffusion and reaction with the sample/phase transfer/adsorption); c) reverse step collection of unconsumed reagent above an inert sample (collection efficiency determined by geometry); d) reverse step above a reactive sample (collection efficiency determined by the geometry and conversion at the interface); e) simplified and exaggerated depiction of the potential steps and the current responses above an inert sample (1) and a reactive sample (2).

kinetics of which can be followed electrochemically (see Figure 12c in Section 4.1).[127–133] The method can be carried out elegantly with conducting SFM cantilevers that allow subsequent characterization of the removed material.[134–136] Conceptually similar, desorption equilibria have been studied at solid–liquid interfaces.[137]

4. SECM as a Tool for Microstructuring

The idea to use the UME of an SECM for local surface modification has been documented since the beginning of the SECM development.[138–143] The current development status has been documented in several review articles.[16,144–147] The SECM methodology allows chemically diverse and defined surface modifications that are often not accessible by alternative methods. The advantages become particularly evident if the SECM is used both for the generation of the structures and for their functional characterization. The quantitative treatment of the SECM experiments eases the mechanistic understanding of the procedures, which helps to transfer the chemical principle to other technological variations of the same chemical reactions. Surface modification by SECM, as a sequential procedure, has a limited processing speed. The use of microelectrodes with complicated shapes can increase the processing speed. However, parallel microstructuring techniques exhibit fundamental advantages for production processes. Despite the disadvantages mentioned, SECM surface modification procedures are very valuable in research and prototype development.

4.1. Local Generation of Reagents

To achieve local surface modification with SECM, four basic configurations can be applied (Figure 12).

Conceptually analogous to the FB mode, the UME can be used to generate an etchant that leads to local oxidative dissolution or chemical oxidation of the substrate (Figure 12a). In this way, the reagent is often regenerated for

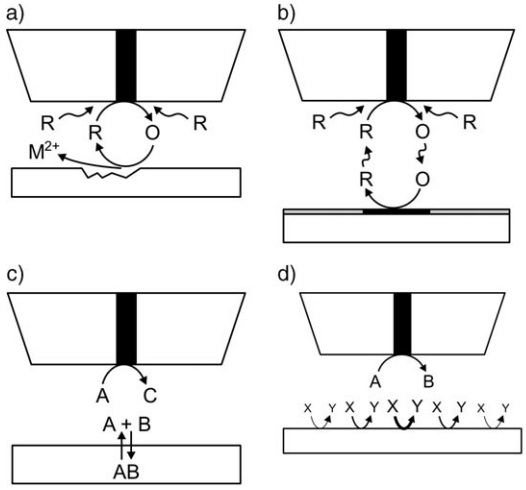

Figure 12. Possibilities for local surface modifications. a) Local generation of an etchant for sample dissolution; b) local generation of a reagent for the local conversion of a thin film on the electrode surface; c) local disturbance of an established heterogeneous equilibrium, and d) use of the UME as a microscopic counter electrode.

the reaction at the UME so that electrochemical feedback is produced and the progress of the surface modification can be monitored by recording i_T. Etching was performed in this manner on Cu,[148] GaAs,[141,143] and Si.[149,150] Charge injection followed by a local color change was performed at tungsten oxide.[151] Locally generated oxidants have also been applied to convert organic thin films at substrate surfaces. Matsue and co-workers deactivated enzyme films with locally generated Br_2 or HBrO.[152] Shiku et al. generated hydroxyl radicals by reduction of Fe^{3+} in an H_2O_2-containing solution and used it for the modification of alkyl silane layers on glass.[153] By subsequent adsorption or covalent attachment, micropatterned protein layers were formed. Protein adsorption and cell adhesion can be locally controlled by using different substrates. Kaji et al. discovered that a bromide oxidation pulse at a UME in physiological buffer solutions can

eliminate the protein-resistent and cytophobic properties of a physisorbed albumin layer.[154–156] This phenomenon was used to "write" lines of attached cells and to introduce multiple cell populations onto surfaces. More recent developments involved a template structure consisting of a cytophobic polymer and fibronectin.[157] The fibronectin layers were activated microelectrochemically for cell adhesion. The limits of the activated areas were defined by the template pattern. Zhao et al. later showed that a bromide oxidation pulse can also lift the cytophobic properties of oligo(ethylenglycol)-terminated SAMs, which are very popular cell-rejecting monolayers in connection with SAM-based micropatterning procedures.[158]

Microelectrochemically generated organic radical anions (e.g. phthalonitile) can graphitize (reduce) the surface of fluoropolymers.[159–163] The resulting surfaces show locally varying wetting behavior[162] and can be subsequently metallized[163] or modified by another oligomer after an oxidation step.[160]

Local material deposition could be carried out by applying a precursor as a thin film to a substrate and converting it by means of a microelectrochemically generated oxidant or reductant into the desired microstructure (Figure 12b). For example, polyvinylpyridine films were loaded with $PdCl_4^{2-}$ and $AuCl_4^-$ and converted by locally generated $[Ru(NH_3)_6]^{2+}$ into Pd and Au microstructures.[142] Electrochemically formed hydroquinone can be used to locally reduce an evaporated AgCl film to elemental Ag.[164] After dissolution of the AgCl, a line of silver remains on the insulating substrate.[165] Polymer microstructures can be formed if a monomer film at the substrate that is insoluble in the working solution is polymerized by an oxidant generated at the UME.[165–167] Poly[2,5-bis(1-ethylpyrrol-2-yl)thiophene] and Poly(4,4′-dimethoxy-2,2′-bithiophene) were deposited in such a way. The opposite approach has also been described: A UME-induced local pH shift activated the immobilized oxidant film (MnO_2), thus leading to local polymerization of the dissolved monomer (thiophene).[168] Polyaniline has been deposited onto different substrates by using a UME-induced pH shift in the interelectrode space, which initiated the electropolymerization in the vicinity of the UME, whereas it did not occur outside this region.[169]

Shohat and Mandler used a local pH increase for the irreversible deposition of $Ni(OH)_2$.[170] In contrast to the methods mentioned above, this proton-consuming reaction proceeded at the substrate surface but not at the UME. Methyl viologen is reduced at a Hg UME to the methyl viologen radical anion, which is catalytically oxidized by protons at a Pt substrate thus producing a local pH increase.

The SECM probe can be used in various ways to locally inject metal ions into the solution that are reduced after diffusion to the substrate. Gold UMEs can be dissolved in the presence of complexing agents. Gold nanoparticles, arranged in micropatterns, can be deposited on conducting and semiconducting substrates by reduction of the aureates generated at the UME.[171,172] The released complexing agents close the electrochemical feedback and become the limiting factor of the overall reaction. Schindler and co-workers formed individual nanoclusters from cobalt by galvanically depositing cobalt on an Au tip mounted in an ECSTM.[173–176] Cobalt ions were then released from the tip by a short anodic pulse, thus leading to a local increase of the Co^{2+} concentration and subsequent deposition onto a conductive sample. The selection of the sample potential is crucial for the experiment. It is selected in such a way that it is close to but not below the Nernst potential in the Co^{2+} solution. A small increase of the Co^{2+} concentration immediately causes the local onset of a galvanic cobalt deposition. Larger cobalt microstructures are accessible by dissolution of Co UMEs.[177]

Liquid–liquid interfaces prepared at the orifice of micropipettes can be used for the potential-controlled transfer of metal ions to generate discontinuous metal structures.[178,179] Sauter and Wittstock deposited catalytically active metal hexacyanoferrates by dissolution of Co and Ni UMEs and precipitation with $[Fe(CN)_6]^{4-}$, which was formed electrochemically at the substrate.[180,181]

4.2. Coupling of Heterogeneous and Homogeneous Reactions

The expansion of diffusion layers limits the lateral resolution of SECM both for local surface modifications and for imaging experiments. Several setups are able to limit the extension of the diffusion layers by utilizing homogeneous reactions in the interelectrode space that limit the lifetime (and hence the spreading) of the species formed at the interface. Prerequisites are that the homogeneous reactions are sufficiently fast, and that the reaction system be chosen in such a way that the reagents of the homogeneous reaction do not enter into an electrochemical reaction at the UME. As early as 1992, Engstrom et al. used the special redox chemistry of the neurotransmitter epinephrine (E).[182] After oxidation at the sample, the initially formed quinone (EQ) reacts homogeneously to adenochrome (A), which can be reduced at more negative potentials than EQ. The UME is operated in such a way that it can reduce EQ but not A in the GC mode. Wittstock and Schuhmann used the enzyme catalase for the catalytic disproportionation of H_2O_2 to limit the lifetime of the H_2O_2 formed at the sample by immobilized glucose oxidase.[73] Besides the importance for enhancing the image quality, such experiments may serve in the identification of products in complex interfacial processes (e.g. corrosion reactions).

Heinze and co-workers developed the concept of the "chemical lens" for FB experiments.[164] A scavenger added to the solution bulk reacts homogeneously with the compound formed at the UME, thereby limiting the expansion of the diffusion layer around the UME. The area of the substrate that is modified becomes independent of the reaction kinetics at the substrate. Suitable reaction systems were developed for local metal depositions,[165,183,184] polymer deposition,[145] and local etching.[185] The local deposition of Ag is taken an illustrative example (Figure 13).

The solution contains NO_2^- and the complex $[Ag(NH_3)_2]^+$. The substrate is kept at a potential that is sufficient for the reduction of $[Ag(H_2O)_6]^+$, but not for the reduction of $[Ag(NH_3)_2]^+$. The electrochemical oxidation of nitrite according to Equation (7) leads to a decrease in pH and to local

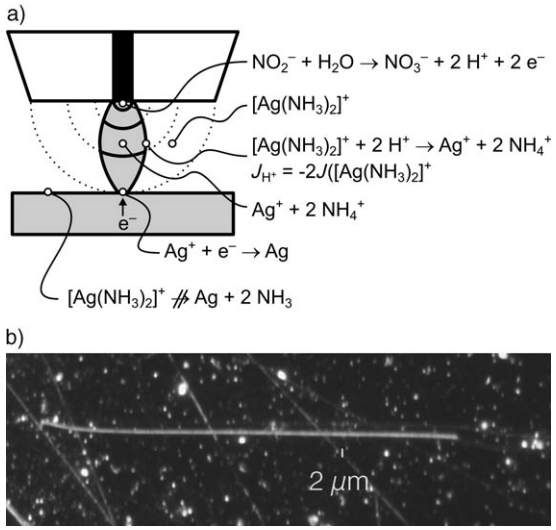

Figure 13. Chemical lens in FB experiments. a) Reaction scheme; b) deposition of a 1-μm-wide line of silver onto gold. Reproduction of (b) from reference [184] with permission. Copyright 2005, The Royal Society of Chemistry.

formation of the aqua complex according to Equation (8). The silver aqua complex is used for galvanic deposition at the substrate (Figure 13).

$$NO_2^- + H_2O \rightarrow NO_3^- + 2\,H^+ + 2\,e^- \quad (7)$$

$$[Ag(NH_3)_2]^+ + 2\,H^+ + 6\,H_2O \rightarrow [Ag(H_2O)_6]^+ + 2\,NH_4^+ \quad (8)$$

When the solution contains an excess of NH_3, the pH shift is observed only in the immediate vicinity of the electrode because NH_3 from the bulk solution reacts with the generated H^+. In case of a fast homogeneous reaction, a thin reaction zone is formed where the flux of H^+ away from the UME and the flux of NH_3 from the solution bulk towards the UME have the same magnitude. Within this zone, $[Ag(H_2O)_6]^+$ is the dominating silver species, whereas $[Ag(NH_3)_2]^+$ dominates outside this region. Deposition occurs only if the substrate surface is inside the reaction zone. The modified area at the substrate can be smaller than the size of the UME.

4.3. Direct Mode

In direct mode, the substrate acts as a counter electrode for the UME. A current at the UME causes an equally large but oppositely directed current i_S at the substrate electrode. If i_S can be confined to a small area around the UME, i_S can be used for substrate modifications by local dissolution or local deposition (Figure 12c). In contrast to FB mode, the reactions at the UME and the substrate do not necessarily need to be oxidations and reductions of the same redox couple.

The confinement of the reaction can be achieved by various methods. An Ag electrode covered with a thin nafion film was used as a substrate in early experiments.[139,186] The contact area between a metal tip penetrating into the film was used as the active electrode area. The small separation between the tip and the substrate resulted in an inhomogeneous field distribution. Silver ions were galvanically reduced at the tip. During the horizontal translation, a line of Ag is formed embedded in nafion. The counter reaction is the dissolution of Ag at the substrate–nafion interface. This mechanism was also used in a slightly modified arrangement for high-resolution etching[186] and for the deposition of polyaniline in nafion.[187] Because of the considerable restrictions in the choice of reaction systems, these experiments were not continued.

However, the confinement can also be achieved by pulse experiments in combination with electropolymerization.[188] Besides the oxidation of the monomer, the deposition of electrically conductive polymers requires homogeneous follow-up reactions until an insoluble oligomer deposits on the surface. When working in a potentiostatic mode, the interelectrode space is depleted of monomers and deposition does not occur. Schuhmann and co-workers introduced suitable pulse sequences, in which the monomers are resupplied to the interelectrode space after an initial oxidation pulse.[188,189] In this way, sufficiently high monomer concentrations for deposition are achieved periodically in the interelectrode space. Starting from a conductive substrate, the deposition can also be carried out on insulating substrates.[190] Three-dimensional polymer structures were formed by retracting the UME during electropolymerization.[191] The use of functionalized monomers opens up the prospect for application in biosensors and biochips (Section 5.7.1).[192]

El Giar et al. generated Cu needles with a length of 2000 μm and a diameter of 25 μm by galvanic Cu deposition onto a Cu substrate in direct mode with a retracting UME as counter electrode (Figure 14).[193]

Another confinement mechanism was developed for the local desorption of self-assembled monolayers (SAM).[194–196] The UME is positioned in a distance $d \approx r_T$ above an SAM-covered Au substrate electrode. An AC voltage (2–10 kHz, ± 1 V) is applied between the substrate and the UME. At negative potentials, alkane thiolates desorb, whereas they oxidatively decompose at positive potentials.[197] The desorption commences directly beneath the UME because of the inhomogeneous field distribution, whereby the electrochemical double-layer capacitance of the substrate is increased locally. Because the UME can only deliver a limited current, the polarization of the substrate collapses once the desorbed area has reached approximately the size of the UME. The desorbed regions can be generated in close proximity to each other without mutual interference.[196] This technique was applied for the modification of monolayers; in particular, the possibility was used to modify the cleared gold surface with another, ω-functionalized thiol or disulfide that constitutes an anchor group for the attachment of biochemical functional units.[198] If the second thiol/disulfide is present in the desorption solution, desorption and refilling of the Au surface can be carried out in one step.[196]

Oxide layers can also be formed if a sample is oxidized in the presence of a microscopic counter electrode.[199] One variation of nanolithography with conductive SFM tips is based on a similar principle.[200] One has to keep in mind that

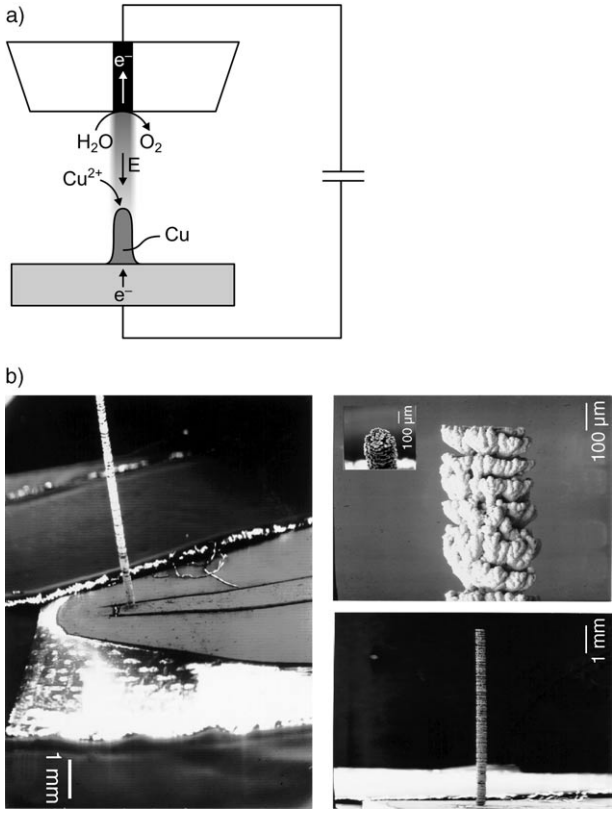

Figure 14. Copper needles generated in direct mode. a) Overview, b) antenna on a cantilever. Reproduction of (b) from reference [193] with permission. Copyright 2000, The Electrochemical Society.

local mechanical interactions might be important along with the local electrochemistry.

Further surface modifications that are observed or intentionally created in STM or SFM experiments will surely be based on the direct mode. Because it can be difficult to separate the various possible near-field interactions (field-induced, local mechanical interaction, local electrochemistry) for each individual case, we will refrain from a more detailed discussion herein.

5. Application Areas and Specific Requirements

This section covers some applied research in which the use of SECM can be foreseen even outside specialized electrochemical laboratories. The instrumentation cannot be considered a real barrier for more applied research because the equipment is available from various commercial suppliers or through cooperations with research groups established in the field.

5.1. Applications in Corrosion Research

The SECM technique can be regarded as an ideal new tool for the investigation of local corrosion phenomena. It can image passivated and active regions of surfaces and also initiate pitting corrosion by local generation of aggressive ions such as Cl^- and Br^-. The concentrations of various relevant species such as Fe^{2+}, Fe^{3+}, O_2, and H_2 can be measured above active regions. Because of the higher lateral resolution and the larger variability of experimental approaches, SECM will contribute to corrosion studies beside or instead of other electrochemical methods with spatial resolution, for example SRET (scanning reference electrode technique).[201,202]

5.1.1. Identification of Precursor Regions for Pitting Corrosion

For most metallic materials, a thin oxidic passive layer prevents their further oxidative dissolution. The local damage of such passive layers leads to active regions in which rapid dissolution of the metal (pitting) proceeds under extreme reaction conditions and pH values. The initiation of the local breakdown of passive layers is not yet fully understood. SECM investigations on precursor regions for pitting corrosion have been carried out on steel,[203–207] Ti,[208–212] Ta,[213,214] Ni,[215] and Al.[216,217] A metal sample is polarized in the passive potential region in such a way that the conversion of a dissolved compound (Br^-, I^-, $[Ru(NH_3)_6]^{3+}$, nitrobenzene, etc.) proceeds at selected regions of the passive layer. The reaction products are detected amperometrically at the UME in SG/TC mode. In the case of Ti/TiO_2, regions in which such electron-transfer reactions occurred in the passive state were the preferred locations for the initiation of pitting corrosion after switching of the polarization to the region of active corrosion.[208,209]

One advantage of the SECM methodology lies in its destruction-free character, which allows the identification of precursor sites in the passive state. From the theory of mass transport through individual pores, it was estimated that 69% of the current at a macroscopic Ti/TiO_2 electrode with surface area of 0.79 cm^2 flowed through 11 precursor sites, which comprised just 0.1% of the total Ti/TiO_2 area.[211] These precursor sites can be defined by inclusions.[212] For inclusion-free samples, detailed structural information about the precursor sites is not currently available. Interesting differences can be observed between different metals. Precursor sites on Ti/TiO_2 do not exhibit chemical selectivity for the conversion of $[Fe(CN)_6]^{4-}$ and Br^- whereas precursor sites on Ta/Ta_2O_5 show a clearly different reactivity for I^- and $[Ru(NH_3)_6]^{3+}$ (Figure 15).[213]

Precursor regions on stainless steel are presumably associated with sulfur-rich inclusions (MnS). Williams et al. developed a methodology to follow the progression of pitting in the vicinity of such inclusions by combining complementary microscopic techniques, including SECM.[218] Sulfidic inclusions on Ni(200) were investigated with a similar approach.[215] Sulfur-containing compounds (HS^-, $S_2O_3^{2-}$) that are released from such inclusions can be chemically detected selectively by reaction with I_3^-. Spatially resolved detection can be achieved by forming I_3^- at the UME.[206,219] Lister and Pinhero expanded the detection principle to the measurement of the local electric-field strength.[206] Later, a microelectrode array was used to obtain microscopic images with an improved temporal resolution in comparison with conventional SECM by avoiding the time-consuming scan-

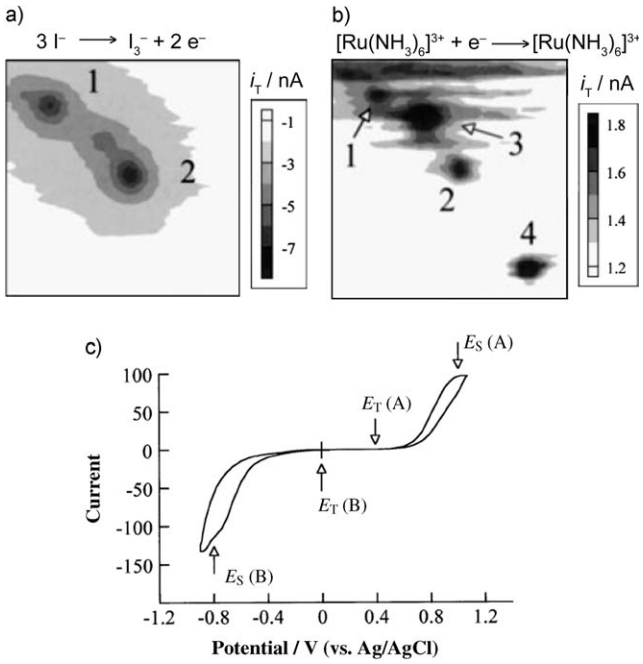

Figure 15. Precursor sites for pitting corrosion on a 200×200-μm² Ta/Ta_2O_5 sample imaged in SG/TC mode in a solution containing both $[Ru(NH_3)_6]^{3+}$ (2.5 mM) and I^- (10 mM). a) Oxidation of I^- occurs in regions 1 and 2 only ($E_S = 1.0$ V, $E_T = 0.0$ V); b) Reduction of $[Ru(NH_3)_6]^{3+}$ occurs in regions 1–4 ($E_S = -0.8$ V, $E_T = +0.4$ V). c) The cyclic voltammogram of the macroscopic Ta/Ta_2O_5 sample shows the sum of the reactions at all precursor sites and does not reveal the chemical selectivity of individual regions ($\nu = 20$ mV s^{-1}). Reprinted with permission in modified form from reference [213]. Copyright 1999, American Chemical Society.

ning with an individual UME. However, the lateral resolution was much lower than in typical SECM images.[220]

5.1.2. *Local Initiation of Pitting Corrosion*

Pitting corrosion can be initiated by high Cl^- concentrations. SECM allows such high Cl^- concentrations to be generated locally, thus inducing the formation of individual active pits.[221,222] The generation of Cl^- was achieved through electrochemical reduction of CCl_3COOH at an amalgamated Au UME. The current at the steel substrate showed the typical behavior for the formation, growth, and repassivation of an isolated corrosion pit in response to the high local Cl^- concentration.

5.1.3. *Following Active Corrosion and Passivation*

A UME can also be used to monitor the active corrosion of a range of materials. The locally released species can be identified by cyclic voltammetry at the UME or by use of ion-selective potentiometric microelectrodes. Investigated materials besides steel[64,223,224] include dental fillings made from amalgams and metallic implants,[225,226] titanium,[227] alloys,[63,228–233] organic coatings on metallic substrates,[234–236] potentiometric sensors from AgI in cyanide solutions,[237] silicon in etching baths,[238] unprotected and carbon-coated ZnSe wave guides,[239] and amperometric biosensors for NADH-dependent dehydrogenases consisting of a composite that served as a reservoir for the controlled release of a redox mediator.[240] SECM is also a powerful tool for following simulated corrosion during the fabrication of integrated circuits.[241]

The formation of locally different passive layers was studied on polycrystalline Ti/TiO_2 electrodes in the FB mode.[227] The regions showing different kinetics with respect to $[Fe(CN)_6]^{3-}$ reduction agreed with the different crystallites that were accessible by optical microscopy.[242]

Impedance measurements at the UME may further expand the possibilities for elucidation of local corrosion phenomena.[229,234,243–245] They were applied to visualize defects in organic coatings[234] and passive layers,[229] although the origin of the contrast is not always clear and a number of factors seem to be involved.[244]

5.2. *Analysis in Surface Technology*

SECM offers a complementary microscopic technique for the characterization of technological surfaces when the surface functionality depends on the progression or inhibition of an interfacial chemical reaction. Topographic images, which can also be recorded, are more easily obtained with better spatial resolution, for example, by scanning force microscopy.

5.2.1. *Investigation of Electrode Materials*

Differently structured electrodes constitute an important research area. The redox kinetics at electrode materials applied as pastes or sprays have been characterized. These materials have been tested because of their technological advantages for various fields of application.[41,246] Because the material consists of conducting particles and an insulating binder and filler, local characterization of the electrochemical behavior is necessary. The distribution of conducting and insulating regions can be obtained very easily by SECM for microstructured transducers used in electrochemical analysis.[245,247–254] This holds also for electrochemically active regions that are located in pores and that are therefore not accessible by other techniques such as SFM. The characterization of the electron-transfer kinetics after different processing steps that may lead to an inhibition by adsorption of process chemicals or to an activation by thermal treatment is also possible.[41] The two phases of a semiconducting copper tetracyanoquinone dimethane were investigated by SECM.[255] Likewise, one of the semiconducting phases was also generated by SECM.[256] Shen et al. investigated the kinetics of dye regeneration in dye-sensitized ZnO electrodes that were developed for electrochemical solar cells.[257]

5.2.2. *Investigation of Self-Assembled Monolayers*

The local inhibition of electron transfer is also the basis for imaging of patterned SAMs on gold by SECM.[43,194,195,258]

A defect-free monolayer passivates the Au substrate so strongly that it behaves like an insulator in SECM experiments. The SECM signal responds very sensitively to defects in the monolayer, because no passivation occurs at the defects and high i_T values result. A good contrast between SAM-covered and bare Au surfaces proves the low defect density on the SAM-covered areas. In contrast to cyclic voltammetry, which is often used to characterize the passivating behavior, the application of extreme potentials (at which the SAM may be modified) can be avoided in SECM investigations of SAMs.[259] By sequential application of different potentials to the sample, potential-dependent properties can be studied. The formation of the SAM was followed by approach curves over time. The evaluation was based on a model of a partially covered electrode in which the uncovered areas are smaller than the UME.[43] Different contributions to the electron transfer across SAMs were determined by Liu et al. by investigating the system under different reaction conditions.[260] SECM was suitable for differentiating the properties of terminally functionalized SAMs that are different in chain length, protonation state, or complexation state.[261,262] The change of the passivating properties of a DNA-containing SAM after binding of divalent cations was also investigated.[263] The approach of Abbou et al. is also notable.[264] They labeled one end of a polymer chain with a ferrocene unit and grafted the other end to a surface. The layers could be contacted in solution by using an electrically conducting cantilever, and SECM approach curves could be recorded that reflect the flexibility of the polymer chains of the monolayers that were only a few nanometers thick.

Particular advantages result from the possibility to pattern SAMs in solution by SECM (Sections 4.1 and 4.3) and to characterize the resulting structures by using the same setup.

5.2.3. Investigation of Polymer Coatings

SECM complements other established procedures for the investigation of polymer coatings on conductive substrates. This investigation is necessary because charge transport across polymer layers may be based on very different mechanisms, whose detailed analysis repeatedly causes difficulties because several mechanisms may be in effect simultaneously. Important mechanisms are schematically shown in Figure 16.

An inert, insulating and nonpermeable film hinders the diffusion of the mediator, as shown in Figure 4, curves 1–4. Pinholes in coatings on conductive substrates may be analyzed very well by SECM (Figure 16b). Only those pores that penetrate the entire film and reach the conductive substrate will cause a significant signal in FB mode or GC mode—a significant advantage over SFM images, which show every pore independent of their depth when the tip geometry prevents the bottom of the pore being reached. The procedure was applied in the investigation of conducting polymers that can be used in a new procedure for through-hole plating.[265] If the distance between the pores is sufficiently large, pores can be detected in FB mode that are as small as 10% of the size of the UME. In GC mode, the pores can be even smaller.

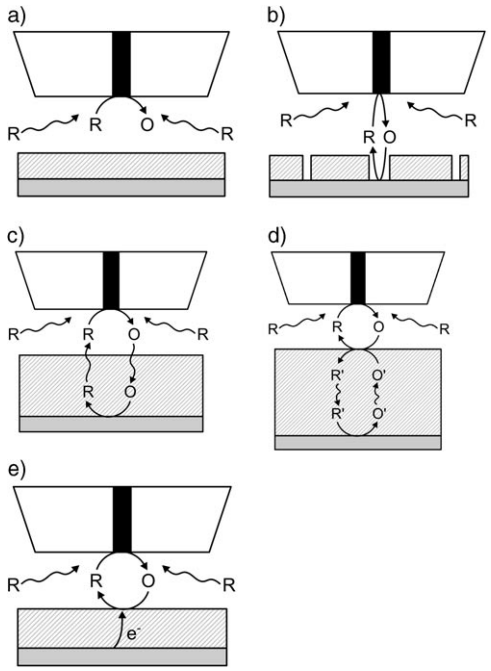

Figure 16. Charge transport through polymer layers and its investigation by SECM. a) An inert, insulating and nonpermeable film hinders the diffusion of mediator as in Figure 4, curves 1–4; b) dissolved redox-active species reach the support surface through pinholes; c) the redox-active species are soluble in the polymer film and diffuse towards the support; d) dissolved redox-active species react with a mediator confined within the polymer film; e) dissolved species exchange electrons with an electronically conducting polymer at the film–electrolyte interface.

The permeation of differently sized dissolved species through insulating polymer films (Figure 16c) was quantified by Williams et al.[266–268] Shiku et al. investigated the influence of a plasma treatment on the O_2 permeability of poly(dimethylsiloxane).[269] Gyurcsányi et al. conducted an important investigation of ion transport through ion-selective membranes.[270] Direct experimental evidence was obtained for the existence of diffusion layers at ion-selective electrodes (ISEs), which for a long time were regarded as completely equilibrated systems. The consideration of mass-transport phenomena at such electrodes under conditions of low analyte concentrations allowed a dramatic improvement of the detection limits at ISEs.[271]

Electron transfer in redox systems dissolved in a polymer film has been investigation in the penetration mode (Figure 16d) by using a conical UME that penetrates the film from the solution side.[272,273] The redox systems can be either dissolved in the film or covalently bound to the polymer chains. In the latter case, the charge transport can only occur by electron hopping between neighboring redox-active moieties.[273]

Charge transport across electronically conductive polymers (Figure 16e) can be investigated expediently in FB mode.[48,274–285] The current at the UME depends on the diffusion of the mediator between the UME and the polymer surface, the electron-transfer rate at the polymer–solution interface, the charge transport within the polymer film, and

the electron-transfer rate between the polymer and the metallic substrate. By variation of the film thickness, the electrode potential, and the distance between the UME and the polymer film, the rate of three of the considered processes can be varied over large ranges. This allows a detailed analysis of the charge-transfer processes. Moreover, electronically conducting regions within polymer blends[277] as well as aging processes[282] can be identified. Electronically conducting polymers can be electrochemically switched between conducting and insulating states. To maintain charge neutrality, counterions are incorporated into or expelled from the film. The counterion exchange can be followed from the solution side by using an amperometric or potentiometric microelectrode.[48,283–286] Similarly, the release of substances from technologically important photoresist materials was analyzed.[287]

Finally the investigation of polymer microstructures benefits from the fact that SECM can be used to generate such structures (Section 4).

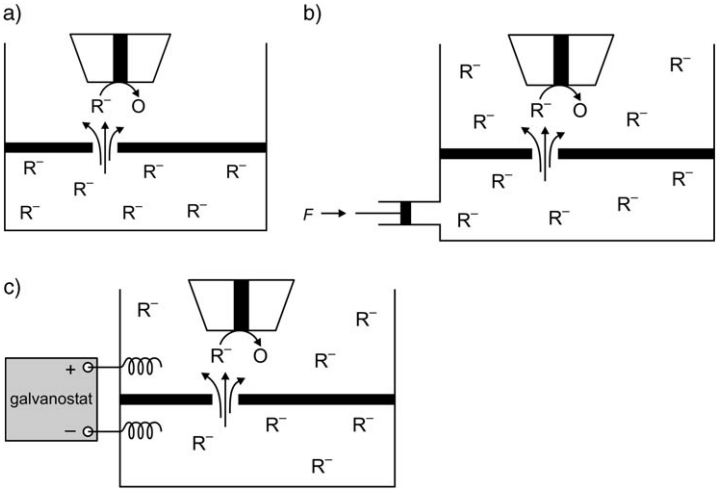

Figure 17. Typical arrangement for the investigation of mass-transport processes in biological membranes. The driving force for the transport can be a) a concentration gradient between a donor and an acceptor compartment, b) a pressure gradient between the compartments, or c) a potential gradient between the two compartments.

5.3. Transport through Membranes and Biological Tissue

SECM seems to be ideally suited for the investigation of local mass-transport processes across membranes and tissue. In a typical setup, the membrane to be investigated is mounted as a separator of a donor and an acceptor compartment. The UME moves in the acceptor compartment and measures in SG/TC mode the local concentrations of the substances emerging from the membrane. The use of selective UMEs (either ISEs or by working at defined E_T) enables the determination of transport quantities for individual species. The transport processes can be driven by concentration, pressure, or potential gradients across the membrane (Figure 17).

If the mass transport is uniformly distributed over the membrane, such as in the case of lipid double layers, the UME can be used to measure concentration profiles in the acceptor compartment under different hydrodynamic conditions, for example, to refine transport models.[59–62]

However, the transport proceeds at least partially through microscopic pore systems in most technical membranes and biological tissues such as skin, dentine, or cartilage. The relative contributions of different transport pathways are often not accurately known. They become increasingly important in the development of controllable transdermal drug-delivery systems and the noninvasive sampling of body fluids for diagnostic purposes. Correspondingly, SECM applications in this area have been pursued with industrial participation. A comprehensive review of the theory and published applications is available.[288] For reasons of brevity, this Review can only summarize the theory and list a selection of experimental studies.

When a substance emerges from a pore, the transport in the acceptor compartment occurs mainly by diffusion and is independent of the prevailing transport mechanism inside the pore. Steady-state concentration gradients are formed above the pore opening in the acceptor compartment if the pore radius r_{pore} is smaller than approximately 50 μm. The diffusive flux J emerging from the pore opening is described, in analogy to Eq. (1), by Equation (9),[5] in which $c(z=0, r=0)$ is the local concentration at the pore opening, and z and r are the vertical and radial distances, respectively, from the pore center in cylindrical coordinates.

$$J = 4\,D\,c(z=0,\,r=0)\,r_{pore} \tag{9}$$

Because of the steady-state character of J and the continuity relation, the flux at the pore opening equals the flux inside an individual pore. The local concentration at the pore opening is calculated from measured concentration distributions above a pore [Eq. (10)].[5,289]

$$c(z,r) = \frac{2\,c(z=0,r=0)}{\pi}\tan^{-1}\frac{\sqrt{2}r_{pore}}{\sqrt{(r^2+z^2-r_{pore}^2)+\sqrt{(r^2+z^2-r_{pore}^2)^2+4\,z^2\,r_{pore}^2}}} \tag{10}$$

A locally enhanced concentration is established above each pore that can be measured with SECM. In this way, individual pores can be localized. If the separation distance of the pores is sufficiently large, the UME can be positioned above a pore center ($r=0$, current maximum). There, the local concentration is measured as a function of the vertical distance [Eq. (11)].[290]

$$c(r=0,z) = \frac{2\,c(r=0,z=0)}{\pi}\tan^{-1}\frac{r_{pore}}{z} \tag{11}$$

A curve fitting of the $(c(z),z)$ data points with Equation (11) provides the unknown parameters $c(r=0,z=0)$ and r_{pore}, which, inserted in Equation (9), yield the flux in an individual pore. Strictly speaking, these relations are valid only if a passive sensor, for example, an ISE, that does not alter the local concentration of the measured species is used.

The published applications, however, have been carried out with amperometric UMEs. The diffusion layers of the pore opening and the UME intersect and the UME constitutes a local sink for the recorded species. Nevertheless, the data can be treated with the above detailed models if the UME is as small as possible and only values for $z \geq 2r_{pore}$ are included when fitting Equation (11), as has been experimentally verified by extensive studies on model membranes.[291] Theoretical descriptions for limiting cases in which the conditions cannot be met are also available.[292,293] The local mass transport was investigated across skin samples in different stages of development[289,294–299] and in dentine.[292,300–302] Transport mechanisms other than diffusion (iontophoresis, hydrodynamic flux) were used. In all cases, the flux was not evenly distributed over the tissue. The contributions of various transport mechanisms were also intensively investigated at technical membranes, such as nafion.[290]

A slightly different approach was used for the investigation of cartilage.[303–305] The cartilage sample was mounted at the bottom of a conventional cell. A highly charged redox system that does not permeate into cartilage allows the topography of the cartilage surface to be estimated. Through reduction of oxygen at the UME, the solution above the cartilage sample is depleted of oxygen, which is re-supplied from the cartilage. The permeability of the tissue for oxygen can be estimated from the difference between the measured curve and the expected values for hindered diffusion in Figure 4. A further increase of the chemical selectivity of such measurements was obtained by Kueng et al. by integration of amperometric enzyme electrodes in SFM sensors.[306–308] The release of glucose and ATP from model membranes was investigated by using this system. Other recent developments with model systems include the combination of topographic and functional information[309] and the testing of new measuring modes[310] similar to those involved in scanning ion-conductance microscopy.[311,312] The blocking of nanoscopic pores by nanoparticles over time could also be followed.[313]

5.4. Catalytical Electrodes and Fuel Cells

The microscopic characterization of electrocatalytic electrodes plays an important role in areas such as chemical sensors, electrosynthesis, and the development of fuel cell technology. The signal dependence on heterogeneous kinetics makes SECM a reasonable complement to existing methods. The modification of glassy carbon electrodes with 4-aminobenzoic acid serves as an example of covalent electrode modification for special reactivity effects. The kinetics of the resulting electrodes was characterized in the FB mode [Eqs. (5) and (6)] and compared with model calculations.[314] Halaoui et al. studied an electrosynthetic application of similar electrodes for the preparation of hydroxylamine from nitric acid.[315] SECM was used to detect reaction intermediates and products at fixed UME positions.

Further studies were devoted to reactions that are important in fuel-cell technology. The use of the mediator system H^+/H_2 was investigated in FB mode.[316–319] In contrast to most redox systems discussed above, the kinetics of the H^+/H_2 system depends strongly on the electrocatalytic properties of the electrode material. Equations (5) and (6) were used for the determination of potential-dependent rate constants to make use of the advantages described in Section 3.1.1.[320] Also, more complex reactions such as methanol oxidation[317] and the catalytic activity of polycrystalline Pt electrodes in the presence of carbon monoxide were investigated.[321] The procedures were also used to investigate combinatorial arrays of PtRu- and PtRuMo electrocatalysts.[322,323] Pt–TiO_2 nanocomposite electrodes were also studied with the H^+/H_2 system.[324]

The reactivity of metallic nanoclusters, which are particularly important in fuel-cell technology, has been characterized on different supporting materials in the GC mode. The setup corresponded to ECSTM instruments with the possibility to retract the tip outside of the tunneling distance. Besides the reactivity of Pt colloids on highly oriented graphite (HOPG),[325] reactivity effects at individual Pd nanoclusters were investigated on gold substrates.[326] In the second case, an isolated nanocluster was generated by a tip-induced effect and characterized regarding topography by ECSTM.[327] The electrocatalytic properties of the cluster were measured in the SG/TC mode after an increase of the working distance. A dramatic dependence of the activity on the thickness of the cluster was found.[328]

The oxygen reduction reaction (ORR) is technologically and biologically very important, yet mechanistically complicated. At least three reaction steps must be considered even in an extremely simplified version of the mechanism [Eq. (12)–(14)].

$$O_2 + 4\,e^- + 4\,H^+ \rightarrow 2\,H_2O \quad (12)$$

$$O_2 + 2\,e^- + 2\,H^+ \rightarrow H_2O_2 \quad (13)$$

$$H_2O_2 + 2\,e^- + 2\,H^+ \rightarrow 2\,H_2O \quad (14)$$

The reaction rate strongly depends on the electrode material. The kinetic limitation by the ORR constitutes an important limitation of the efficiency of fuel cells and electrosynthetic procedures. Because the ORR is an irreversible reaction, it cannot be investigated in the FB mode. Some investigations were performed in the TG/SC mode (Figure 6c).[1,329–332] The UME is positioned at a distance of 0.5–$3\,r_T$ above the sample in an oxygen-free solution and used to generate molecular oxygen by electrolysis. The locally generated oxygen diffuses towards the sample and is reduced there. The local ORR rate can be mapped by plotting the sample current i_S versus the lateral position of the UME. Such measurements have been used for example to screen catalyst preparations (Figure 18).

The principle was also applied for the investigation of oxygen-reducing enzymes for biofuel cells[331] and investigations of libraries of metallic reduction catalysts.[1,332] In the latter case, an array of alloy dots consisting of Pd, Au, and Co with systematically varied composition was investigated within one measurement. The composition with the highest ORR activity showed the highest i_S value during passage of

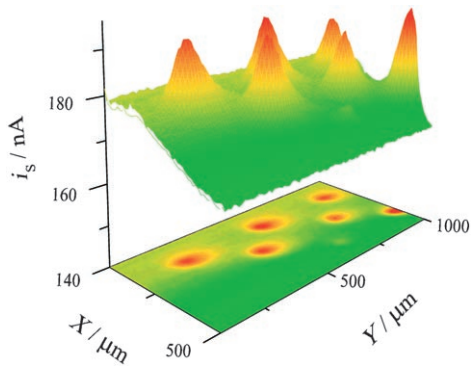

Figure 18. TG/SC image of the ORR activity of an array of Pt spots on glassy carbon. O_2 formed at the UME ($i_T = 22$ nA) is catalytically converted at the sample ($E_S = 0.1$ V). Electrolyte: 0.5 M H_2SO_4. Reprinted from reference [329] with permission. Copyright 2003, American Chemical Society.

the UME. The ORR can also be investigated at pH 12 in FB mode because hydroxide ions act as a mediator under such conditions.[333] They are oxidized to O_2 at the UME, then they are regenerated by reduction at the Pt sample. The application of this variation is very limited not only by the small pH range but also by the sample materials because the ORR leads to a significant generation of H_2O_2 at many metals. H_2O_2 reduces the amount of mediator for the feedback cycle, thus making the quantitative analysis of such cases very difficult.

5.5. Investigation of Biotechnological Surfaces

5.5.1. Imaging of Enzymatic Reactions

SECM has become an important method for the characterization of the kinetics and the distribution of immobilized enzymes at surfaces and is applicable for the optimization of biochemical sensors, biochips, or supporting materials for enzymes (membranes, foams, gels). The activity of immobilized enzymes can be imaged in FB or GC mode. Although only oxidases can be investigated in FB mode (Table 1), further enzymes can be characterized in GC mode (Table 2). Suitable substrates were found, for example, for the enzymes alkaline phosphatase (ALP) and galactosidase (Gal), both of which are significant in biotechnology and molecular biology. The substrates are not oxidized at the potential of the UME, but the product of the enzymatic reaction (*p*-aminophenol) is oxidized.[74,334,335]

Tables 1 and 2 can be expanded according to the principles outlined below and are in no way final. An attractive possibility of SECM is the characterization of enzymes on transducer surfaces independent of the transducer itself. Inhibition of electron-transfer reactions is often observed as a consequence of enzyme immobilization on electrode surfaces. This scenario can be distinguished from a deactivation of the enzyme itself by the use of SECM. Furthermore, the continuing trend towards miniaturization of sensors and chip system calls for appropriate analytical methods that allow the imaging of the relative positions of active surfaces and immobilized enzymes.[350] Some enzymes can be investigated in GC mode as well as in FB mode (Tables 1 and 2). The following guidelines may be helpful in selecting a working mode and interpreting the results.

1) If enzymes are immobilized on conductive surfaces (electrodes), only the GC mode can be used in most cases.[73] If oxidoreductases are investigated on conducting surfaces, a superposition is observed between the mediator regeneration originating from the enzymatic reaction and that from heterogeneous electron transfer to the conducting surface (Figure 19).

Although it is possible in principle to isolate both contributions by suitable control experiments,[192] this working mode is usually not a good choice because the heterogeneous electron transfer proceeds at a larger rate and a small additional contribution from the enzymatic reaction is difficult to identify because of the nonlinearity of the current–distance relation with respect to κ (Figure 5).

2) If the FB mode is possible in principle, it allows a much better lateral resolution but has a very limited sensitivity.

Table 1: FB imaging of immobilized oxidoreductases.

Imaged enzyme	Substrate	Mediator/Reaction at the UME	Ref.
glucose oxidase, EC 1.1.3.4	50–100 mM glucose	0.05–2 mM ferrocenecarboxylic acid, dimethylaminomethylferrocene, oxidation	[46, 192, 336]
		0.05–2 mM $K_4[Fe(CN)_6]$, oxidation	[46]
		0.02–2 mM hydroquinone, oxidation	[46, 337]
		0.5 mM [Os(fpy)(bpy)$_2$Cl]Cl,[a] oxidation	[192]
	50 mM glucose	0.05–2 mM ferrocenecarboxylic acid,	[338]
PQQ-dependent glucose dehydrogenase, EC 1.1.99.17		0.05–2 mM ferrocenemethanol, 0.05–2 mM *p*-aminophenol, oxidation	
NADH-cytochrome *c* reductase, EC 1.6.99.3 within mitochondria	50 mM NADH	0.5 mM *N*,*N*,*N*′,*N*′-tetramethyl-*p*-phenylenediamine, oxidation	[337]
diaphorase (NADH acceptor oxidoreductase, EC 1.6.99.–)	5.0 mM NADH	0.5 mM hydroxymethylferrocene, oxidation	[339]
horseradish peroxidase, EC 1.11.1.7	0.5 mM H_2O_2	1 mM hydroxymethylferrocenium, reduction	[340]
nitrate reductase, EC 1.7.99.4	23–65 mM NO_3^-	0.25 mM methyl viologen, reduction	[341, 342]

[a] fpy = formylpyridine, bpy = bipyridine.

Table 2: GC imaging of local enzyme activities.

Imaged enzyme	Species detected at the UME	UME[a]	Ref.
glucose oxidase EC1.1.3.4	H_2O_2	amperom. Pt UME amperom. enzyme electrode	[73, 343] [344]
PQQ-dependent glucose dehydrogenase, EC1.1.99.17	$[Fe(CN)_6]^{4-}$	amperom. Pt UME	[338]
urease EC3.5.1.5	H^+ NH_4^+	potentiom. Sb UME liquid-membrane ISE	[49] [53]
horseradish peroxidase EC1.11.1.7	ferrocene derivatives	amperom. Pt UME	[196, 340, 345]
alkaline phosphatase EC3.1.3.1	4-aminophenol	amperom. Pt UME	[74, 336, 346]
galactosidase EC3.2.1.23	4-aminophenol	amperom. Pt UME	[334, 335, 347, 348]
alcohol dehydrogenase EC1.1.1.1	H^+	potentiom. Sb UME	[61]
NADPH-dependent oxidase in osteoclasts	$O_2^{\bullet-}$	cytochrome *c* modified Au UME (amperom.)	[349]

[a] amperom.: amperometric; potentiom.: potentiometric.

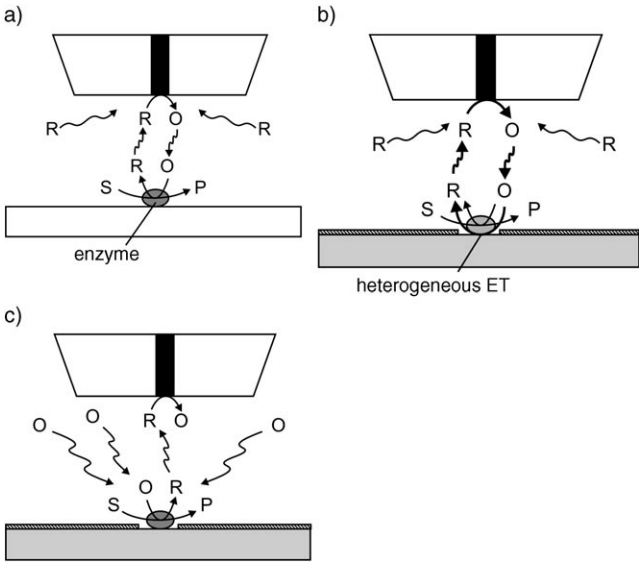

Figure 19. Imaging of immobilized enzymes on surfaces. a) Oxidoreductase on an insulating surface (FB imaging and quantification possible); b) oxidoreductase on a conducting surface (mediator recycling can occur in FB mode by the enzymatic reaction and the electron transfer to the support); c) GC-mode experiments do not depend on the nature of the support.

Therefore, it is applicable only for very active enzymes or enzymes at high interfacial concentrations Γ_{enz}. Pierce et al. described the detection limit quantitatively through Equation (15).[46]

$$k_{cat}\,\Gamma_{enz} \geq 10^{-3}\,D\,c/r_T \qquad (15)$$

The left-hand side of Equation (15) summarizes the enzyme-dependent quantities: the turnover number k_{cat} and Γ_{enz} (to be replaced by volume concentration × layer thickness if necessary). The right-hand side contains the experimental conditions: diffusion coefficient D of the mediator, mediator concentration c, and the UME radius r_T. The smaller r_T and the larger c, the more difficult it is to fulfill the detection condition.

Horrocks and Wittstock suggested a detection limit for the GC mode [Eq. (16)] that is analogous to Equation (15).[72]

$$k_{cat}\,\Gamma_{enz} \geq D\,c'/r_S \qquad (16)$$

If one assumes realistic values for the radius of the active sample r_S of 50 μm, electrochemical detection limit for the compound collected at the UME $c' = 1\ \mu M$, $D = 5 \times 10^{-6}\ cm^2\,s^{-1}$, and a monolayer of enzymes ($\Gamma_{enz} = 1 \times 10^{-12}\ mol\,cm^{-2}$), enzymes with an activity of $k_{cat} \geq 1\ s^{-1}$ can be detected.[72]

3) To evaluate GC measurements quantitatively by means of Equations (10) and (11), the enzyme-modified region must be a microstructure by itself that forms steady-state diffusion layers. This limitation does not exist for FB experiments.

4) The FB mode requires d to be as small as possible. The GC mode is less critically dependent on d. Therefore, a larger d can be selected such that protruding sample regions or a tilt between sample surface and scanning plane have a less critical effect on the experiment.

5) The concentration of the enzyme substrate must be selected carefully. It should be considerably larger than the corresponding Michaelis–Menten constant. The presence of the UME with its glass sheath hinders also the diffusion of the enzyme substrate to sample regions directly under the UME,[344] which can lead to an underestimation of the enzyme activity in corresponding experiments or cause distorted images.[351] The use of UMEs with RG values as small as possible is always advantageous in GC experiments.

6) Investigations of immobilized enzymes should always be accompanied by corresponding control experiments.

Because of the very small currents often involved, other factors (e.g., sample roughness, locally different permeabilities of coatings) could be the cause of variations in the signal that are erroneously ascribed to the enzymatic reaction.

5.5.2. *New Sensor Architectures*

The possibility of imaging specific enzyme activities and surface modification in aqueous solution (Section 3) makes SECM an ideal tool for exploring the potential of microstructured surfaces used for sensor applications.[343,352,353] For example, Kuhr and co-workers immobilized enzymes only on one part of the electrode and used the unmodified regions for electrochemical detection with a particularly short response time.[353] Thereby, the contrary requirements of both functions could be fulfilled without compromising the performance. The different reaction kinetics were visualized by SECM.[352] SECM was also used for microderivatization of the surface in this context.[354]

Wilhelm and Wittstock generated a surface with a defined arrangement of glucose oxidase (GOx) and horseradish peroxidase (HRP) by a combination of microcontact printing and SECM-based modification.[198] The surface was investigated after microcontact printing as well as after the local electrochemical modification with respect to its reactivity.[196,355]

A pattern was formed in which one region was modified by GOx and surrounded by a periodic grid of immobilized HRP (Figure 20a). GOx converts glucose and O_2 into gluconolactone and H_2O_2. The latter serves as a substrate in the HRP-catalyzed oxidation of ferrocenemethanol (Figure 20b). A GC image of the emerging ferrocinium derivative shows the combined action of both enzymes (Figure 20c). The image shows that considerable conversion is observed at the HRP grid only in the immediate vicinity of the GOx-modified regions. Further expansion of the H_2O_2 diffusion layer along the sample is prevented. The activity of the enzyme layers can be studied separately after solution exchange and switching of E_T. The GOx activity in a solution containing glucose and O_2 (no ferrocenemethanol) can be obtained by direct oxidation of H_2O_2 at the UME (Figure 20d,e). The HRP activity can be followed if H_2O_2 and ferrocenemethanol are added to the solution bulk and ferrocinium methanol is dectected (no glucose, Figure 20f,g). The larger reduction currents in periodic intervals indicate the position of the HRP-modified regions. The different signals in Figure 20c can be traced back to the different availability of H_2O_2 and can be distinguished clearly from local variation of immobilized HRP activity.

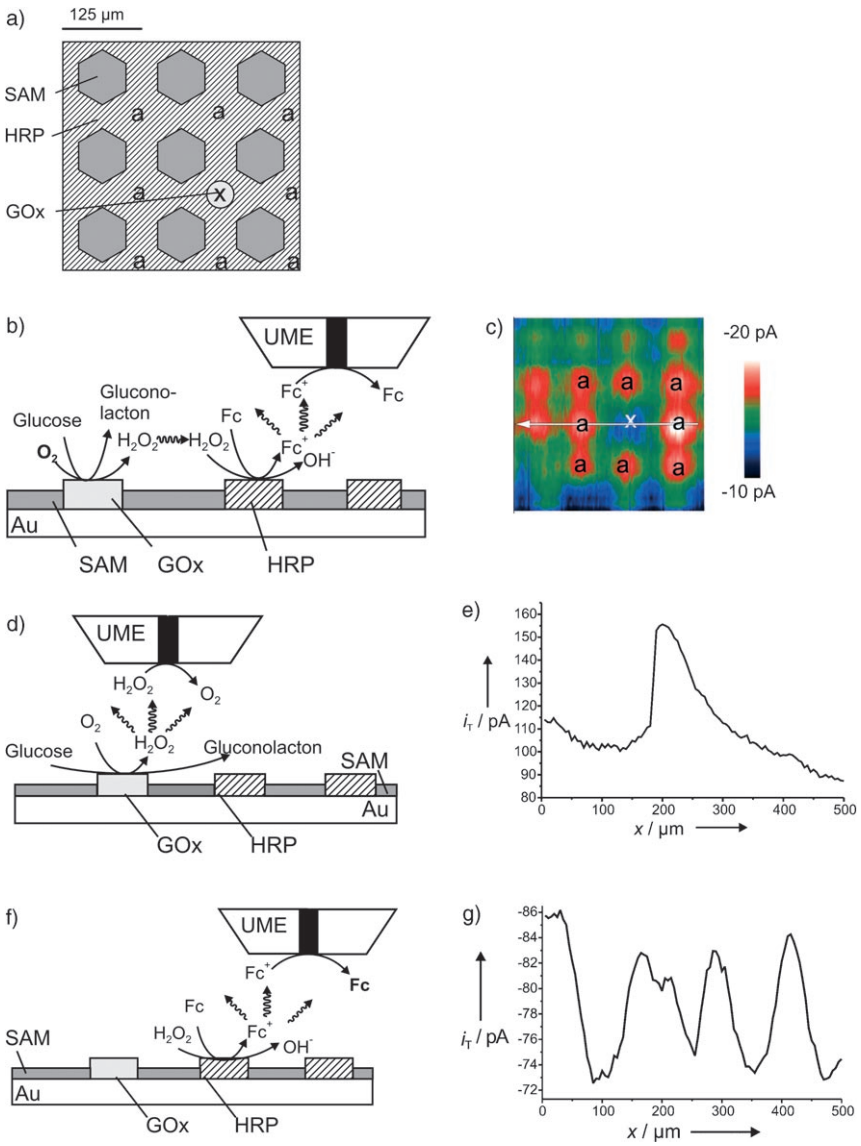

Figure 20. Investigation of a patterned bienzymatic surface with HRP and GOx. a) Arrangement of the enzymes after local derivatization with GOx; b) GC-mode experiment; c) experimental GC image in the presence of O_2, glucose, and ferrocenemethanol (500×500 µm^2); d) GC-mode experiment for imaging the GOx activity; e) experimental GC line scan for the detection of H_2O_2 along the line shown in (c) (the solution initially contains only glucose and O_2); f) GC-mode experiment for the detection of HRP activity; g) experimental GC line scan along the line shown in (c). The UME detects ferrociniummethanol. Initially, the solution contains only H_2O_2 and ferrocenemethanol. Reprinted from reference [198].

5.5.3. *Screening Procedures for Combinatorial Tests*

SECM has also been applied for the characterization of a number of new, nonmanual immobilization procedures for microstructured transducers. Examples include enzyme-loaded hydrogels,[356] the deposition of polyelectrolytes by a local, electrochemically induced pH shift,[357] and the use of microdispensers.[358] Great promise exists for the combinatorial testing of gradient materials in which different sensor surfaces are simulated on a substrate for the purpose of optimizing preparation protocols.[358–360] The region with the

highest i_T value corresponds to the optimal architecture, which might be a starting point for further optimization. In this way, the time-consuming testing of preparation protocols with a multitude of variable parameters could be shortened.

5.6. Studies on Metabolism of Tissue and Cells

Electrochemical methods, particularly amperometry and voltammetry, have been used in the investigation of cellular processes, primarily the release of neurotransmitters, for quite some time.[361,362] The possibility of gaining new insights into biological structure–function relationships with SECM was demonstrated at the inception of SECM and the area has expanded extensively since then.[17] The applications involve the FB or the GC mode. Further difficulties are encountered if cellular systems are investigated. In the conventional SECM procedure, the UME moves in one plane above the surface, which ensures a constant working distance d if tilting between the sample surface and the scanning plane is avoided and the sample roughness is small relative to r_T (5–20 μm). Cells, however, are corrugated objects with micrometer-sized height differences, that is, they are comparable in size to r_T. To keep d constant, a mechanism must be employed that retraces the topography of the sample with the UME. As discussed in Section 2.1.4, i_T itself cannot be used for distance regulation. The most convincing results have been obtained by distance regulation based on shear forces (Section 6). Positioning has also been carried out by means of an optical microscope,[349,363,364] or cells were grown in special cavities with whose upper rim they formed a flat surface after cultivation.[365–368] Alternatively, double microelectrodes were applied in which one UME converts a mediator that does not interact with the sample and allows distance determination according to Equation (3).[369] The second UME detects the biologically interesting molecule. Another approach is the simultaneous measurement of a DC signal for the detection of neurotransmitters and an AC signal for monitoring d and keeping it constant.[370]

5.6.1. Investigation of the Photosynthetic Oxygen Production, the Local Oxygen Demand, and In Vitro Toxicity Tests

SECM was applied for the investigation of local oxygen production of leaves from *Tradescantia fluminensis* while still connected to the intact plant.[363] The topography of the bottom side of the leaf was obtained in the dark with O_2 as a mediator and showed individual stomata cells. The leaves of *T. fluminensis* possess white regions in which chloroplasts are present only in the stomata cells. Tsionsky et al. recorded the O_2 production of individual stomata cells during illumination.[363] This approach clearly illustrates the advantages of the SECM methodology: localization of single cells of interest on the basis of topography or biochemical activity, positioning of the UME directly above these objects, and a more detailed, often time-dependent investigation at a fixed location. A similar appoach is also feasible to measure the influence of toxic substances, such as Cd^{2+}, on the photosynthetic O_2 production.[371] Yasukawa et al. investigated the O_2 production of individual protoplasts of *Bryopsis plumosa* and its change after addition of various chemicals.[369,372]

The oxygen consumption of individual cells or tissue can be monitored in a similar way: The UME detects less O_2 above respiratorally active cells relative to the rest of the sample. Particular attention must be paid to the distinction between a larger oxygen consumption and the shielding of mass transport by protruding cells. The described examples include HeLa cells[373] and cells of the line SW-480.[374] The oxygen demand was also monitored after addition of cell poisons to evaluate the toxicity of chemicals or to select suitable cytostatica for therapeutic applications.[375–377] Other approaches for in vitro toxicity tests used a mutant of *S. typhimurium* that started to express the UmuC–LacZ fusion protein with galactosidase activity after addition of a mutagen. The galactosidase activity was followed with high sensitivity by SECM.[348] Shiku et al. demonstrated in a series of papers a method for the evaluation of in vitro fertilized bovine embryos.[2,378,379] The UME was used for a differential measurement of the oxygen content in the bulk solution and in the vicinity of the embryo. The derived respiratory activity correlated with the survival rate and the gender of the embryos.[380]

5.6.2. Release of Messengers

The release of neurotransmitters during the transmission of nerve signals between cells was successfully recorded some time ago at isolated cells by using carbon-fiber UMEs.[361] Hengstenberg et al. used carbon-fiber UMEs in combination with a shear-force distance regulation to record a rough topographic image of an adherently growing PC12 cell[381] and subsequently to position the UME above a selected part of the cell without mechanically touching it. After stimulation of the cells by adding K^+ ions, the catecholamine release was observed with high temporal resolution at a fixed UME position. The release of adrenaline and noradrenaline from individual secretory vesicles of chromaffine cells was investigated in a similar way.[382]

The release of nitrogen monoxide from endothelia cells was also investigated. NO plays an important role as a messenger compound in, for example, the vascular system. It was detected by an electrocatalytic sensor based on a substituted nickel porphyrine (∅ 50 μm)[364] and combined with a conventional Pt UME (∅ 10 μm) to form a double UME. The sensor was then positioned above the cell by using O_2 reduction as well as Equation (3). The catalytic electrode then detected the NO release of the cell.

5.6.3. Function and Regulation of Bone-Resorbing Cells

Deeper insights into physiological processes of bone resorption by osteoclasts could be gained by the application of SECM.[55,383,384] Osteoclasts cause bone resorption by releasing Ca^{2+} and other substances. A balance exists between the resorption and formation of bone. An imbalance between these two processes is a component of many diseases, such as osteoporosis. Assays on the resorptive activity of osteoclasts conventionally involve incubation of bone slices for 18–

20 hours and subsequent electron-microscopic examination of the resorption pits. The investigation of the resorption activity by SECM is faster and more precise; the release of Ca^{2+} from individual cells can be detected after a 10-minute incubation. The reduced bone resorption rate after fluoride treatment could also be observed.

The cells respond to stimulation by parathyroid hormone (PTH) with a burst of superoxide radicals. The superoxide anion was detected amperometrically by a cytochrome *c* modified Au UME.[349] The short time span between PTH stimulation and superoxide release together with the inhibitory action of cholera toxin and other inhibitors suggested the direct action of PTH on a G-protein-coupled receptor.

5.6.4. Redox Capacity of Individual Cells

Liu et al. showed that the redox recycling of an SECM mediator can be directly linked to the internal metabolism of living cells.[385] Various imaging modes have been realized: 1) Hydrophilic mediators cannot cross the cell membrane. An image with these mediators provides topographic information according to Equation (3). 2) If a redox-active compound is distributed between the interior of a cell and the surounding medium, its concentration can be locally decreased above the cell by electrolysis at the UME. The cell can react with a release of the substance. The time dependence of i_T allows conclusions to be drawn about the transport kinetics across the cell membrane. 3) The mediator can be regenerated by redox enzymes located in the cell membrane. Thus, they transport charge into the interior of the cell. 4) Neutral redox mediators such as menadione and naphtoquinone can diffuse through the lipid layers and directly consume redox equivalents inside the cell.[386] Feng et al. observed differences between normal and metastatic tumor cells, which were then correlated with the expression profiles of the cells.[387] The same general approach was also applied to the study of bacteria cells.[388] The SECM data were interpreted by using a theory developed for charge-transfer processes at liquid–liquid interfaces. It remains to be seen whether such models will also promote a deeper understanding of the complex internal regulation processes of biological cells.

Nagamine et al. observed the metabolic regulation of bacteria embedded in collagen micropads and exposed to osmotic stress.[389,390] The change of the osmotic conditions changed the permeability of the cell membrane for the hydrophilic mediator $[Fe(CN)_6]^{4-}$. Furthermore, the response depended on whether the cells grew on a medium with D-glucose as the only carbon source, which suggested that the electron-transfer chain in which the SECM mediator is involved is located upstream of the respiratory chain.[389]

5.7. SECM as a Detection Method in Biochemical Assays and in Electropherograms

SECM detection in bioanalytical assays has been carried out by three fundamentally different methods. Miniaturized immunoassays and DNA tests have been developed by using enzyme labels. Furthermore, there are recent developments with metallic labels and label-free detection methods.

5.7.1. Enzyme Labels

The use of enzyme labels depends on the SECM imaging of local enzyme activity, which correlates with the amount of bound analyte.[74,340] The selection of the working mode is determined by the principles explained in Section 5.5. Zhao and Wittstock provided a systematic comparison of the detection principles with the example of the PQQ-dependent glucose dehydrogenase (PQQ = pyrroloquinoline quinone).[351] In summary, the GC mode has been used for

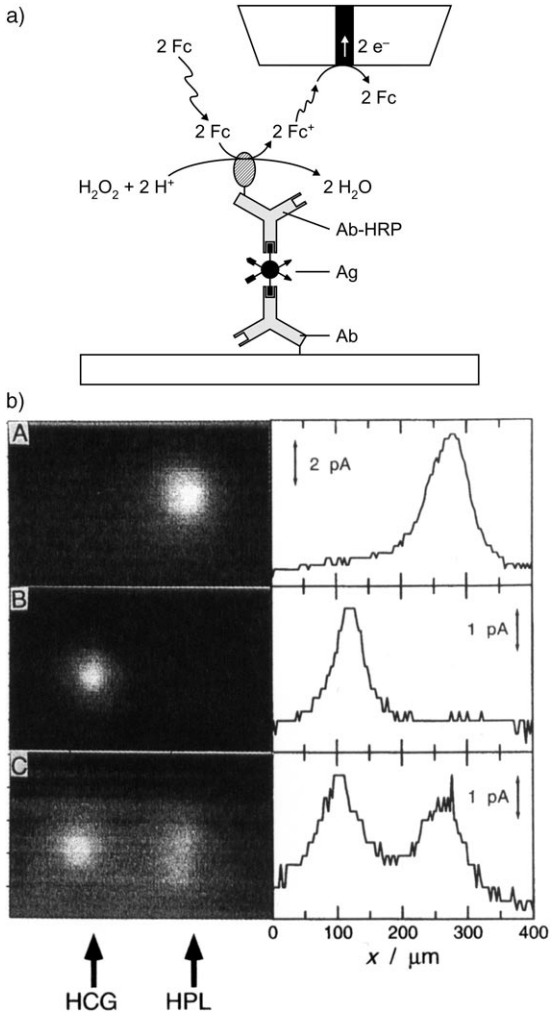

Figure 21. a) SECM detection of a sandwich immunoassay by Shiku et al.;[345] b) SECM images and cross-sectional profiles of a microstructured glass support with (anti-HCG)-Ab and (anti-HPL)-Ab immobilized at two distinct regions. The images were recorded after contact with the following solutions A) 56 ng mL^{-1} HPL; B) 2.0 IU mL^{-1} HCG; C) a mixture containing 31 ng mL^{-1} HPL + 0.63 IU mL^{-1} HCG. The glass support was rinsed and then dipped into a solution of 20 µg mL^{-1} (anti-HCG)-Ab-HRP + 7 µg mL^{-1} (anti-HPL)-Ab-HRP. Working solution for the detection step: 1.0 mM ferrocenemethanol + 0.5 mM H_2O_2 + 0.1 M KCl + 0.1 M phosphate buffer, pH 7.0; $\nu_T = 9.8$ µm s^{-1}; $E_T = +0.05$ V (Ag/AgCl). Reprinted from *J. Electroanal. Chem.*, *438*, H. Shiku, Y. Hara, T. Matsue, I. Uchida, T. Yamauchi, pp. 187–190,[345] Copyright 1997, with permission from Elsevier.

most investigations in this context.[74,336,340,345,346,391] The product of the enzymatic reaction is detected in the immediate vicinity of the enzyme label, which avoids dilution of the compound into a large solution volume. Therefore, the long incubation times required for many conventional ELISA protocols are not required. A number of immunoassays with SECM detection have been realized.[340,345,391–395] Figure 21 shows a dual immunoassay for human placental lactogen (HPL) and human chorionic gonadotropin (HCG) as an example.[345] The analyte is identified by the position on the chip, and the UME current at the corresponding position enables quantification. The detection was carried out in GC mode. The enzyme horseradish peroxidase converts H_2O_2 and ferrocene methanol, and the produced ferrocinium ion is reduced at the UME.

Magnetic microparticles can be used as new materials for immunoassays. Wijayawardhana et al. obtained acceptable detection limits of 6.4×10^{-11} mol L^{-1} or 1.4×10^{-15} mol for murine immunoglobulin G in a nonoptimized model assay using alkaline phosphatase (ALP) as a label enzyme.[346,396] Further options for optimization are the use of galactosidase as the label enzyme (avoidance of the air-sensitive substrate *p*-aminophenyl phospate for ALP) and the use of catalytical signal enhancement by coupling a second enzymatic reaction (Figure 22).[334,347] In this case, *p*-quinone imine, which is formed at the UME from *p*-aminophenol (PAP), acts as a cofactor for glucose dehydrogenase. In this reaction, PAP is regenerated and can be detected at the UME. Enzyme labels have also been used to label annual rings in wood and to image them with SECM.[397]

Fortin et al.[398] reported a new approach in which DNA microarrays were constructed on the basis of local deposition of polypyrrole according to Kranz et al.[188] Through incorporation of single-strand DNA–monomer conjugates into the polymer, a sensitive surface was obtained.[399] This surface was hybridized with biotinylated complementary DNA, and then horseradish peroxidase was bound through a strepavidin–biotin bond and used for the conversion of 4-chloro-1-naphthol. The formed insoluble, insulating reaction product blocked the metal surface of the supporting chip. Successful hybridization was detected in FB mode by reduced currents.[400] Komatsu et al. and Takenaka reported current enhancement over hybridized, immobilized DNA if the regions were imaged in FB mode with a ferrocene-substituted intercalating substance as a mediator.[401,402]

The main disadvantages of SECM detection compared with conventional fluorescence detection are the long measurement times and the associated difficulties in accomplishing high throughput. In contrast, the more affordable instrumentation at comparable sensitivity and the reduced problems with background signals can be regarded as the main advantages. One can therefore expect that SECM detection will gain importance in the area of protein arrays, in which a limited number of array elements is detected and reading times are less critical than in high-density DNA arrays. The SECM represents an ideal tool for the optimization of such detection methods because of its flexibility. Matsue and co-workers and Nishizawa and co-workers successfully transferred SECM operation principles into miniaturized electrochemical cells, in which assays could be read out without mechanically demanding and time-consuming scanning of the sample,[403,404] or in which surfaces were modified.[405]

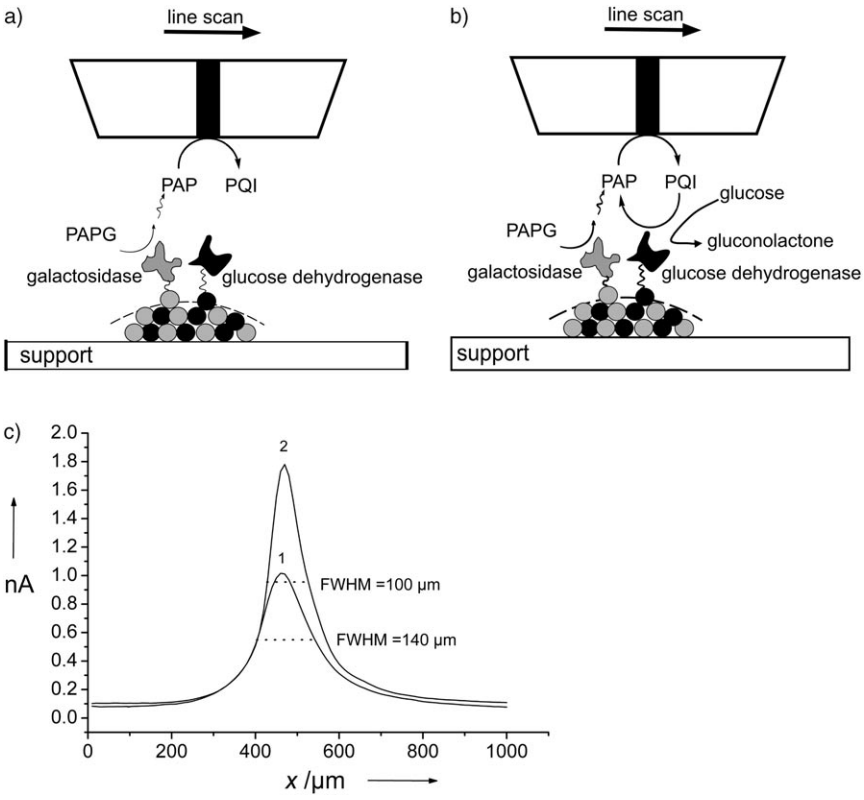

Figure 22. a) Measurement principle in conventional GC mode for galactosidase; b) signal amplification by glucose dehydrogenase in the presence of glucose. PAPG: *p*-aminophenyl-β-D-galactopyranoside; PAP: *p*-aminophenol; PQI: *p*-quinonimine; c) SECM line scan over the center of a microspot in the conventional GC mode (according to (a), curve 1, without glucose) and with signal amplification (according to (b), curve 2, with glucose). The representations are not to scale. Reprinted from reference [347].

5.7.2. *Metallic Labels*

Metallic labels have been used for staining electrophoresis gels and for the reading out of DNA and protein chips for quite some time. SECM can be applied for reading such labels and can be made significantly more sensitive than the corresponding optical detection method. Wang et al. labeled single-strand DNA (ssDNA) with Au nanoparticles.[406] After these were bound to the complementary strand, which was immobilized at the chip surface, the Au

particles served as a catalyst for electroless deposition. The formed metal layer was subsequently imaged in FB mode with $[Ru(NH_3)_6]^{3+}$ as a mediator. In this example, silver served as an inert metal electrode to allow positive FB by heterogeneous electron transfer from the reduced mediator. Carano et al. applied a slightly different principle for the detection of proteins on poly(vinylidene difluoride) (PVDF) membranes.[407] These membranes are used for electroblotting from polyacrylamide gels after electrophoretic separation. The proteins were labeled by separately prepared Ag nanoparticles in initial experiments. $[Os(bpy)_3]^{3+}$ generated at the UME dissolved the Ag nanoparticles. Meanwhile a similar approach was demonstrated with Cu staining and detection with ferrocene methanol as a mediator.[408]

5.7.3. Label-Free Detection of DNA Chips

Wang and Zhou determined hybridized DNA on chip surfaces by generating the strong oxidizer $[Ru(bpy)_3]^{3+}$ at the UME, which then oxidized guanine within the DNA strands.[409] Turcu et al. immobilized ssDNA as microspots on Au surfaces.[410,411] The negatively charged DNA strands inhibited the redox recycling of the negatively charged mediator $[Fe(CN)_6]^{3-/4-}$ in FB mode in a similar way to the investigation of self-assembled monolayers (Section 5.2.2). The current over the DNA spots was decreased further after hybridization because the negative charge density increased at the chip surface.

6. Developments of New Methods and Instruments

Despite the variety of applications and the availability of commercial instruments, the development until around 2002 was dominated by methodical studies, for a number of very different reasons. Successful results, in particular with non-ideal samples, require a thorough understanding of the underlying electrochemical principles and practical experience to design and to realize suitable experiments. Because i_T depends not only on d but also on the reactivity of the sample (Figure 5), it has been obvious for a long time that current-independent positioning methods are urgently required for the unambiguous assignment of measured data to differences in reactivity and adjustment for sample tilt. From a current perspective, some trends can be identified, namely, the use of UMEs with dimensions in the nanometer range in connection with shear-force systems as well as the combination of SECM with other experimental techniques.

6.1.1. Positioning through Shear Forces

An increasing number of groups have prepared UMEs with diameters less than or equal to 1 μm and defined disk-shaped geometry for imaging experiments involving shear-force detection at laterally vibrating UMEs.[70,412–418] Because the shear forces are measured in a viscous liquid, different filling levels are often unavoidable in practical experiments (addition of solutions), and the mechanical properties of the UME vary, the routine measurement of shear forces remains challenging. Two variations exist: A piezoelectric actuator excites the UME with a frequency tuned to the mechanical properties of the UME as first demonstrated by Ludwig et al.[412] The amplitude was estimated to be 50 nm ($\ll r_T$). The amplitude and phase shift of the lateral motion are recorded either by projection of a diffraction pattern onto a split photodiode[412] or by a second piezoelectric element.[58,245,254,415,419,420] The optical detection requires a minimum diameter of the UME, whereas the piezoelectrical detection is also suitable for very small electrodes. Figure 23a shows the attachment of the piezoelectric actuator and receiver to a UME. Simultaneously recorded images of the electrochemical signals and the topography of a Pt band array are also shown (Figure 23b,c) and illustrate the correction for the sample tilt and the contrast enhancement in the FB image by means of small working distances.[415]

Alternatively, the UME can be attached to one leg of a quartz tuning fork.[258,397,413,414,416,417] The resonance frequency is determined in this case mainly by the quartz resonator, which allows the use of electronics specified for a smaller frequency range than in the method described above. Because of the insulating sheath, the mass of the UME is significantly larger than that of the quartz resonator and sensitivity problems occur in this case as well. In each case, the complexity of the experiments is increased by application of the shear-force mode because not only the electrochemical but also the mechanical properties of the UME have to be adjusted to the experimental task.

6.1.2. Coupling with SFM and ECSTM

SFM and electrochemical scanning tunneling microscopy (ECSTM) routinely allow imaging with a lateral and vertical resolution that is clearly superior to that of SECM. However, neither method directly delivers chemically specific information. SECM can be coupled with other methods by integration of a UME into the sensors used for other scanning probe techniques (SFM, ECSTM, SNOM). These coupled systems are directed towards two tasks: 1) The solution composition should be modified locally (and hence rapidly) by microelectrochemical methods so that the resulting topographic changes can be measured by SFM or ECSTM. SFM cantilevers coated with metals[134,136] or special ECSTM cell constructions are suitable for this purpose.[421] Dissolution processes at crystals and proton exchange at polyaniline films have been studied.[134,136,421] The region influenced by the electrochemical reaction is significantly larger than the region imaged by SFM or ECSTM. 2) Another approach aims at recording spatially correlated images. As SECM and ECSTM share some experimental similarities, coupling of the two methods is a logical strategy for obtaining topographical information from ECSTM images that can be directly related to SECM measurements.[30,218,325,422] The first system utilized rather large electrodes.[218] Later, Kucernak et al. described a system in which the topography of the sample was imaged by ECSTM, the probe was then retracted at a defined distance, and finally a SECM image was recorded at a constant plane (and hence with different d).[325] Other experiments used the topographic information from an ECSTM line scan to guide

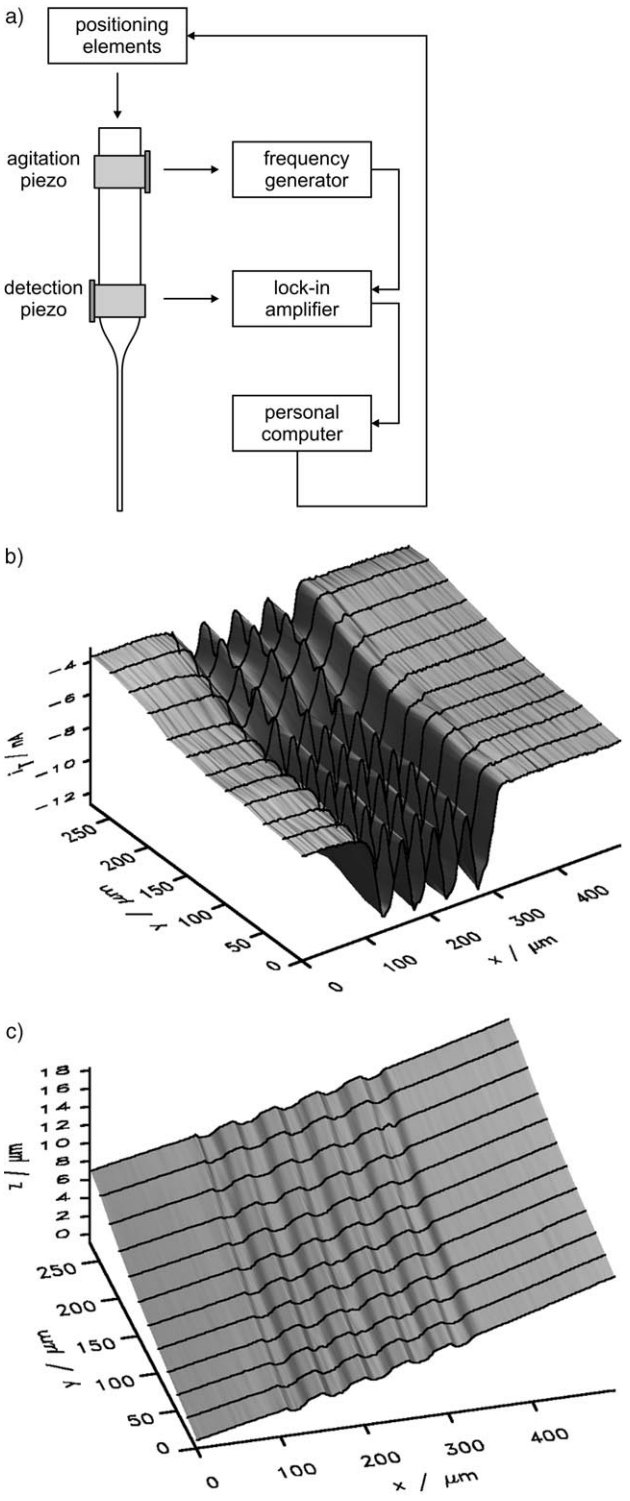

Figure 23. The use of shear-force measurements for distance control in SECM. a) Piezoelectric detection system for shear forces; b) amperometric FB; and c) topographic images of a Pt band electrode array ($500 \times 250\ \mu m^2$). The two images were recorded simultaneously in constant-distance mode. Reprinted from reference [415]. Copyright 2003, Wiley-VCH.

the probe at constant d over the sample during the SECM image ("lift off").[30,422]

ECSTM coupled systems are principally restricted in their application because they are not applicable to insulating samples. Therefore, the coupling of SECM with SFM is of greater importance. The development was decisively initiated by Macpherson and co-workers[135,309,423–427] as well as Kranz and co-workers[428–431] and has meanwhile been taken up by other groups in various conceptual details.[231,233,432–437] The combined probes of Kranz and co-workers proved to be useful for a number of applications. These were obtained by coating SFM cantilevers with metals and an insulating layer followed by cutting with a focused ion beam (FIB).[428–431] In this procedure, a central thorn is carved from the cantilever tip, which is surrounded by a recessed frame-shaped electrode (Figure 24a).

The thorn keeps d constant so that an SFM and an SECM image can be recorded simultaneously, and thus double scanning of the sample is avoided. The probes possessed very good imaging properties for SFM and are suitable for tapping mode,[431] which is advantageous for the investigation of soft samples. The development has advanced so far that practically relevant investigation of enzyme-loaded microstructures[308,438,439] was performed. Figure 25 shows images of the topography and the enzymatic activity of horseradish peroxidase that was immobilized on an SAM on gold. A control experiment was performed in the absence of H_2O_2 (Figure 25b, top), and measurement with H_2O_2 showed the localized enzyme activity by high probe currents (Figure 25b, bottom right), which correlated very well with the topography imaged in contact mode.

The method is robust enough to allow further modification of the integrated electrodes to enzyme electrodes, thereby increasing the chemical selectivity of the measurements.[440,441] A limiting factor is that each probe must be fabricated individually.

Macpherson et al. formed cantilevers from Pt wires that were used as combined electrochemical force sensors after insulation with an electrophoretic paint (Figure 24b),[135] which were used in lift-off mode[423] for the characterization of electrocatalytic electrodes,[424] pore diffusion,[309,425] and other model samples.[135] Recent developments aimed at the preparation of combined probes in parallel processes (Figure 24c)[427,442,443] and the integration of microdisk electrodes.[426]

Fasching et al. presented the first probe arrays with integrated electrodes (Figure 24d).[433] Consequently, a number of new applications will become feasible in the near future in which the enhanced information content and the improved lateral resolution can be exploited, for example, for the investigation of electrochemical processes at grain boundaries, for biogeochemical problems of phase formation, or to answer cell-biological questions.

6.1.3. *Other Combined Methods*

Both electrochemical and optical methods provide important functional information about surfaces. The coupling of scanning near-field optical microscopy (SNOM) and SECM is thus reasonable.[444–447] An optical fiber or a capillary serves as a wave guide and a metallic coating forms the electrode

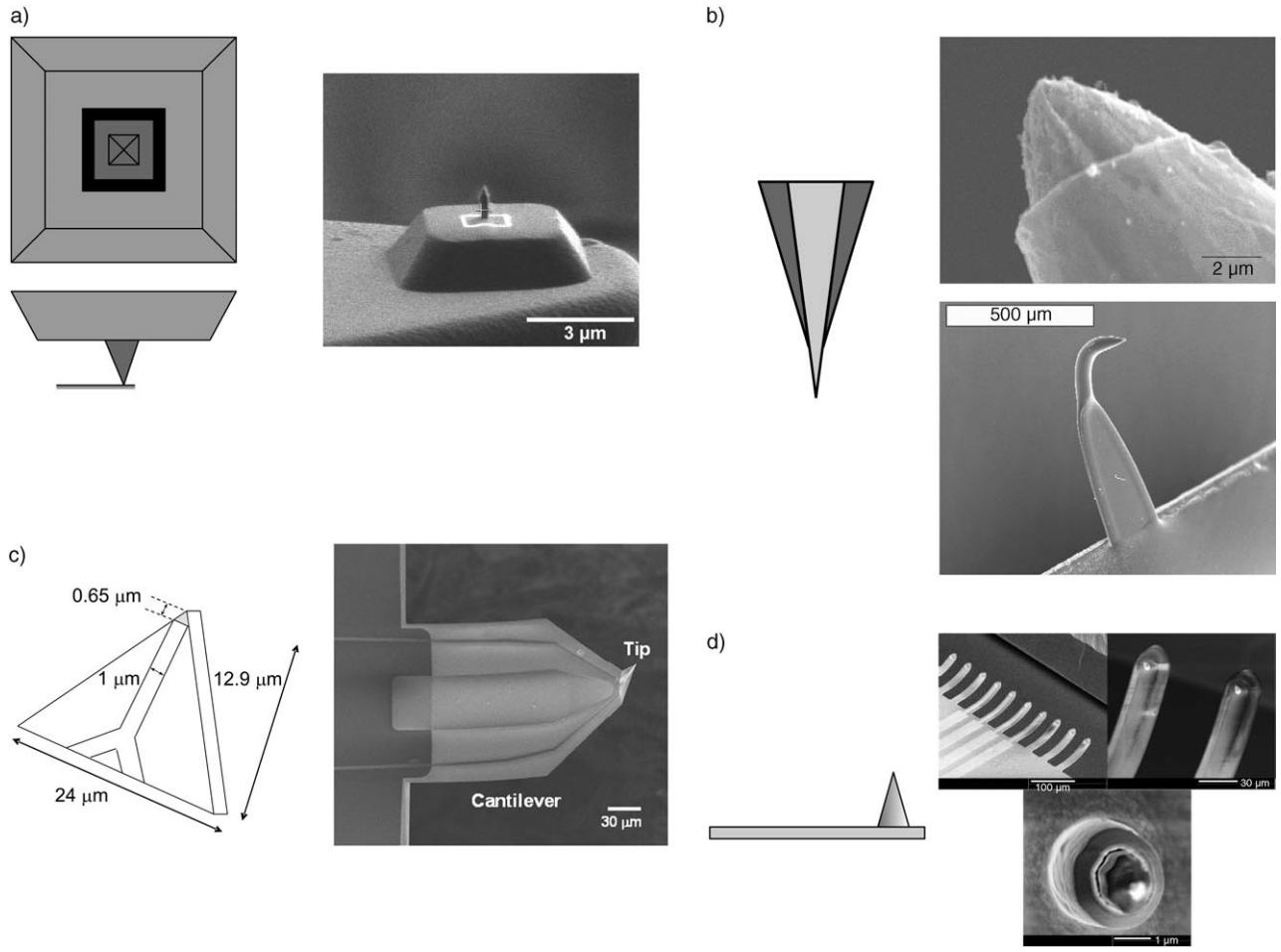

Figure 24. Integrated SFM–SECM probes. a) Recessed frame electrode according to Kranz and co-workers; b) coated Pt wire according to Macpherson and co-workers; c) bent Pt electrode shielded in glass or quartz according to Dobson et al.; d) multitip arrangement with integrated electrodes according to Fasching et al. Reproduction of (a) with kind permission of C. Kranz. Reproduction of (b) from references [135] and [423] with permission. Copyright 2000, 2001, American Chemical Society. Reproduction of (c) from reference [443] with permission. Copyright 2005, American Chemical Society. Reproduction of (d) from *Sens. Actuators B*, *108*, R. J. Fasching, Y. Tao, F. B. Prinz, pp. 964–972,[433] Copyright 2005, with permission from Elsevier.

material. The insulation of the side walls against the electrolyte solution is critical for their function. A metal ring forms the active electrode area at the cross section of the coated fiber.[414,447–449] The inverse principle has also been demonstrated: Electrogenerated luminiscence was triggered by a UME and was used to record an optical image of a model sample.[450]

The combination of SECM and confocal microscopy is also very interesting because confocal microscopy allows a three-dimensional investigation of diffusion layers[451] at a spatial resolution that is compatible with the lateral resolution of SECM without any modification.[451,452] Furthermore, photochemical excitation processes can be followed electrochemically and local variation of the solution composition can be used as driving force for interfacial reactions that are then characterized optically.[452] In this way, Boldt et al. generated a local pH shift that drove the enzyme ATP synthase.[452] The movement of the ATP synthase could be followed simultaneously by fluorescent resonant energy transfer (FRET) measurements.

Finally, the combination of SECM with the quartz-crystal microbalance,[453–457] optical spectroscopy,[414] or surface plasmon resonance spetroscopy[399,458,459] should be mentioned. In these systems, the UME is used for initiating a local reaction.[459] Alternatively, property changes of the sample, for example, mass or optical signals, can be recorded while the UME follows the ejection or uptake of substance from the solution side.[460]

6.1.4. Limits to Lateral Resolution

The extension of the diffusion layer above the sample determines the resolution in GC mode. If r_T is smaller than the diffusion layer, further miniaturization of the UME does not lead to improved resolution. Nevertheless, small UMEs are always advantageous in GC mode, in particular, for quantitative investigation (Section 2.2.2). The use of conical electrodes is possible without diminishing the performance.

The resolution in FB mode is primarily determined by r_T. Furthermore, the resolution becomes better as d is decreased.

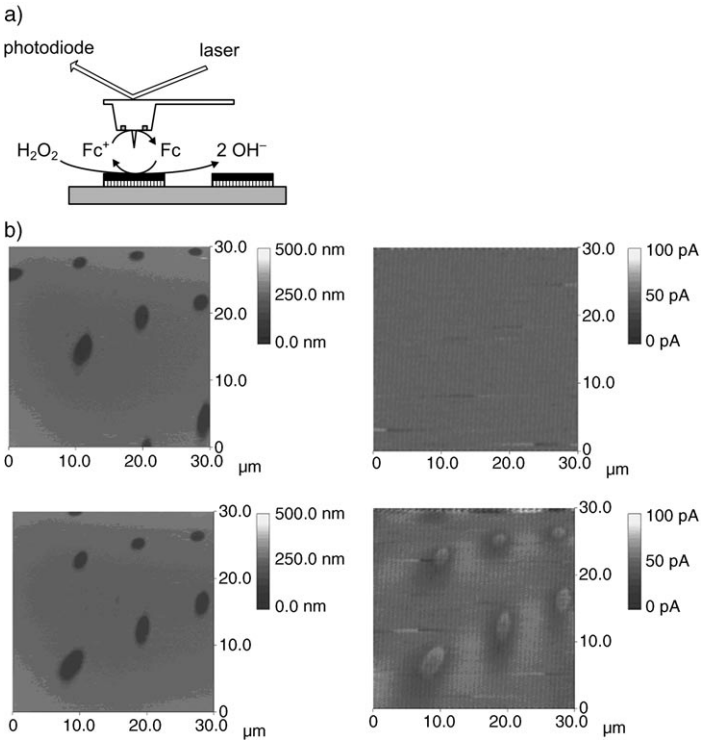

Figure 25. Images of enzyme spots obtained by an integrated SFM–SECM probe with recessed frame electrode. a) Horseradish peroxidase immobilized on a patterned SAM catalyzes the oxidation of ferrocenemethanol (Fc) to ferroceniummethanol (Fc^+) by H_2O_2. The distance between the sample and the frame electrode is given by the length of the central thorn (410 nm). b) Simultaneously recorded topography (left) and SECM feedback signals (right) with (bottom) and without (top) enzyme substrate H_2O_2. Reproduction of (b) from *Ultramicroscopy, 100*, C. Kranz, A. Kueng, A. Lugstein, E. Bertagnolli, B. Mizaikoff, pp. 127–134,[438] Copyright 2004, with permission from Elsevier.

Because the normalized distance d/r_T is important in this case, smaller UMEs require a proportionally decreased d, which can be achieved by current-independent distance control modes (Section 6.1.1). These modes require UMEs in which the active electrode area is at the apex of the usually shallow-cone-shaped face of the electrode body.[254] This is very difficult to achieve with electrodes in which $r_T \approx 100$ nm. Finally, lateral resolution and sensitivity are linked to each other. It can be seen from the curves in Figure 5 that an active region can be detected if it causes a signal at least corresponding to curve 3 with $\kappa = 0.3$. Because $\kappa = k_{eff} r_T/D$ represents a normalized rate constant, the minimum k_{eff} grows with decreasing r_T. Table 3 illustrates this fact: At $r_T = 5$ nm, k_{eff} must be larger than 3 cm s^{-1} to be detectable by SECM. In conventional electrochemical experiments, this value corresponds to a rate constant of an almost diffusion-controlled reaction. The SECM becomes "blind" to all slower reactions. Although UMEs with such dimensions and defined geometry have been prepared,[461] their use for FB imaging is unlikely on kinetic grounds even if the vertical positioning can be achieved. Therefore, it is not surprising that many research groups use very small electrodes but apply these in the more sensitive GC mode even though this mode offers lower lateral resolution than FB mode.[70,233,254,426,438]

Table 3: Heterogeneous rate constants k_{eff} required to obtain approach curve 3 in Figure 5 ($\kappa = 0.3$). $D = 5 \times 10^{-6}$ cm^2 s^{-1}.

r_T [µm]	12.5	5	1	0.5	0.1	0.05	0.025	0.005
k_{eff} [cm s^{-1}]	0.0012	0.003	0.015	0.03	0.15	0.3	0.6	3

7. Summary and Outlook

Scanning electrochemical microscopy can be applied for the investigation of numerous reactions at solid–liquid interfaces. The method provides a direct image of the reactivity, even in cases in which the topography of the interface remains unchanged. Examples with strong application potential include the investigation of corrosion mechanisms of passivated metals, transport processes through coatings and membranes, heterogeneous catalysis at fuel cell materials, enzyme catalysis at sensor surfaces, and the metabolic activity of intact cells and organs. Additionally, the results can often be described by simple continuum models for diffusive mass transport and interfacial kinetics. These possibilities have been very stimulating for fundamental electrochemical research, for which SECM has become an essential tool. Owing to the steady-state character at the microscopic surfaces, this technique offers great advantages over more conventional techniques that are often limited by charging currents, limited rise times of the instruments, and ohmic drops within the electrochemical cell. SECM can investigate heterogeneous electron-transfer reaction rates even if the interface is not connected to an external potential source. This allows extension of the principle to unusual interfaces such as organized nanoparticles at gas–liquid interfaces.

Finally, it is possible to modify substrates locally by a multitude of clearly defined chemical/electrochemical reactions and to test new approaches for the prototyping of micro- and nanostructured functional surfaces, for example, in biosensors and biochips. The functionality of the generated structure can be tested within the same setup, thus making SECM an ideal tool for such tasks.

The application range of the method is likely to expand greatly in the future if the production of integrated SECM–SFM probes becomes routine in batch processes. This already foreseeable breakthrough will proceed hand in hand with a considerable increase in lateral resolution in routine experiments, which will enable application of the method in all those areas in which scanning force microscopy in liquids is used today. This includes, in particular, further areas in materials science such as the investigation of corrosion processes at grain boundaries or on individual grains, whose mechanisms are not yet fully understood.

Current projects on scanning electrochemical microscopy are funded by the Deutsche Forschungsgemeinschaft (Wi 1617/6 (research group biogeochemistry of tidal flats), Wi 1617/7, Wi 1617/8) and the Lower Saxony–Israeli Foundation. The authors are grateful to Prof. J. Heinze for helpful comments as well as to all colleagues who provided original figures. The

frontispiece was designed by Markus Träuble, Carl von Ossietzky Universität Oldenburg. Dr. Yan Shen was a Fellow of the Alexander von Humboldt Foundation.

Received: July 11, 2006
Published online: February 7, 2007

[1] J. L. Fernandez, D. A. Walsh, A. J. Bard, *J. Am. Chem. Soc.* **2005**, *127*, 357 – 365.
[2] H. Shiku, T. Shiraishi, H. Ohya, T. Matsue, H. Abe, H. Hoshi, M. Kobayashi, *Anal. Chem.* **2001**, *73*, 3751 – 3758.
[3] J. Heinze, *Angew. Chem.* **1993**, *105*, 1327 – 1349; *Angew. Chem. Int. Ed. Engl.* **1993**, *32*, 1268 – 1288.
[4] M. Fleischmann, S. Pons, D. R. Rolison, P. P. Schmidt, *Ultramicroelectrodes*, Datatech Systems, Morganton, **1987**.
[5] Y. Saito, *Rev. Polarogr.* **1968**, *15*, 177 – 187.
[6] R. C. Engstrom, M. Weber, D. J. Wunder, R. Burgess, S. Winquist, *Anal. Chem.* **1986**, *58*, 844 – 848.
[7] H.-Y. Liu, F.-R. F. Fan, C. W. Lin, A. J. Bard, *J. Am. Chem. Soc.* **1986**, *108*, 3838 – 3839.
[8] J. Kwak, A. J. Bard, *Anal. Chem.* **1989**, *61*, 1221 – 1227.
[9] D. O. Wipf, "SECM Bibliography", http://www.msstate.edu/dept/Chemistry/dow1/secm/secm_bib.html.
[10] *Scanning Electrochemical Microscopy* (Eds.: A. J. Bard, M. V. Mirkin), Marcel Dekker, New York, **2001**.
[11] B. R. Horrocks in *Encyclopedia of Electrochemistry*, *Vol. 3* (Eds.: P. R. Unwin, A. J. Bard, M. Stratmann), Wiley-VCH, Weinheim, **2003**, pp. 444 – 490.
[12] H. Shiku, H. Ohya, T. Matsue in *Encyclopedia of Electrochemistry*, *Vol. 9* (Eds.: G. S. Wilson, A. J. Bard, M. Stratmann), **2002**, pp. 257, 259 – 275.
[13] A. J. Bard, F.-R. F. Fan, M. V. Mirkin in *Electroanalytical Chemistry*, *Vol. 18* (Ed.: A. J. Bard), Marcel Dekker, New York, **1994**.
[14] G. Nagy, L. Nagy, *Fresenius J. Anal. Chem.* **2000**, *366*, 735 – 744.
[15] A. L. Barker, M. Gonsalves, J. V. Macpherson, C. J. Slevin, P. R. Unwin, *Anal. Chim. Acta* **1999**, *385*, 223 – 240.
[16] D. Mandler, S. Meltzer, I. Shohat, *Isr. J. Chem.* **1996**, *36*, 73 – 80.
[17] A. J. Bard, F.-R. F. Fan, D. T. Pierce, P. R. Unwin, D. O. Wipf, F. Zhou, *Science* **1991**, *254*, 68 – 74.
[18] R. C. Engstrom, C. M. Pharr, *Anal. Chem.* **1989**, *61*, 1099 – 1104.
[19] S. Amemiya, J. Guo, H. Xiong, D. A. Gross, *Anal. Bioanal. Chem.* **2006**, *386*, 458 – 471.
[20] A. T. Hubbard, F. C. Anson in *Electroanalytical Chemistry*, *Vol. 4* (Ed.: A. J. Bard), Marcel Dekker, New York, **1970**, pp. 129 – 214.
[21] H. Siegenthaler in *Scanning Tunneling Microscopy II* (Eds.: R. Wiesendanger, H. J. Güntherodt), Springer, Berlin, **1992**, pp. 7 – 49.
[22] R. Guckenberger, M. Heim, G. Cevc, H. F. Knapp, W. Wiegräbe, A. Hillebrand, *Science* **1994**, *266*, 1538 – 1540.
[23] R. Guckenberger, E. Hartmann, W. Wiegräbe, W. Bauermeister in *Scanning Tunneling Microscopy II* (Eds.: R. Wiesendanger, H. J. Güntherodt), Springer, Berlin, **1992**, pp. 84 – 92.
[24] R. Guckenberger, M. Heim, *Science* **1995**, *270*, 1849 – 1851.
[25] F.-R. F. Fan, A. J. Bard, *Science* **1995**, *267*, 871 – 874.
[26] F. Forouzan, A. J. Bard, *J. Phys. Chem. B* **1997**, *101*, 10876 – 10879.
[27] N. Patel, M. C. Davies, M. Lomas, C. J. Roberts, S. J. B. Tendler, P. M. Williams, *J. Phys. Chem. B* **1997**, *101*, 5138 – 5142.
[28] C. G. Zoski, M. V. Mirkin, *Anal. Chem.* **2002**, *74*, 1986 – 1992.
[29] O. Sklyar, A. Kueng, C. Kranz, B. Mizaikoff, A. Lugstein, E. Bertagnolli, G. Wittstock, *Anal. Chem.* **2005**, *77*, 764 – 771.
[30] O. Sklyar, T. H. Treutler, N. Vlachopoulos, G. Wittstock, *Surf. Sci.* **2005**, *597*, 181 – 195.
[31] M. N. Holder, C. E. Gardner, J. V. Macpherson, P. R. Unwin, *J. Electroanal. Chem.* **2005**, *585*, 8 – 18.
[32] M. V. Mirkin, F.-R. F. Fan, A. J. Bard, *J. Electroanal. Chem.* **1992**, *328*, 47 – 62.
[33] Y. Shao, M. V. Mirkin, *J. Phys. Chem. B* **1998**, *102*, 9915 – 9921.
[34] J. L. Amphlett, G. Denuault, *J. Phys. Chem. B* **1998**, *102*, 9946 – 9951.
[35] Y. Selzer, D. Mandler, *Anal. Chem.* **2000**, *72*, 2383 – 2390.
[36] J. Galceran, J. Cecilia, E. Companys, J. Salvador, J. Puy, *J. Phys. Chem. B* **2000**, *104*, 7993 – 8000.
[37] O. Sklyar, G. Wittstock, *J. Phys. Chem. B* **2002**, *106*, 7499 – 7508.
[38] Q. Fulian, A. C. Fisher, G. Denuault, *J. Phys. Chem. B* **1999**, *103*, 4387 – 4392.
[39] T. Nann, J. Heinze, *Electrochim. Acta* **2003**, *48*, 3975 – 3980.
[40] M. V. Mirkin in *Scanning Electrochemical Microscopy* (Eds.: A. J. Bard, M. V. Mirkin), Marcel Dekker, New York, **2001**, pp. 145 – 199.
[41] G. Wittstock, H. Emons, M. Kummer, J. R. Kirchhoff, W. R. Heineman, *Fresenius J. Anal. Chem.* **1994**, *348*, 712 – 718.
[42] A. J. Bard, M. V. Mirkin, P. R. Unwin, D. O. Wipf, *J. Phys. Chem.* **1992**, *96*, 1861 – 1868.
[43] F. Forouzan, A. J. Bard, M. V. Mirkin, *Isr. J. Chem.* **1997**, *37*, 155 – 163.
[44] D. O. Wipf, A. J. Bard, *J. Electrochem. Soc.* **1991**, *138*, 469 – 474.
[45] C. Wei, A. J. Bard, M. V. Mirkin, *J. Phys. Chem.* **1995**, *99*, 16033 – 16042.
[46] D. T. Pierce, P. R. Unwin, A. J. Bard, *Anal. Chem.* **1992**, *64*, 1795 – 1804.
[47] G. Denuault, G. Nagy, K. Toth in *Scanning Electrochemical Microscopy* (Eds.: A. J. Bard, M. V. Mirkin), Marcel Dekker, New York, **2001**, pp. 397 – 444.
[48] G. Denuault, M. H. T. Frank, L. M. Peter, *Faraday Discuss.* **1992**, *94*, 23 – 35.
[49] B. R. Horrocks, M. V. Mirkin, D. T. Pierce, A. J. Bard, G. Nagy, K. Toth, *Anal. Chem.* **1993**, *65*, 1213 – 1224.
[50] K. Toth, G. Nagy, C. Wei, A. J. Bard, *Electroanalysis* **1995**, *7*, 801 – 810.
[51] C. Wei, A. J. Bard, G. Nagy, K. Toth, *Anal. Chem.* **1995**, *67*, 1346 – 1356.
[52] R. E. Gyurcsanyi, A.-S. Nybäck, K. Toth, G. Nagy, A. Ivaska, *Analyst* **1998**, *123*, 1339 – 1344.
[53] B. R. Horrocks, M. V. Mirkin, *J. Chem. Soc. Faraday Trans.* **1998**, *94*, 1115 – 1118.
[54] I. Kapui, R. E. Gyurcsanyi, G. Nagy, K. Toth, M. Arca, E. Arca, *J. Phys. Chem. B* **1998**, *102*, 9934 – 9939.
[55] C. E. M. Berger, B. R. Horrocks, H. K. Datta, *Electrochim. Acta* **1999**, *44*, 2677 – 2683.
[56] N. J. Gray, P. R. Unwin, *Analyst* **2000**, *125*, 889 – 893.
[57] A. Schulte, S. Belger, W. Schuhmann, *Mater. Sci. Forum* **2002**, *394–395*, 145 – 148.
[58] M. Etienne, A. Schulte, S. Mann, G. Jordan, I. D. Dietzel, W. Schuhmann, *Anal. Chem.* **2004**, *76*, 3682 – 3688.
[59] P. Pohl, S. M. Saparov, Y. N. Antonenko, *Biophys. J.* **1998**, *75*, 1403 – 1409.
[60] P. Pohl, S. M. Saparov, Y. N. Antonenko, *Biophys. J.* **1997**, *72*, 1711 – 1718.
[61] Y. N. Antonenko, P. Pohl, E. Rosenfeld, *Arch. Biochem. Biophys.* **1996**, *333*, 225 – 232.
[62] Y. N. Antonenko, G. A. Denisov, P. Pohl, *Biophys. J.* **1993**, *64*, 1701 – 1710.
[63] J. O. Park, C.-H. Paik, R. C. Alkire, *J. Electrochem. Soc.* **1996**, *143*, L174 – L176.
[64] H. Tanabe, K. Togashi, T. Misawa, U. K. Mudali, *J. Mater. Sci. Lett.* **1998**, *17*, 551 – 553.
[65] C. Wei, A. J. Bard, I. Kapui, G. Nagy, K. Toth, *Anal. Chem.* **1996**, *68*, 2651 – 2655.
[66] C. Lee, J. Kwak, F. C. Anson, *Anal. Chem.* **1991**, *63*, 1501 – 1504.

[67] R. C. Engstrom, *Anal. Chem.* **1984**, *56*, 890 – 894.
[68] A. Hengstenberg, C. Kranz, W. Schuhmann, *Chem. Eur. J.* **2000**, *6*, 1547 – 1554.
[69] R. C. Engstrom, T. Meaney, R. Tople, R. M. Wightman, *Anal. Chem.* **1987**, *59*, 2005 – 2010.
[70] N. Baltes, L. Thouin, C. Amatore, J. Heinze, *Angew. Chem.* **2004**, *116*, 1455 – 1459; *Angew. Chem. Int. Ed.* **2004**, *43*, 1431 – 1435.
[71] O. Sklyar, M. Träuble, C. Zhao, G. Wittstock, *J. Phys. Chem. B* **2006**, *110*, 15869 – 15877.
[72] B. R. Horrocks, G. Wittstock in *Scanning Electrochemical Microscopy* (Eds.: A. J. Bard, M. V. Mirkin), Marcel Dekker, New York, **2001**, pp. 445 – 519.
[73] G. Wittstock, W. Schuhmann, *Anal. Chem.* **1997**, *69*, 5059 – 5066.
[74] G. Wittstock, K.-j. Yu, H. B. Halsall, T. H. Ridgway, W. R. Heineman, *Anal. Chem.* **1995**, *67*, 3578 – 3582.
[75] M. V. Mirkin, T. C. Richards, A. J. Bard, *J. Phys. Chem.* **1993**, *97*, 7672 – 7677.
[76] C. J. Slevin, J. V. Macpherson, P. R. Unwin, *J. Phys. Chem. B* **1997**, *101*, 10851 – 10859.
[77] C. J. Slevin, S. Ryley, D. J. Walton, P. R. Unwin, *Langmuir* **1998**, *14*, 5331 – 5334.
[78] J. Zhang, P. R. Unwin, *Langmuir* **2002**, *18*, 1218 – 1224.
[79] I. Ciani, D. P. Burt, S. Daniele, P. R. Unwin, *J. Phys. Chem. B* **2004**, *108*, 3801 – 3809.
[80] C. J. Slevin, P. R. Unwin, *J. Am. Chem. Soc.* **2000**, *122*, 2597 – 2602.
[81] J. Zhang, P. R. Unwin, *Phys. Chem. Chem. Phys.* **2002**, *4*, 3814 – 3819.
[82] D. Mandler, P. R. Unwin, *J. Phys. Chem. B* **2003**, *107*, 407 – 410.
[83] J. Zhang, A. L. Barker, D. Mandler, P. R. Unwin, *J. Am. Chem. Soc.* **2003**, *125*, 9312 – 9313.
[84] J. Zhang, D. Mandler, P. R. Unwin, *Chem. Commun.* **2004**, 450 – 451.
[85] A. L. Whitworth, D. Mandler, P. R. Unwin, *Phys. Chem. Chem. Phys.* **2005**, *7*, 356 – 365.
[86] B. M. Quinn, I. Prieto, S. K. Haram, A. J. Bard, *J. Phys. Chem. B* **2001**, *105*, 7474 – 7476.
[87] B. M. Quinn, P. Liljeroth, K. Kontturi, *J. Am. Chem. Soc.* **2002**, *124*, 12915 – 12921.
[88] P. Liljeroth, B. M. Quinn, V. Ruiz, K. Kontturi, *Chem. Commun.* **2003**, 1570 – 1571.
[89] D. G. Georganopoulou, M. V. Mirkin, R. W. Murray, *Nano Lett.* **2004**, *4*, 1763 – 1767.
[90] P. Liljeroth, D. Vanmaekelbergh, V. Ruiz, K. Kontturi, H. Jiang, E. Kauppinen, B. M. Quinn, *J. Am. Chem. Soc.* **2004**, *126*, 7126 – 7132.
[91] P. Liljeroth, B. M. Quinn, *J. Am. Chem. Soc.* **2006**, *128*, 4922 – 4923.
[92] H. H. Girault, D. J. Schiffrin in *Electroanalytical Chemistry, Vol. 15* (Ed.: A. J. Bard), Marcel Dekker, New York, **1989**, pp. 1 – 141.
[93] Y. Shao, M. V. Mirkin, *J. Electroanal. Chem.* **1997**, *439*, 137 – 143.
[94] A. L. Barker, P. R. Unwin, S. Amemiya, J. Zhou, A. J. Bard, *J. Phys. Chem. B* **1999**, *103*, 7260 – 7269.
[95] B. Liu, M. V. Mirkin, *J. Am. Chem. Soc.* **1999**, *121*, 8352 – 8355.
[96] A. L. Barker, P. R. Unwin, *J. Phys. Chem. B* **2001**, *105*, 12019 – 12031.
[97] P. Sun, Z. Zhang, Z. Gao, Y. Shao, *Angew. Chem.* **2002**, *114*, 3595 – 3598; *Angew. Chem. Int. Ed.* **2002**, *41*, 3445 – 3448.
[98] F. Li, Y. Chen, P. Sun, M. Zhang, Z. Gao, D. Zhan, Y. Shao, *J. Phys. Chem. B* **2004**, *108*, 3295 – 3302.
[99] Y. Selzer, D. Mandler, *J. Phys. Chem. B* **2000**, *104*, 4903 – 4910.
[100] B. Liu, M. V. Mirkin, *J. Phys. Chem. B* **2002**, *106*, 3933 – 3940.
[101] C. Shi, F. C. Anson, *J. Phys. Chem. B* **2001**, *105*, 1047 – 1049.
[102] Y. Bai, P. Sun, M. Zhang, Z. Gao, Z. Yang, Y. Shao, *Electrochim. Acta* **2003**, *48*, 3447 – 3453.
[103] Z. Ding, B. M. Quinn, A. J. Bard, *J. Phys. Chem. B* **2001**, *105*, 6367 – 6374.
[104] A. L. Barker, C. J. Slevin, P. R. Unwin, J. Zhang in *Liquid Interfaces in Chemical, Biological, and Pharmaceutical Applications* (Ed.: A. G. Volkov), Marcel Dekker, New York, **2001**, pp. 283 – 324.
[105] Y. Zu, F.-R. F. Fan, A. J. Bard, *J. Phys. Chem. B* **1999**, *103*, 6272 – 6276.
[106] M. V. Mirkin in *Scanning Electrochemical Microscopy* (Eds.: A. J. Bard, M. V. Mirkin), Marcel Dekker, New York, **2001**, pp. 299 – 342.
[107] A. L. Barker, P. R. Unwin, J. Zhang, *Electrochem. Commun.* **2001**, *3*, 372 – 378.
[108] Z. Zhang, Y. Yuan, P. Sun, B. Su, J. Guo, Y. Shao, H. H. Girault, *J. Phys. Chem. B* **2002**, *106*, 6713 – 6717.
[109] J. Zhang, P. R. Unwin, *Phys. Chem. Chem. Phys.* **2002**, *4*, 3820 – 3827.
[110] X. Lu, L. Hu, X. Wang, *Electroanalysis* **2005**, *17*, 953 – 958.
[111] M.-H. Delville, M. Tsionsky, A. J. Bard, *Langmuir* **1998**, *14*, 2774 – 2779.
[112] J. Zhang, P. R. Unwin, *Phys. Chem. Chem. Phys.* **2003**, *5*, 3979 – 3983.
[113] S. Amemiya, Z. Ding, J. Zhou, A. J. Bard, *J. Electroanal. Chem.* **2000**, *483*, 7 – 17.
[114] J. Zhang, J. Strutwolf, S. Cannan, P. R. Unwin, *Electrochem. Commun.* **2003**, *5*, 105 – 110.
[115] S. Amemiya, A. J. Bard, *Anal. Chem.* **2000**, *72*, 4940 – 4948.
[116] P. R. Unwin in *Scanning Electrochemical Microscopy* (Eds.: A. J. Bard, M. V. Mirkin), Marcel Dekker, New York, **2001**, pp. 241 – 298.
[117] P. R. Unwin, A. J. Bard, *J. Phys. Chem.* **1991**, *95*, 7814 – 7824.
[118] F. Zhou, P. R. Unwin, A. J. Bard, *J. Phys. Chem.* **1992**, *96*, 4917 – 4924.
[119] C. Demaille, P. R. Unwin, A. J. Bard, *J. Phys. Chem.* **1996**, *100*, 14137 – 14143.
[120] T. C. Richards, A. J. Bard, A. Cusanelli, D. Sutton, *Organometallics* **1994**, *13*, 757 – 759.
[121] M. V. Mirkin, H. Yang, A. J. Bard, *Electrochem. Soc. Interface* **1992**, *139*, 2212 – 2217.
[122] F. Zhou, A. J. Bard, *J. Am. Chem. Soc.* **1994**, *116*, 393 – 394.
[123] S. Bollo, P. Jara-Ulloa, S. Finger, L. J. Nunez-Vergara, J. A. Squella, *J. Electroanal. Chem.* **2005**, *577*, 235 – 242.
[124] S. Bollo, L. Nunez-Vergara, J. A. Squella, *J. Electrochem. Soc.* **2004**, *151*, E322-E325.
[125] D. P. Burt, J. Cervera, D. Mandler, J. V. Macpherson, J. A. Manzanares, P. R. Unwin, *Phys. Chem. Chem. Phys.* **2005**, *7*, 2955 – 2964.
[126] P. R. Unwin, J. V. Macpherson, R. D. Martin, C. F. McConville, *Proc. Electrochem. Soc.* **2000**, *99–28*, 104 – 121.
[127] J. V. Macpherson, P. R. Unwin, *J. Phys. Chem.* **1994**, *98*, 1704 – 1713.
[128] J. V. Macpherson, P. R. Unwin, *J. Phys. Chem.* **1994**, *98*, 11764 – 11770.
[129] J. V. Macpherson, P. R. Unwin, *J. Chem. Soc. Faraday Trans. 1* **1993**, *89*, 1883 – 1884.
[130] J. V. Macpherson, P. R. Unwin, *J. Phys. Chem.* **1996**, *100*, 19475 – 19483.
[131] P. R. Unwin, J. V. Macpherson, *Chem. Soc. Rev.* **1995**, *24*, 109 – 119.
[132] J. V. Macpherson, P. R. Unwin, *J. Phys. Chem.* **1995**, *99*, 3338 – 3351.
[133] J. V. Macpherson, P. R. Unwin, *J. Phys. Chem.* **1995**, *99*, 14824 – 14831.
[134] C. E. Jones, P. R. Unwin, J. V. Macpherson, *ChemPhysChem* **2003**, *4*, 139 – 146.

[135] J. V. Macpherson, P. R. Unwin, *Anal. Chem.* **2000**, *72*, 276 – 285.
[136] J. V. Macpherson, P. R. Unwin, A. C. Hillier, A. J. Bard, *J. Am. Chem. Soc.* **1996**, *118*, 6445 – 6452.
[137] P. R. Unwin, A. J. Bard, *J. Phys. Chem.* **1992**, *96*, 5035 – 5045.
[138] C. W. Lin, F.-R. F. Fan, A. J. Bard, *J. Electrochem. Soc.* **1987**, *134*, 1038 – 1039.
[139] D. H. Craston, C. W. Lin, A. J. Bard, *J. Electrochem. Soc.* **1988**, *135*, 785 – 786.
[140] A. J. Bard, G. Denuault, C. Lee, D. Mandler, D. O. Wipf, *Acc. Chem. Res.* **1990**, *23*, 357 – 363.
[141] D. Mandler, A. J. Bard, *Langmuir* **1990**, *6*, 1489 – 1494.
[142] D. Mandler, A. J. Bard, *J. Electrochem. Soc.* **1990**, *137*, 1079 – 1086.
[143] D. Mandler, A. J. Bard, *J. Electrochem. Soc.* **1990**, *137*, 2468 – 2472.
[144] S. Krämer, R. R. Fuierer, C. B. Gorman, *Chem. Rev.* **2003**, *103*, 4367 – 4418.
[145] V. Radtke, J. Heinze, *Z. Phys. Chem.* **2004**, *218*, 103 – 121.
[146] D. Mandler in *Scanning Electrochemical Microscopy* (Eds.: A. J. Bard, M. V. Mirkin), Marcel Dekker, New York, **2001**, pp. 593 – 627.
[147] H. Shiku, T. Matsue in *Sensors Update*, *Vol. 6* (Eds.: H. Baltes, W. Göpel, J. Hesse), Wiley-VCH, Weinheim, **2000**.
[148] D. Mandler, A. J. Bard, *J. Electrochem. Soc.* **1989**, *136*, 3143 – 3144.
[149] S. Meltzer, D. Mandler, *J. Chem. Soc. Faraday Trans. 1* **1995**, *91*, 1019 – 1024.
[150] Y. Zu, L. Xie, B. Mao, Z. Tian, *Electrochim. Acta* **1998**, *43*, 1683 – 1690.
[151] I. Turyan, U. O. Krasovec, B. Orel, T. Saraidorov, R. Reisfeld, D. Mandler, *Adv. Mater.* **2000**, *12*, 330 – 333.
[152] H. Shiku, T. Takeda, H. Yamada, T. Matsue, I. Uchida, *Anal. Chem.* **1995**, *67*, 312 – 317.
[153] H. Shiku, I. Uchida, T. Matsue, *Langmuir* **1997**, *13*, 7239 – 7244.
[154] H. Kaji, K. Tsukidate, T. Matsue, M. Nishizawa, *J. Am. Chem. Soc.* **2004**, *126*, 15026 – 15027.
[155] H. Kaji, K. Tsukidate, M. Hashimoto, T. Matsue, M. Nishizawa, *Langmuir* **2005**, *21*, 6966 – 6969.
[156] H. Kaji, M. Kanada, D. Oyamatsu, T. Matsue, M. Nishizawa, *Langmuir* **2004**, *20*, 16 – 19.
[157] H. Kaji, T. Kawashima, M. Nishizawa, *Langmuir* **2006**, *22*, 10784 – 10787.
[158] C. Zhao, I. Witte, G. Wittstock, *Angew. Chem.* **2006**, *118*, 5595 – 5597; *Angew. Chem. Int. Ed.* **2006**, *45*, 5469 – 5471.
[159] C. Combellas, J. Ghilane, F. Kanoufi, D. Mazouzi, *J. Phys. Chem. B* **2004**, *108*, 6391 – 6397.
[160] C. Combellas, A. Fuchs, F. Kanoufi, D. Mazouzi, S. Nunige, *Polymer* **2004**, *45*, 4669 – 4675.
[161] C. Combellas, F. Kanoufi, D. Mazouzi, *J. Phys. Chem. B* **2004**, *108*, 19260 – 19268.
[162] F. Kanoufi, C. Combellas, M. E. R. Shanahan, *Langmuir* **2003**, *19*, 6711 – 6716.
[163] C. Combellas, F. Kanoufi, D. Mazouzi, A. Thiebault, *J. Electroanal. Chem.* **2003**, *556*, 43 – 52.
[164] C. Hess, K. Borgwarth, C. Ricken, D. G. Ebling, J. Heinze, *Electrochim. Acta* **1997**, *42*, 3065 – 3073.
[165] K. Borgwarth, C. Ricken, D. G. Ebling, J. Heinze, *Ber. Bunsen-Ges.* **1995**, *99*, 1421 – 1426.
[166] K. Borgwarth, N. Rohde, C. Ricken, M. L. Hallensleben, D. Mandler, J. Heinze, *Adv. Mater.* **1999**, *11*, 1221 – 1226.
[167] C. Marck, K. Borgwarth, J. Heinze, *Adv. Mater.* **2001**, *13*, 47 – 51.
[168] C. Marck, K. Borgwarth, J. Heinze, *Chem. Mater.* **2001**, *13*, 747 – 752.
[169] J. Zhou, D. O. Wipf, *J. Electrochem. Soc.* **1997**, *144*, 1202 – 1207.
[170] I. Shohat, D. Mandler, *J. Electrochem. Soc.* **1994**, *141*, 995 – 999.
[171] S. Meltzer, D. Mandler, *J. Electrochem. Soc.* **1995**, *142*, L82 – L84.
[172] E. Ammann, D. Mandler, *J. Electrochem. Soc.* **2001**, *148*, C533 – C539.
[173] M. Hugelmann, P. Hugelmann, W. J. Lorenz, W. Schindler, *Surf. Sci.* **2005**, *597*, 156 – 172.
[174] W. Schindler, D. Hofmann, J. Kirschner, *J. Electrochem. Soc.* **2001**, *148*, 124 – 130.
[175] W. Schindler, D. Hofmann, J. Kirschner, *J. Appl. Phys.* **2000**, *87*, 7007 – 7009.
[176] D. Hofmann, W. Schindler, J. Kirschner, *Appl. Phys. Lett.* **1998**, *73*, 3279 – 3281.
[177] O. de Abril, D. Mandler, P. R. Unwin, *Electrochem. Solid-State Lett.* **2004**, *7*, C71 – C74.
[178] Y. Yatziv, I. Turyan, D. Mandler, *J. Am. Chem. Soc.* **2002**, *124*, 5618 – 5619.
[179] I. Turyan, M. Etienne, D. Mandler, W. Schuhmann, *Electroanalysis* **2005**, *17*, 538 – 542.
[180] S. Sauter, G. Wittstock, *J. Solid State Electrochem.* **2001**, *5*, 205 – 211.
[181] S. Sauter, G. Wittstock, R. Szargan, *Phys. Chem. Chem. Phys.* **2001**, *3*, 562 – 569.
[182] R. C. Engstrom, B. Small, L. Kattan, *Anal. Chem.* **1992**, *64*, 241 – 244.
[183] K. Borgwarth, J. Heinze, *J. Electrochem. Soc.* **1999**, *146*, 3285 – 3289.
[184] J. Ufheil, C. Hess, K. Borgwarth, J. Heinze, *Phys. Chem. Chem. Phys.* **2005**, *7*, 3185 – 3190.
[185] J. Ufheil, F. M. Boldt, M. Börsch, K. Borgwarth, J. Heinze, *Bioelectrochemistry* **2000**, *52*, 103 – 110.
[186] O. E. Hüsser, D. H. Craston, A. J. Bard, *J. Electrochem. Soc.* **1989**, *136*, 3222 – 3229.
[187] Y.-M. Wuu, F.-R. F. Fan, A. J. Bard, *J. Electrochem. Soc.* **1989**, *136*, 885 – 886.
[188] C. Kranz, M. Ludwig, H. E. Gaub, W. Schuhmann, *Adv. Mater.* **1995**, *7*, 38 – 40.
[189] W. Schuhmann, C. Kranz, H. Wohlschläger, J. Strohmeier, *Biosens. Bioelectron.* **1997**, *12*, 1157 – 1167.
[190] C. Kranz, M. Ludwig, H. E. Gaub, W. Schuhmann, *Adv. Mater.* **1995**, *7*, 568 – 571.
[191] C. Kranz, H. E. Gaub, W. Schuhmann, *Adv. Mater.* **1996**, *8*, 634 – 637.
[192] C. Kranz, G. Wittstock, H. Wohlschläger, W. Schuhmann, *Electrochim. Acta* **1997**, *42*, 3105 – 3111.
[193] E. M. El-Giar, R. A. Said, G. E. Bridges, D. J. Thomson, *J. Electrochem. Soc.* **2000**, *147*, 586 – 591.
[194] G. Wittstock, R. Hesse, W. Schuhmann, *Electroanalysis* **1997**, *9*, 746 – 750.
[195] T. Wilhelm, G. Wittstock, *Microchim. Acta* **2000**, *133*, 1 – 9.
[196] T. Wilhelm, G. Wittstock, *Electrochim. Acta* **2001**, *47*, 275 – 281.
[197] C. A. Widrig, C. Chung, M. D. Porter, *J. Electroanal. Chem.* **1991**, *310*, 335 – 359.
[198] T. Wilhelm, G. Wittstock, *Angew. Chem.* **2003**, *115*, 2349 – 2353; *Angew. Chem. Int. Ed.* **2003**, *42*, 2247 – 2250.
[199] R. C. Tenent, D. O. Wipf, *J. Electrochem. Soc.* **2003**, *150*, E131 – E139.
[200] J. A. Dagata, *Science* **1995**, *270*, 1625 – 1626.
[201] H. S. Isaacs, *Corros. Sci.* **1989**, *29*, 313 – 323.
[202] H. S. Isaacs, G. Kissel, *J. Electrochem. Soc.* **1972**, *119*, 1628 – 1632.
[203] H. Tanabe, Y. Yamamura, T. Misawa, *Mater. Sci. Forum* **1995**, *185–188*, 991 – 1000.
[204] Y. Zhu, D. E. Williams, *J. Electrochem. Soc.* **1997**, *144*, 43 – 45.
[205] B. T. Luong, A. Nishikata, T. Tsuru, *Electrochemistry* **2003**, *71*, 555 – 561.
[206] T. E. Lister, P. J. Pinhero, *Electrochim. Acta* **2003**, *48*, 2371 – 2378.

[207] T. E. Lister, P. J. Pinhero, *Proc. Electrochem. Soc.* **2002**, *2002–24*, 368–376.
[208] N. Casillas, S. J. Charlebois, W. H. Smyrl, H. S. White, *J. Electrochem. Soc.* **1993**, *140*, 142–144.
[209] N. Casillas, S. J. Charlebois, W. H. Smyrl, H. S. White, *J. Electrochem. Soc.* **1994**, *141*, 636–642.
[210] S. B. Basame, H. S. White, *J. Phys. Chem.* **1995**, *99*, 16430–16435.
[211] S. B. Basame, H. S. White, *J. Phys. Chem. B* **1998**, *102*, 9812–9819.
[212] L. F. Garfias-Mesias, M. Alodan, P. James, W. H. Smyrl, *J. Electrochem. Soc.* **1998**, *145*, 2005–2010.
[213] S. B. Basame, H. S. White, *Langmuir* **1999**, *15*, 819–825.
[214] S. B. Basame, H. S. White, *Anal. Chem.* **1999**, *71*, 3166–3170.
[215] C. H. Paik, R. C. Alkire, *J. Electrochem. Soc.* **2001**, *148*, B276–B281.
[216] I. Serebrennikova, H. S. White, *Electrochem. Solid-State Lett.* **2001**, *4*, B4–B6.
[217] I. Serebrennikova, S. Lee, H. S. White, *Faraday Discuss.* **2002**, *121*, 199–210.
[218] D. E. Williams, T. F. Mohiuddin, Y. Y. Zhu, *J. Electrochem. Soc.* **1998**, *145*, 2664–2672.
[219] C.-H. Paik, H. S. White, R. C. Alkire, *J. Electrochem. Soc.* **2000**, *147*, 4120–4124.
[220] T. E. Lister, P. J. Pinhero, *Anal. Chem.* **2005**, *77*, 2601–2607.
[221] D. O. Wipf, *Colloids Surf. A* **1994**, *93*, 251–261.
[222] J. W. Still, D. O. Wipf, *J. Electrochem. Soc.* **1997**, *144*, 2657–2664.
[223] K. Fushimi, M. Seo, *Electrochim. Acta* **2001**, *47*, 121–127.
[224] E. Voelker, C. G. Inchauspe, E. J. Calvo, *Electrochem. Commun.* **2006**, *8*, 179–183.
[225] J. L. Gilbert, S. M. Smith, E. P. Lautenschlager, *J. Biomed. Mater. Res.* **1993**, *27*, 1357–1366.
[226] J. L. Gilbert, L. Zarka, E. Chang, C. H. Thomas, *J. Biomed. Mater. Res.* **1998**, *42*, 321–330.
[227] K. Fushimi, T. Okawa, M. Seo, *Electrochemistry* **2000**, *68*, 950–954.
[228] J. C. Seegmiller, D. A. Buttry, *J. Electrochem. Soc.* **2003**, *150*, B413–B418.
[229] A. Schulte, S. Belger, M. Etienne, W. Schuhmann, *Mater. Sci. Eng. A* **2004**, *378*, 523–526.
[230] S. Belger, A. Schulte, C. Hessing, M. Pohl, W. Schuhmann, *Materialwiss. Werkstofftech.* **2004**, *35*, 276–279.
[231] A. Davoodi, J. Pan, C. Leygraf, S. Norgren, *Electrochem. Solid-State Lett.* **2005**, *8*, B21–B24.
[232] T. E. Lister, P. J. Pinhero, T. L. Trowbridge, R. E. Mizia, *J. Electroanal. Chem.* **2005**, *579*, 291–298.
[233] A. Davoodi, J. Pan, C. Leygraf, S. Norgren, *Appl. Surf. Sci.* **2006**, *252*, 5499–5503.
[234] B. Ballesteros Katemann, C. G. Inchauspe, P. A. Castro, A. Schulte, E. J. Calvo, W. Schuhmann, *Electrochim. Acta* **2003**, *48*, 1115–1121.
[235] A. C. Bastos, A. M. Simoes, S. Gonzalez, Y. Gonzalez-Garcia, R. M. Souto, *Prog. Org. Coat.* **2005**, *53*, 177–182.
[236] R. M. Souto, Y. Gonzalez-Garcia, S. Gonzalez, *Corros. Sci.* **2005**, *47*, 3312–3323.
[237] K. Toth, G. Nagy, B. R. Horrocks, A. J. Bard, *Anal. Chim. Acta* **1993**, *282*, 239–246.
[238] G. A. Shreve, C. D. Karp, K. E. Pomykal, N. S. Lewis, *J. Phys. Chem.* **1995**, *99*, 5575–5580.
[239] M. Janotta, D. Rudolph, A. Kueng, C. Kranz, H.-S. Voraberger, W. Waldhauser, B. Mizaikoff, *Langmuir* **2004**, *20*, 8634–8640.
[240] B. Gründig, G. Wittstock, U. Rüdel, B. Strehlitz, *J. Electroanal. Chem.* **1995**, *395*, 143–157.
[241] C. Gabrielli, E. Ostermann, H. Perrot, V. Vivier, L. Beitone, C. Mace, *Electrochem. Commun.* **2005**, *7*, 962–968.
[242] K. Fushimi, T. Okawa, K. Azumi, M. Seo, *J. Electrochem. Soc.* **2000**, *147*, 524–529.
[243] B. Ballesteros Katemann, A. Schulte, E. J. Calvo, M. Koudelka-Hep, W. Schuhmann, *Electrochem. Commun.* **2002**, *4*, 134–138.
[244] A. S. Baranski, P. M. Diakowski, *J. Solid State Electrochem.* **2004**, *8*, 683–692.
[245] M. Etienne, A. Schulte, W. Schuhmann, *Electrochem. Commun.* **2004**, *6*, 288–293.
[246] K. Borgwarth, J. Heinze in *Scanning Electrochemical Microscopy* (Eds.: A. J. Bard, M. V. Mirkin), Marcel Dekker, New York, **2001**, S. 201–240.
[247] G. Wittstock, H. Emons, T. H. Ridgway, E. A. Blubaugh, W. R. Heineman, *Anal. Chim. Acta* **1994**, *298*, 285–302.
[248] G. Wittstock, B. Gründig, B. Strehlitz, K. Zimmer, *Electroanalysis* **1998**, *10*, 526–531.
[249] O. Köster, W. Schuhmann, H. Vogt, W. Mokwa, *Sens. Actuators B* **2001**, *76*, 573–581.
[250] C. G. Zoski, N. Simjee, O. Guenat, M. Koudelka-Hep, *Anal. Chem.* **2004**, *76*, 62–72.
[251] S. Ramirez-Garcia, S. Alegret, F. Cespedes, R. J. Forster, *Analyst* **2002**, *127*, 1512–1519.
[252] O. Sklyar, J. Ufheil, J. Heinze, G. Wittstock, *Electrochim. Acta* **2003**, *49*, 117–128.
[253] J. Ufheil, K. Borgwarth, J. Heinze, *Anal. Chem.* **2002**, *74*, 1316–1321.
[254] M. Etienne, E. C. Anderson, S. R. Evans, W. Schuhmann, I. Fritsch, *Anal. Chem.* **2006**, *78*, 7317–7324.
[255] A. P. O'Mullane, A. K. Neufeld, A. M. Bond, *Anal. Chem.* **2005**, *77*, 5447–5452.
[256] A. K. Neufeld, A. P. O'Mullane, A. M. Bond, *J. Am. Chem. Soc.* **2005**, *127*, 13846–13853.
[257] Y. Shen, K. Nonomura, D. Schlettwein, C. Zhao, G. Wittstock, *Chem. Eur. J.* **2006**, *12*, 5832–5839.
[258] H. Yamada, M. Ogata, T. Koike, *Langmuir* **2006**, *22*, 7923–7927.
[259] L. Svobodova, M. Snejdarkova, K. Toth, R. E. Gyurcsanyi, T. Hianik, *Bioelectrochemistry* **2004**, *63*, 285–289.
[260] B. Liu, A. J. Bard, M. V. Mirkin, S. E. Creager, *J. Am. Chem. Soc.* **2004**, *126*, 1485–1492.
[261] F.-M. Boldt, N. Baltes, K. Borgwarth, J. Heinze, *Surf. Sci.* **2005**, *597*, 51–64.
[262] D. Burshtain, D. Mandler, *J. Electroanal. Chem.* **2005**, *581*, 310–319.
[263] B. Liu, A. J. Bard, C.-Z. Li, H.-B. Kraatz, *J. Phys. Chem. B* **2005**, *109*, 5193–5198.
[264] J. Abbou, A. Anne, C. Demaille, *J. Am. Chem. Soc.* **2004**, *126*, 10095–10108.
[265] G. Wittstock, T. Asmus, T. Wilhelm, *Fresenius J. Anal. Chem.* **2000**, *367*, 346–351.
[266] M. E. Williams, K. D. Benkstein, C. Abel, P. H. Dinolfo, J. T. Hupp, *Proc. Natl. Acad. Sci. USA* **2002**, *99*, 5171–5177.
[267] M. E. Williams, J. T. Hupp, *J. Phys. Chem. B* **2001**, *105*, 8944–8950.
[268] M. E. Williams, K. J. Stevenson, A. M. Massari, J. T. Hupp, *Anal. Chem.* **2000**, *72*, 3122–3128.
[269] H. Shiku, T. Saito, C.-C. Wu, T. Yasukawa, M. Yokoo, H. Abe, T. Matsue, H. Yamada, *Chem. Lett.* **2006**, *35*, 234–235.
[270] R. E. Gyurcsanyi, E. Pergel, R. Nagy, I. Kapui, B. T. T. Lan, K. Toth, I. Bitter, E. Lindner, *Anal. Chem.* **2001**, *73*, 2104–2111.
[271] E. Bakker, P. Bühlmann, E. Pretsch, *Electroanalysis* **1999**, *11*, 915–933.
[272] M. V. Mirkin, F.-R. F. Fan, A. J. Bard, *Science* **1992**, *257*, 364–366.
[273] F.-R. F. Fan, M. V. Mirkin, A. J. Bard, *J. Phys. Chem.* **1994**, *98*, 1475–1481.
[274] C. Lee, A. J. Bard, *Anal. Chem.* **1990**, *62*, 1906–1913.

[275] J. Kwak, C. Lee, A. J. Bard, *J. Electrochem. Soc.* **1990**, *137*, 1481 – 1484.
[276] K. Borgwarth, D. G. Ebling, J. Heinze, *Electrochim. Acta* **1995**, *40*, 1455 – 1460.
[277] K. Borgwarth, C. Ricken, D. G. Ebling, J. Heinze, *Fresenius J. Anal. Chem.* **1996**, *356*, 288 – 294.
[278] G. Wittstock, C. Kranz, D. J. Strike, W. Schuhmann, H. L. Schmidt, *European Microscopy and Analysis* **1996**, 5 – 7.
[279] M. Arca, M. V. Mirkin, A. J. Bard, *J. Phys. Chem.* **1995**, *99*, 5040 – 5050.
[280] M. Tsionsky, A. J. Bard, D. Dini, F. Decker, *Chem. Mater.* **1998**, *10*, 2120 – 2126.
[281] M. Quinto, S. A. Jenekhe, A. J. Bard, *Chem. Mater.* **2001**, *13*, 2824 – 2832.
[282] I. C. Jeon, F. C. Anson, *Anal. Chem.* **1992**, *64*, 2021 – 2028.
[283] J. Kwak, F. C. Anson, *Anal. Chem.* **1992**, *64*, 250 – 256.
[284] C. Lee, F. C. Anson, *Anal. Chem.* **1992**, *64*, 528 – 533.
[285] M. H. T. Frank, G. Denuault, *J. Electroanal. Chem.* **1993**, *354*, 331 – 339.
[286] V. Syritski, R. E. Gyurcsanyi, A. Oepik, K. Toth, *Synth. Met.* **2005**, *152*, 133 – 136.
[287] J. C. Taylor, R. J. LeSuer, C. R. Chambers, F.-R. F. Fan, A. J. Bard, W. E. Conley, C. G. Willson, *Chem. Mater.* **2005**, *17*, 4194 – 4203.
[288] B. D. Bath, H. S. White, E. R. Scott in *Scanning Electrochemical Microscopy* (Eds.: A. J. Bard, M. V. Mirkin), Marcel Dekker, New York, **2001**, pp. 343 – 395.
[289] E. R. Scott, H. S. White, J. B. Phipps, *Anal. Chem.* **1993**, *65*, 1537 – 1545.
[290] B. D. Bath, R. D. Lee, H. S. White, *Anal. Chem.* **1998**, *70*, 1047 – 1058.
[291] E. R. Scott, H. S. White, J. B. Phipps, *J. Membr. Sci.* **1991**, *58*, 71 – 87.
[292] S. Nugues, G. Denuault, *J. Electroanal. Chem.* **1996**, *408*, 125 – 140.
[293] O. D. Uitto, H. S. White, K. Aoki, *Anal. Chem.* **2002**, *74*, 4577 – 4582.
[294] E. R. Scott, A. I. Laplaza, H. S. White, J. B. Phipps, *Pharm. Res.* **1993**, *10*, 1699 – 1709.
[295] E. R. Scott, J. B. Phipps, H. S. White, *J. Invest. Dermatol.* **1995**, *104*, 142 – 145.
[296] B. D. Bath, E. R. Scott, J. B. Phipps, H. S. White, *J. Pharm. Sci.* **2000**, *89*, 1537 – 1549.
[297] B. D. Bath, J. B. Phipps, E. R. Scott, O. D. Uitto, H. S. White, *Stud. Surf. Sci. Catal.* **2001**, *132*, 1015 – 1019.
[298] O. D. Uitto, H. S. White, *Anal. Chem.* **2001**, *73*, 533 – 539.
[299] O. D. Uitto, H. S. White, *Pharm. Res.* **2003**, *20*, 646 – 652.
[300] J. V. Macpherson, M. A. Beeston, P. R. Unwin, *J. Chem. Soc. Faraday Trans. 1* **1995**, *91*, 899 – 904.
[301] J. V. Macpherson, M. A. Beeston, P. R. Unwin, N. P. Hughes, D. Littlewood, *Langmuir* **1995**, *11*, 3959 – 3963.
[302] P. R. Unwin, J. V. Macpherson, M. A. Beeston, N. J. Evans, D. Littlewood, N. P. Hughes, *Adv. Dent. Res.* **1997**, *11*, 548 – 559.
[303] N. J. Evans, M. Gonsalves, N. J. Gray, A. L. Barker, J. V. Macpherson, P. R. Unwin, *Electrochem. Commun.* **2000**, *2*, 201 – 206.
[304] M. Gonsalves, A. L. Barker, J. V. Macpherson, P. R. Unwin, D. O'Hare, P. C. Winlove, *Biophys. J.* **2000**, *78*, 1578 – 1588.
[305] J. V. Macpherson, D. O'Hare, P. R. Unwin, C. P. Winlove, *Biophys. J.* **1997**, *73*, 2771 – 2781.
[306] A. Kueng, C. Kranz, B. Mizaikoff, *Biosens. Bioelectron.* **2004**, *19*, 1301 – 1307.
[307] A. Kueng, C. Kranz, B. Mizaikoff, *Biosens. Bioelectron.* **2005**, *21*, 346 – 353.
[308] A. Kueng, C. Kranz, A. Lugstein, E. Bertagnolli, B. Mizaikoff, *Angew. Chem.* **2003**, *115*, 3358 – 3360; *Angew. Chem. Int. Ed.* **2003**, *42*, 3238 – 3240.
[309] C. E. Gardner, P. R. Unwin, J. V. Macpherson, *Electrochem. Commun.* **2005**, *7*, 612 – 618.
[310] E. N. Ervin, H. S. White, L. A. Baker, *Anal. Chem.* **2005**, *77*, 5564 – 5569.
[311] P. K. Hansma, B. Drake, O. Marti, S. A. C. Gould, C. B. Prater, *Science* **1989**, *243*, 641 – 643.
[312] E. N. Ervin, H. S. White, L. A. Baker, *Anal. Chem.* **2005**, *77*, 5564 – 5569.
[313] S. Lee, Y. Zhang, H. S. White, C. C. Harrell, R. Martin Charles, *Anal. Chem.* **2004**, *76*, 6108 – 6115.
[314] J. Ye, J. Liu, Z. Zhang, J. Hu, S. Dong, Y. Shao, *J. Electroanal. Chem.* **2001**, *508*, 123 – 128.
[315] L. I. Halaoui, H. Sharifian, A. J. Bard, *J. Electrochem. Soc.* **2001**, *148*, E386 – E393.
[316] J. Zhou, Y. Zu, A. J. Bard, *J. Electroanal. Chem.* **2000**, *491*, 22 – 29.
[317] B. C. Shah, A. C. Hillier, *J. Electrochem. Soc.* **2000**, *147*, 3043 – 3048.
[318] S. Ahmed, S. Ji, L. Petrik, V. M. Linkov, *Anal. Sci.* **2004**, *20*, 1283 – 1287.
[319] C. G. Zoski, *J. Phys. Chem. B* **2003**, *107*, 6401 – 6405.
[320] K. Jambunathan, B. C. Shah, J. L. Hudson, A. C. Hillier, *J. Electroanal. Chem.* **2001**, *500*, 279 – 289.
[321] K. Jambunathan, A. C. Hillier, *J. Electroanal. Chem.* **2002**, *524–525*, 144 – 156.
[322] S. Jayaraman, A. C. Hillier, *J. Comb. Chem.* **2004**, *6*, 27 – 31.
[323] S. Jayaraman, A. C. Hillier, *J. Phys. Chem. B* **2003**, *107*, 5221 – 5230.
[324] S. Daniele, C. Bragato, M. A. Baldo, G. A. Battiston, R. Gerbasi, *Mater. Sci. Forum* **2003**, *413*, 147 – 152.
[325] A. R. Kucernak, P. B. Chowdhury, C. P. Wilde, G. H. Kelsall, Y. Y. Zhu, D. E. Williams, *Electrochim. Acta* **2000**, *45*, 4483 – 4491.
[326] J. Meier, A. K. Friedrich, U. Stimming, *Faraday Discuss.* **2002**, *121*, 365 – 372.
[327] M. G. Del Popolo, E. P. M. Leiva, H. Kleine, J. Meier, U. Stimming, M. Mariscal, W. Schmickler, *Electrochim. Acta* **2003**, *48*, 1287 – 1294.
[328] J. Meier, J. Schiotz, P. Liu, J. K. Norskov, U. Stimming, *Chem. Phys. Lett.* **2004**, *390*, 440 – 444.
[329] J. L. Fernandez, A. J. Bard, *Anal. Chem.* **2003**, *75*, 2967 – 2974.
[330] J. L. Fernandez, A. J. Bard, *Anal. Chem.* **2004**, *76*, 2281 – 2289.
[331] J. L. Fernandez, N. Mano, A. Heller, A. J. Bard, *Angew. Chem.* **2004**, *116*, 6515 – 6517; *Angew. Chem. Int. Ed.* **2004**, *43*, 6355 – 6357.
[332] D. A. Walsh, J. L. Fernandez, A. J. Bard, *J. Electrochem. Soc.* **2006**, *153*, E99 – E103.
[333] B. Liu, A. J. Bard, *J. Phys. Chem. B* **2002**, *106*, 12801 – 12806.
[334] C. Zhao, J. K. Sinha, C. A. Wijayawardhana, G. Wittstock, *J. Electroanal. Chem.* **2004**, *561*, 83 – 91.
[335] T. Kaya, K. Nagamine, N. Matsui, T. Yasukawa, H. Shiku, T. Matsue, *Chem. Commun.* **2004**, 248 – 249.
[336] C. A. Wijayawardhana, G. Wittstock, H. B. Halsall, W. R. Heineman, *Anal. Chem.* **2000**, *72*, 333 – 338.
[337] D. T. Pierce, A. J. Bard, *Anal. Chem.* **1993**, *65*, 3598 – 3604.
[338] C. Zhao, G. Wittstock, *Anal. Chem.* **2004**, *76*, 3145 – 3154.
[339] H. Yamada, H. Shiku, T. Matsue, I. Uchida, *Bioelectrochem. Bioenerg.* **1994**, *33*, 91 – 93.
[340] H. Shiku, T. Matsue, I. Uchida, *Anal. Chem.* **1996**, *68*, 1276 – 1278.
[341] G. Wittstock, T. Wilhelm, S. Bahrs, P. Steinrücke, *Electroanalysis* **2001**, *13*, 669 – 675.
[342] J. Zaumseil, G. Wittstock, S. Bahrs, P. Steinrücke, *Fresenius J. Anal. Chem.* **2000**, *367*, 352 – 355.
[343] J. Wang, L.-H. Wu, R. Li, *J. Electroanal. Chem.* **1989**, *272*, 285 – 292.

[344] B. R. Horrocks, D. Schmidtke, A. Heller, A. J. Bard, *Anal. Chem.* **1993**, *65*, 3605 – 3614.
[345] H. Shiku, Y. Hara, T. Matsue, I. Uchida, T. Yamauchi, *J. Electroanal. Chem.* **1997**, *438*, 187 – 190.
[346] C. A. Wijayawardhana, G. Wittstock, H. B. Halsall, W. R. Heineman, *Electroanalysis* **2000**, *12*, 640 – 644.
[347] C. Zhao, G. Wittstock, *Angew. Chem.* **2004**, *116*, 4264 – 4267; *Angew. Chem. Int. Ed.* **2004**, *43*, 4170 – 4172.
[348] N. Matsui, T. Kaya, K. Nagamine, T. Yasukawa, H. Shiku, T. Matsue, *Biosens. Bioelectron.* **2006**, *21*, 1202 – 1209.
[349] C. E. M. Berger, B. R. Horrocks, H. K. Datta, *J. Endocrinol.* **1998**, *158*, 311 – 318.
[350] T. Wilhelm, G. Wittstock, R. Szargan, *Fresenius J. Anal. Chem.* **1999**, *365*, 163 – 167.
[351] C. Zhao, G. Wittstock, *Biosens. Bioelectron.* **2005**, *20*, 1277 – 1284.
[352] W. B. Nowall, N. Dontha, W. G. Kuhr, *Biosens. Bioelectron.* **1998**, *13*, 1237 – 1244.
[353] S. E. Rosenwald, N. Dontha, W. G. Kuhr, *Anal. Chem.* **1998**, *70*, 1133 – 1140.
[354] W. B. Nowall, D. O. Wipf, W. G. Kuhr, *Anal. Chem.* **1998**, *70*, 2601 – 2606.
[355] T. Wilhelm, G. Wittstock, *Langmuir* **2002**, *18*, 9485 – 9493.
[356] M. Niculescu, S. Gaspar, A. Schulte, E. Csoregi, W. Schuhmann, *Biosens. Bioelectron.* **2004**, *19*, 1175 – 1184.
[357] C. Kurzawa, A. Hengstenberg, W. Schuhmann, *Anal. Chem.* **2002**, *74*, 355 – 361.
[358] S. Gaspar, M. Mosbach, L. Wallman, T. Laurell, E. Csöregi, W. Schuhmann, *Anal. Chem.* **2001**, *73*, 4254 – 4261.
[359] F. Turcu, G. Hartwich, D. Schaefer, W. Schuhmann, *Macromol. Rapid Commun.* **2005**, *26*, 325 – 330.
[360] M. Maciejewska, D. Schaefer, W. Schuhmann, *Electrochem. Commun.* **2006**, *8*, 1119 – 1124.
[361] R. N. Adams, *Prog. Neurobiol.* **1990**, *35*, 297 – 311.
[362] R. M. Wightman, *Science* **2006**, *311*, 1570 – 1574.
[363] M. Tsionsky, Z. G. Cardon, A. J. Bard, R. B. Jackson, *Plant Physiol.* **1997**, *113*, 895 – 901.
[364] S. Isik, M. Etienne, J. Oni, A. Bloechl, S. Reiter, W. Schuhmann, *Anal. Chem.* **2004**, *76*, 6389 – 6394.
[365] Y.-S. Torisawa, H. Shiku, T. Yasukawa, M. Nishizawa, T. Matsue, *Biomaterials* **2005**, *26*, 2165 – 2172.
[366] Y.-S. Torisawa, H. Shiku, S. Kasai, M. Nishizawa, T. Matsue, *Int. J. Cancer* **2004**, *109*, 302 – 308.
[367] Y.-S. Torisawa, H. Shiku, S. Kasai, M. Nishizawa, T. Matsue, *Chem. Senses* **2003**, *19*, 28 – 30.
[368] Y.-S. Torisawa, T. Kaya, Y. Takii, D. Oyamatsu, M. Nishizawa, T. Matsue, *Anal. Chem.* **2003**, *75*, 2154 – 2158.
[369] T. Yasukawa, T. Kaya, T. Matsue, *Anal. Chem.* **1999**, *71*, 4631 – 4641.
[370] R. T. Kurulugama, D. O. Wipf, S. A. Takacs, S. Pongmayteegul, P. A. Garris, J. E. Baur, *Anal. Chem.* **2005**, *77*, 1111 – 1117.
[371] R. Zhu, S. M. Macfie, Z. Ding, *J. Exp. Bot.* **2005**, *56*, 2831 – 2838.
[372] T. Yasukawa, T. Kaya, T. Matsue, *Chem. Lett.* **1999**, *9*, 975 – 976.
[373] M. Nishizawa, K. Takoh, T. Matsue, *Langmuir* **2002**, *18*, 3645 – 3649.
[374] T. Yasukawa, Y. Kondo, I. Uchida, T. Matsue, *Chem. Lett.* **1998**, 767 – 768.
[375] Y.-S. Torisawa, A. Takagi, H. Shiku, T. Yasukawa, T. Matsue, *Oncol. Rep.* **2005**, *13*, 1107 – 1112.
[376] K. B. Holt, A. J. Bard, *Biochemistry* **2005**, *44*, 13214 – 13223.
[377] Y.-S. Torisawa, H. Shiku, T. Yasukawa, M. Nishizawa, T. Matsue, *Sens. Actuators B* **2005**, *108*, 654 – 659.
[378] H. Shiku, T. Shiraishi, S. Aoyagi, Y. Utsumi, M. Matsudaira, H. Abe, H. Hoshi, S. Kasai, H. Ohya, T. Matsue, *Anal. Chim. Acta* **2004**, *522*, 51 – 58.
[379] H. Shiku, Y.-S. Torisawa, A. Takagi, S. Aoyagi, H. Abe, H. Hoshi, T. Yasukawa, T. Matsue, *Sens. Actuators B* **2005**, *108*, 597 – 602.
[380] B. Agung, T. Otoi, H. Abe, H. Hoshi, M. Murakami, N. W. K. Karja, M. K. Murakami, P. Wongsrikeao, H. Watari, T. Suzuki, *Reprod. Domest. Anim.* **2005**, *40*, 51 – 56.
[381] A. Hengstenberg, A. Blöchl, I. D. Dietzel, W. Schuhmann, *Angew. Chem.* **2001**, *113*, 942 – 946; *Angew. Chem. Int. Ed.* **2001**, *40*, 905 – 908.
[382] L. Pitta Bauermann, W. Schuhmann, A. Schulte, *Phys. Chem. Chem. Phys.* **2004**, *6*, 4003 – 4008.
[383] C. E. M. Berger, H. Rathod, J. I. Gillespie, B. R. Horrocks, H. K. Datta, *J. Bone Miner. Res.* **2001**, *16*, 2092 – 2102.
[384] C. E. M. Berger, B. R. Horrocks, H. K. Datta, *Mol. Cell. Endocrinol.* **1999**, *149*, 53 – 59.
[385] B. Liu, S. A. Rotenberg, M. V. Mirkin, *Proc. Natl. Acad. Sci. USA* **2000**, *97*, 9855 – 9860.
[386] B. Liu, S. A. Rotenberg, M. V. Mirkin, *Anal. Chem.* **2002**, *74*, 6340 – 6348.
[387] W. Feng, S. A. Rotenberg, M. V. Mirkin, *Anal. Chem.* **2003**, *75*, 4148 – 4154.
[388] B. Liu, W. Cheng, S. A. Rotenberg, M. V. Mirkin, *J. Electroanal. Chem.* **2001**, *500*, 590 – 597.
[389] K. Nagamine, N. Matsui, T. Kaya, T. Yasukawa, H. Shiku, T. Nakayama, T. Nishino, T. Matsue, *Biosens. Bioelectron.* **2005**, *21*, 145 – 151.
[390] K. Nagamine, T. Kaya, T. Yasukawa, H. Shiku, T. Matsue, *Sens. Actuators B* **2005**, *108*, 676 – 682.
[391] S. Kasai, A. Yokota, H. Zhou, M. Nishizawa, T. Onouchi, K. Niwa, T. Matsue, *Anal. Chem.* **2000**, *72*, 5761 – 5765.
[392] N. Motochi, Y. Hirano, Y. Abiko, D. Oyamatsu, M. Nishizawa, T. Matsue, K. Ushizawa, S. Kawabata, *Chem. Senses* **2002**, *18*, 172 – 174.
[393] X. Zhang, X. Peng, W. Jin, *Anal. Chim. Acta* **2006**, *558*, 110 – 114.
[394] D. Ogasawara, Y. Hirano, T. Yasukawa, H. Shiku, T. Matsue, K. Kobori, K. Ushizawa, S. Kawabata, *Chem. Senses* **2004**, *20*, 139 – 141.
[395] Y. Hirano, Y. Mase, D. Oyamatsu, T. Yasukawa, H. Shiku, T. Matsue, *Chem. Senses* **2004**, *20*, 754 – 755.
[396] C. A. Wijayawardhana, N. J. Ronkainen-Matsuno, S. M. Farrel, G. Wittstock, H. B. Halsall, W. R. Heineman, *Anal. Sci.* **2001**, *17*, 535 – 538.
[397] M. Florencia Garay, J. Ufheil, K. Borgwarth, J. Heinze, *Phys. Chem. Chem. Phys.* **2004**, *6*, 4028 – 4033.
[398] E. Fortin, P. Mailley, L. Lacroix, S. Szunerits, *Analyst* **2006**, *131*, 186 – 193.
[399] S. Szunerits, N. Knorr, R. Calemczuk, T. Livache, *Langmuir* **2004**, *20*, 9236 – 9241.
[400] E. Fortin, P. Mailley, L. Lacroix, S. Szunerits, *Analyst* **2006**, *131*, 186 – 193.
[401] M. Komatsu, K. Yamashita, K. Uchida, H. Kondo, S. Takenaka, *Electrochim. Acta* **2006**, *51*, 2023 – 2029.
[402] S. Takenaka, *Polym. J.* **2004**, *36*, 503 – 512.
[403] T. Kaya, K. Nagamine, N. Matsui, T. Yasukawa, H. Shiku, T. Matsue, *Chem. Commun.* **2004**, 248 – 249.
[404] D. Ogasawara, Y. Hirano, T. Yasukawa, H. Shiku, T. Matsue, K. Kobori, K. Ushizawa, S. Kawabata, *Chem. Sens.* **2004**, *20*, 139 – 141.
[405] H. Kaji, M. Hashimoto, M. Nishizawa, *Anal. Chem.* **2006**, *78*, 5469 – 5473.
[406] J. Wang, F. Song, F. Zhou, *Langmuir* **2002**, *18*, 6653 – 6658.
[407] M. Carano, N. Lion, J.-P. Abid, H. H. Girault, *Electrochem. Commun.* **2004**, *6*, 1217 – 1221.
[408] M. Carano, N. Lion, H. H. Girault, *Chimia* **2005**, *59*, 105 – 108.
[409] J. Wang, F. Zhou, *J. Electroanal. Chem.* **2002**, *537*, 95 – 102.

[410] F. Turcu, A. Schulte, G. Hartwich, W. Schuhmann, *Angew. Chem.* **2004**, *116*, 3564 – 3567; *Angew. Chem. Int. Ed.* **2004**, *43*, 3482 – 3485.
[411] F. Turcu, A. Schulte, G. Hartwich, W. Schuhmann, *Biosens. Bioelectron.* **2004**, *20*, 925 – 932.
[412] M. Ludwig, C. Kranz, W. Schuhmann, H. E. Gaub, *Rev. Sci. Instrum.* **1995**, *66*, 2857 – 2860.
[413] P. James, L. F. Garfias-Mesias, P. J. Moyer, W. H. Smyrl, *J. Electrochem. Soc.* **1998**, *145*, 64 – 66.
[414] Y. Lee, A. J. Bard, *Anal. Chem.* **2002**, *74*, 3626 – 3633.
[415] B. Ballesteros Katemann, A. Schulte, W. Schuhmann, *Chem. Eur. J.* **2003**, *9*, 2025 – 2033.
[416] M. F. Garay, J. Ufheil, K. Borgwarth, J. Heinze, *Phys. Chem. Chem. Phys.* **2004**, *6*, 4028 – 4033.
[417] H. Yamada, H. Fukumoto, T. Yokoyama, T. Koike, *Anal. Chem.* **2005**, *77*, 1785 – 1790.
[418] D. Oyamatsu, Y. Hirano, N. Kanaya, Y. Mase, M. Nishizawa, T. Matsue, *Bioelectrochemistry* **2003**, *60*, 115 – 121.
[419] B. Ballesteros Katemann, A. Schulte, W. Schuhmann, *Electroanalysis* **2004**, *16*, 60 – 65.
[420] L. P. Bauermann, W. Schuhmann, A. Schulte, *Phys. Chem. Chem. Phys.* **2004**, *6*, 4003 – 4008.
[421] E. Ammann, C. Beuret, P. F. Indermuhle, R. Kotz, N. F. de Rooij, H. Siegenthaler, *Electrochim. Acta* **2001**, *47*, 327 – 334.
[422] T. H. Treutler, G. Wittstock, *Electrochim. Acta* **2003**, *48*, 2923 – 2932.
[423] J. V. Macpherson, P. R. Unwin, *Anal. Chem.* **2001**, *73*, 550 – 557.
[424] J. V. Macpherson, J.-P. Gueneau de Mussy, J.-L. Delplancke, *J. Electrochem. Soc.* **2002**, *149*, B306 – B313.
[425] J. V. Macpherson, C. E. Jones, A. L. Barker, P. R. Unwin, *Anal. Chem.* **2002**, *74*, 1841 – 1848.
[426] D. P. Burt, N. R. Wilson, J. M. R. Weaver, P. S. Dobson, J. V. Macpherson, *Nano Lett.* **2005**, *5*, 639 – 643.
[427] P. S. Dobson, J. M. R. Weaver, D. P. Burt, M. N. Holder, N. R. Wilson, P. R. Unwin, J. V. Macpherson, *Phys. Chem. Chem. Phys.* **2006**, *8*, 3909 – 3914.
[428] C. Kranz, G. Friedbacher, B. Mizaikoff, A. Lugstein, J. Smolier, E. Bertagnolli, *Anal. Chem.* **2001**, *73*, 2491 – 2500.
[429] A. Lugstein, E. Bertagnolli, C. Kranz, A. Kueng, B. Mizaikoff, *Appl. Phys. Lett.* **2002**, *81*, 349 – 351.
[430] A. Lugstein, E. Bertagnolli, C. Kranz, B. Mizaikoff, *Surf. Interface Anal.* **2002**, *33*, 146 – 150.
[431] A. Kueng, C. Kranz, B. Mizaikoff, A. Lugstein, E. Bertagnolli, *Appl. Phys. Lett.* **2003**, *82*, 1592 – 1594.
[432] J. Abbou, A. Anne, C. Demaille, *J. Am. Chem. Soc.* **2004**, *126*, 10095 – 10108.
[433] R. J. Fasching, Y. Tao, F. B. Prinz, *Sens. Actuators B* **2005**, *108*, 964 – 972.
[434] Y. Tao, R. J. Fasching, F. B. Prinz, *Proc. SPIE-Int. Soc. Opt. Eng.* **2004**, *5389*, 431 – 442.
[435] R. J. Fasching, Y. Tao, F. B. Prinz, *Chem. Senses* **2004**, *20*, 318 – 319.
[436] M. R. Gullo, P. L. T. M. Frederix, T. Akiyama, A. Engel, N. F. de Rooij, U. Staufer, *Anal. Chem.* **2006**, *78*, 5436 – 5442.
[437] T. Akiyama, M. R. Gullo, N. F. De Rooij, A. Tonin, H.-R. Hidber, P. L. T. M. Frederix, A. Engel, U. Staufer, *Jpn. J. Appl. Phys. Part 1* **2004**, *43*, 3865 – 3867.
[438] C. Kranz, A. Kueng, A. Lugstein, E. Bertagnolli, B. Mizaikoff, *Ultramicroscopy* **2004**, *100*, 127 – 134.
[439] A. Kueng, C. Kranz, A. Lugstein, E. Bertagnolli, B. Mizaikoff, *Methods Mol. Biol.* **2005**, *300*, 403 – 415.
[440] A. Kueng, C. Kranz, B. Mizaikoff, *Sens. Lett.* **2003**, *1*, 2 – 15.
[441] A. Kueng, C. Kranz, A. Lugstein, E. Bertagnolli, B. Mizaikoff, *Angew. Chem.* **2005**, *117*, 3485 – 3488; *Angew. Chem. Int. Ed.* **2005**, *44*, 3419 – 3422.
[442] A. L. Barker, P. R. Unwin, J. W. Gardner, H. Rieley, *Electrochem. Commun.* **2004**, *6*, 91 – 97.
[443] P. S. Dobson, J. M. R. Weaver, M. N. Holder, P. R. Unwin, J. V. Macpherson, *Anal. Chem.* **2005**, *77*, 424 – 434.
[444] N. Casillas, P. James, W. H. Smyrl, *J. Electrochem. Soc.* **1995**, *142*, 16 – 18.
[445] P. James, N. Casillas, W. H. Smyrl, *J. Electrochem. Soc.* **1996**, *143*, 3853 – 3865.
[446] Y. Lee, Z. Ding, A. J. Bard, *Anal. Chem.* **2002**, *74*, 3634 – 3643.
[447] K. Maruyama, H. Ohkawa, S. Ogawa, A. Ueda, O. Niwa, K. Suzuki, *Anal. Chem.* **2006**, *78*, 1904 – 1912.
[448] G. Shi, L. F. Garfias-Mesias, W. H. Smyrl, *J. Electrochem. Soc.* **1998**, *145*, 2011 – 2016.
[449] H. Xiong, J. Guo, K. Kurihara, S. Amemiya, *Electrochem. Commun.* **2004**, *6*, 615 – 620.
[450] F.-R. F. Fan, D. E. Cliffel, A. J. Bard, *Anal. Chem.* **1998**, *70*, 2941 – 2948.
[451] S. Cannan, I. D. Macklam, P. R. Unwin, *Electrochem. Commun.* **2002**, *4*, 886 – 892.
[452] F.-M. Boldt, J. Heinze, M. Diez, J. Petersen, M. Boersch, *Anal. Chem.* **2004**, *76*, 3473 – 3481.
[453] D. E. Cliffel, A. J. Bard, *Anal. Chem.* **1998**, *70*, 1993 – 1998.
[454] C. Hess, K. Borgwarth, J. Heinze, *Electrochim. Acta* **2000**, *45*, 3725 – 3736.
[455] B. Gollas, P. N. Bartlett, G. Denuault, *Anal. Chem.* **2000**, *72*, 349 – 356.
[456] C. Gabrielli, S. Joiret, M. Keddam, H. Perrot, N. Portail, P. Rousseau, V. Vivier, *J. Electrochem. Soc.* **2006**, *153*, B68 – B74.
[457] X. Tu, Q. Xie, C. Xiang, Y. Zhang, S. Yao, *J. Phys. Chem. B* **2005**, *109*, 4053 – 4063.
[458] E. Fortin, Y. Defontaine, P. Mailley, T. Livache, S. Szunerits, *Electroanalysis* **2005**, *17*, 495 – 503.
[459] J. Xiang, J. Guo, F. Zhou, *Anal. Chem.* **2006**, *78*, 1418 – 1424.
[460] D. E. Cliffel, A. J. Bard, S. Shinkai, *Anal. Chem.* **1998**, *70*, 4146 – 4151.
[461] P. Sun, M. V. Mirkin, *Anal. Chem.* **2006**, *78*, 6526 – 6534.